Synergy-Based Human Grasp Representations and Semi-Autonomous Control of Prosthetic Hands

zur Erlangung des akademischen Grades eines

Doktors der Ingenieurwissenschaften

von der KIT-Fakultät für Informatik
des Karlsruher Instituts für Technologie (KIT)

genehmigte
DISSERTATION

von

M.Sc. Julia Starke

aus Hannover

Tag der mündlichen Prüfung:	20. September 2022
Erster Gutachter:	Prof. Dr.-Ing. Tamim Asfour
Zweiter Gutachter:	Prof. Dr. Antonio Morales Escrig

Deutsche Zusammenfassung

Das sichere und stabile Greifen mit humanoiden Roboterhänden stellt eine große Herausforderung dar. Menschen dagegen können Objekte schnell, zuverlässig und intuitiv greifen. Sie bestimmen geeignete Fingerstellungen, um das Objekt zu Umschließen und die geplante Verwendung des Objektes zu ermöglichen. Zudem erzeugen Menschen mit ihren Händen Kräfte, die das sichere Greifen und Halten von Objekten garantieren ohne diese zu beschädigen. Aus diesem menschlichen Erfahrungswissen kann die Robotik lernen und Greifstrategien für humanoide Roboterhände ableiten. Neben der Pose und Kraft eines Griffs ist die Annäherungsbewegung an das Objekts entscheidend für den Erfolg der Griffausführung.

In der Literatur konnten bei einem Griff Korrelationen sowohl zwischen den Gelenkwinkeln der Finger einer Hand als auch zwischen den Aktivierungen der am Griff beteiligten Muskeln nachgewiesen werden. Die sogenannten Griffsynergien legen nahe, dass die Steuerung komplexer menschlicher Griffe gegenüber dem Handkonfigurationsraum eine erheblich niedrigere Dimensionalität aufweist. Die Betrachtung des niedrigdimensionalen Raums der Griffsynergien ermöglicht damit eine Analyse der Charakteristika erfolgreicher menschlicher Greifstrategien und deren Übertragung auf die Steuerung humanoider Hände in der Robotik.

Ziel dieser Arbeit ist es, Greifstrategien für Roboterhände aus der Beobachtung menschlicher Greifbewegungen abzuleiten. Dabei liegt der Fokus auf der Betrachtung des gesamten Greifvorgangs. Dieser umfasst zum einen die Hand- und Fingertrajektorien während des Greifprozesses und zum anderen die Kon-

taktpunkte sowie den Kraftverlauf zwischen Hand und Objekt vom ersten Kontakt bis zum statisch stabilen Griff. Diese vom Menschen gelernten Greifstrategien sollen für die Steuerung robotischer Prothesenhände angewandt werden. Im Folgenden werden die drei Einzelbeiträge dieser Arbeit vorgestellt:

Posturale und kinematische Griffsynergien Als Grundlage dieser Arbeit dient das Konzept der posturalen Griffsynergien, welches Korrelationen zwischen den Fingergelenken der menschlichen Hand ausnutzt, um statische Griffposen in einem reduzierten Parameterraum beschreiben zu können. Diese Arbeit stellt adaptive posturale Griffsynergien vor, die mithilfe eines tiefen Autoencoders gelernt werden. Die Griffpose der Hand, bestehend aus 16 Fingergelenkwinkeln, kann so in einem dreidimensionalen Synergieraum dargestellt werden. Der Synergieraum ist hinsichtlich des Grifftyps strukturiert und ermöglicht über einen zusätzlichen vierten Parameter die direkte Beeinflussung des gewünschten Objektdurchmessers. Damit können neue, nicht direkt vom Menschen gezeigte Griffe aus dem adaptiven posturalen Synergieraum generiert werden, die dennoch menschenähnlich sind und deren Griffeigenschaften explizit gesteuert werden können.

Zur Beschreibung der gesamten Greifbewegung zum Erreichen der statischen Griffpose werden kinematische Griffsynergien genutzt. Diese stellen die Greifbewegung als Trajektorie im statischen Synergieraum dar. Diese Arbeit stellt kinematische Synergieprimitive vor, die als Via-Punkt-Bewegungsprimitive (engl. *via-point movement primitives*) aus menschlichen Synergietrajektorien eines Grifftyps gelernt werden. Die Synergieprimitive ermöglichen eine generalisierte Darstellung von Greifbewegungen eines Grifftyps, welche hinsichtlich des zeitlichen Verlaufs, der Start- und Endpose, sowie des Verlaufs der Greifbewegung selbst, adaptiert werden kann. Auf diese Weise können neue, menschenähnliche Greifbewegungen eines Grifftyps aus dem Spektrum vom Menschen demonstrierter Bewegungen generiert werden.

Griffkraftsynergien Neben der Handbewegung und -pose spielt auch die Griffkraft eine bedeutende Rolle für Stabilität und Erfolg eines Griffes. Auch zwischen den Griffkräften an verschiedenen Kontaktpunkten zwischen Hand und Objekt können Korrelationen nachgewiesen werden. Dies motiviert eine Darstellung der Kraftkonfiguration von Griffen mittels Griffkraftsynergien. Im Rahmen dieser Arbeit wurde eine allgemeine Darstellung statischer Griffkraftsynergien entwickelt, die Kraftkonfigurationen für viele verschiedene Grifftypen und Objekte berücksichtigt. Auf diese Weise kann die Kraftkonfiguration

an 18 Kontaktpunkten der Hand mit lediglich acht Kraftsynergien beschrieben werden.

Zudem präsentiert diese Arbeit zwei neuartige Methoden zur Beschreibung zeitlicher Griffkraftverläufe mithilfe von Kraftsynergien. Zum einen wird ein statischer Kraftsynergieraum unter Verwendung einer Hauptkomponentenanalyse gelernt. Die Darstellung zeitlicher Griffkraftverläufe erfolgt mittels zeitabhängiger Trajektorien in diesem statischen Synergieraum. Weiterhin wird ein LSTM-Autoencoder mit ganzen Griffkraftverläufen trainiert, um einen zeitabhängigen latenten Synergieraum zu lernen. Dieser zeitabhängige Synergieraum berücksichtigt den zeitlichen Kraftverlauf direkt in der Synergiedarstellung, sodass die Generierung neuer, menschenähnlicher Griffe unter Beachtung des zeitlichen Griffortschritts möglich wird. Zusätzlich sind verschiedene Grifftypen im zeitlichen Kraftsynergieraum räumlich strukturiert, sodass die gewünschte Griffpose bei der Generierung neuer Griffe berücksichtigt werden kann.

Teilautonome Prothesensteuerung Unter Verwendung einer Datenbank menschlicher Greifstrategien wird eine Steuerung für eine unteraktuierte Handprothese entwickelt. Die komplexe menschliche Handbewegung wird dabei auf die Prothesenkinematik mit einer wesentlich geringeren Anzahl unabhängiger Bewegungsfreiheitsgrade übertragen. Unter Verwendung von Kontextinformation über den Zustand der Prothese und die Umgebung wird eine geeignete Greifstrategie ausgewählt und dem Nutzenden vorgeschlagen. Dieser kann den Greifvorgang mit Hilfe von Muskelkontraktionen im Unterarm initiieren und beeinflussen.

Aus der Datenbank menschlicher Griffe werden situationsgerecht Kontrollstrategien ausgewählt, angepasst und ausgeführt. Dabei wird der Nutzende in den Greifprozess eingebunden und kann Griffauswahl und -ausführung beeinflussen. Diese teilautonome Prothesensteuerung zeichnet sich gegenüber dem Stand der Forschung durch die Verwendung menschlicher Greifstrategien und die trajektorienbasierte, kontinuierliche Greifausführung aus. Aufgrund der vom Menschen inspirierten Greifbewegungen ist die teilautonome Steuerung für den Nutzenden intuitiv während die partielle Automatisierung der Greifbewegung die kognitive Belastung des Nutzenden verringert.

Contents

CHAPTER 1

Introduction

Grasping is a significant activity in human daily life. Throughout all our daily actions, we incessantly perform grasps on a wide variety of objects, be it throughout work, in leisure activities, for cooking or in cleaning and personal hygiene. Almost without thinking about it - and sometimes even without looking - humans grasp many objects and even use them as tools to manipulate their environment. This is very impressive, since the kinematics of the human hand are quite complex. With 27 joints and more than 20 degrees of freedom (DoF), the human hand is a complex system driven by several extrinsic and intrinsic muscles ((Jones and Lederman, 2006) and (León et al., 2014)). A significant part of the human motor cortex is specifically concerned with hand control ((Grodd et al., 2001)). Nevertheless, human grasping is done intuitively and is an easy task for most of us.

In humanoid robotics it is desirable to imitate the versatility of the human hand. This is especially interesting when robots are cooperating with humans or dealing with environments made for humans. For prosthetic hands the focus on humanoid appearance and behavior goes even beyond the general needs in humanoid robotics. However, the kinematic complexity of the human hand raises a number of challenges for the mechanical design and the control of robotic hands. Besides the problem of mechanical integration and actuation, especially the planning and control of grasps on known and unknown object geometries is still a hard problem in robotics. Therefore, researchers strive for transferring

the intuitive human grasping knowledge into robotics, making it accessible for grasp planning and control on humanoid robots and prostheses.

1.1 Problem Statement

This thesis aims at developing methods for the control of humanoid robotic and prosthetic hands based on human grasping strategies. To this end, the thesis builds upon the concept of grasp synergies, which reduces the complexity of human grasping postures by exploiting correlations within the hand joints discovered in neuroscience in (Santello et al., 1998). Analyzing these low-dimensional grasp synergies can therefore provide insights on the characteristics of successful human grasp strategies and their transfer to the control of humanoid robot hands and prostheses. These postural synergies describe a static and stable human grasp posture. Extending this concept, kinematic synergies provide a description of an entire grasping motion starting from the relaxed hand towards the static grasp posture. Besides the pose and kinematic grasping motion, the force applied between the hand and an object is crucial for stable grasping. Therefore, in this thesis both characteristics are taken into account to formulate a comprising grasp description. The focus is set on the analysis of the entire grasping process. This includes the hand and finger trajectories during reaching, hand preshaping and finally closing the fingers around the object. In addition, it also involves the development of grasp forces from the initial contact between the hand and the object until the object is lifted and fully supported by the hand contact forces.

Human grasping knowledge is leveraged by applying the robotics concept of programming by demonstration, as shown in Fig. 1.1. In a first step, human grasp strategies are observed based on recordings of human grasping actions. Both motion capture and force sensing are needed to measure the inherent characteristics of human grasping. The recorded grasping data is analyzed with respect to correlations indicating synergistic behavior. In addition, the grasping data is also analyzed in the context of significant grasping characteristics. The following generalization strives to compile a general model from the findings of the human grasp observation. In literature, a generalized postural synergy space has proven to be capable of representing human grasp postures ((Santello et al., 1998), (Jarque-Bou et al., 2020)). However, there is no such comprehensive description for grasp forces and little attention has been paid to the entire process of grasping.

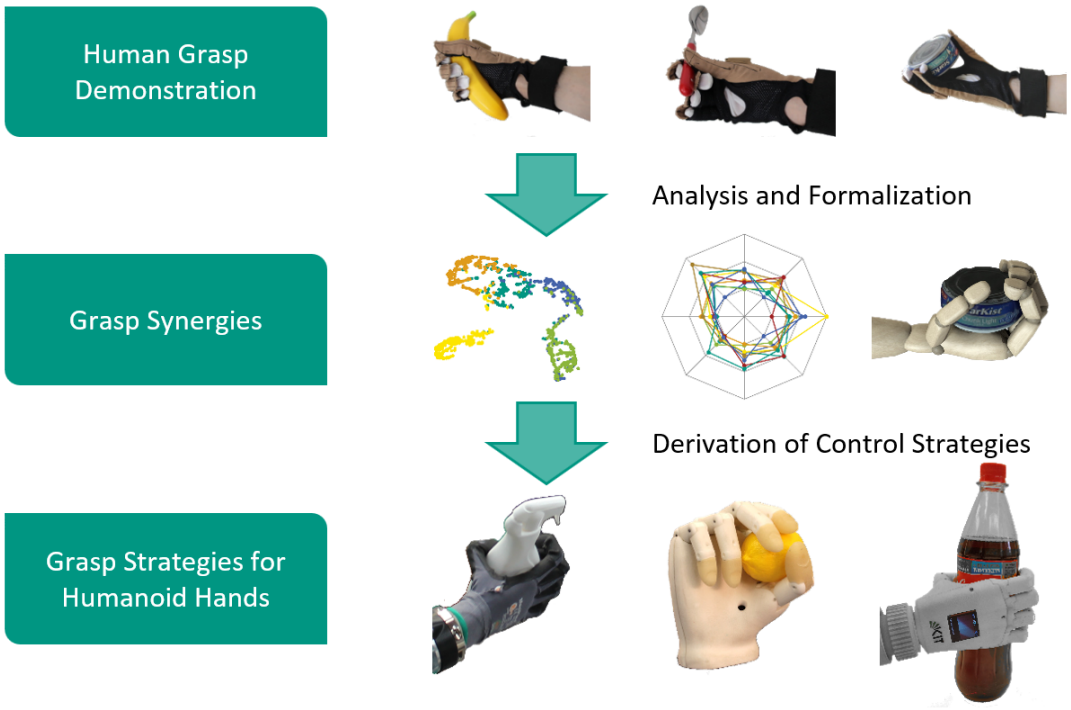

Figure 1.1: Structure of this thesis; demonstrated human grasps are formalized in grasp synergies, which can be used to control humanoid hands

The goal of this thesis is therefore to include the entire grasp process into a generalized synergy description. In addition, a meaningful semantic structure of the synergy space shall be induced to simplify its application in robotic control. Finally, a grasp control based on the general description of human grasping needs to be implemented and evaluated on a robotic hand. The merit of the developed human-like grasps shall therefore be shown in daily life activities on a prosthetic hand, showing a practical example of a real world application.

1.2 Contributions

This thesis contributes to the field of grasp synergies by investigating the kinematic hand and finger trajectories as well as temporally changing grasp force patterns. In addition, it presents a human-inspired grasp control for prosthetic hands, that enables an intuitive semi-autonomous prosthesis control.

Postural and kinematic synergies: Descriptive postural synergies are presented that provide a novel encoding of important grasp characteristics into the synergy space. A deep autoencoder network is applied to learn a non-linear, descriptive latent synergy space. For the first time, a generation of human-like

grasp postures from synergy space is achieved without a corresponding human demonstration. Due to the encoded characteristics of grasp type and object size into the synergy space, these can be explicitly controlled for the generation of new grasps. In addition, this thesis defines kinematic hand synergies that consider the entire grasping process. A novel representation of these kinematic synergies in the form of via-point movement primitives (VMPs) enables the adaptation of human grasp trajectories. By these means, kinematic synergy trajectories demonstrated by the human can be specifically adapted for the execution of novel grasps.

Force synergies: Correlations of grasp contact forces between different contact locations throughout the hand are analyzed for a wide range of grasp types, object shapes and weights. Static grasp force synergies are described and investigated for the first time without restriction of the grasp type or object shape. These static force synergies are learned by a principal component analysis. The dynamic progression of grasp forces is initially described by two models. The description of continuous contact force patterns as trajectories in a static force synergy space is inspired by the methodology of kinematic synergies from literature and is applied on grasp forces for the first time. In addition, a novel dynamic synergy space is proposed, that is learned with an LSTM-autoencoder network. This dynamic synergy space encompasses a notion of grasp progress and is additionally structured to represent grasp characteristics to simplify grasp generation.

Semi-autonomous grasping: Grasps learned from human demonstration are generalized, adapted and applied to a robotic prosthetic hand. Based on grasp recordings with several subjects and a wide range of everyday objects, a human grasp database is generated. This database provides control information for finger and thumb motion as well as wrist orientation to be applied on the prosthetic hand. It is integrated into a novel, semi-autonomous control of prosthetic hands, that focuses on the continuous and simultaneous motion of all degrees of freedom involved in the grasp. By these means, a human-like timing and correlation of the hand's degrees of freedom is ensured, leading to intuitive and successful grasping.

1.3 Structure of the Thesis

The remainder of this thesis is structured as follows: Chapter 2 discusses the state of the art with respect to this thesis. It describes taxonomies as conceptual

grasp representations and introduces computational grasp representations including postural, kinematic and force synergies as well as their application to robotics. In addition, grasp control for prosthetic hands is discussed focusing on semi-autonomous control schemes.

The descriptive postural synergies are presented in Chapter 3. Including an explicit description of grasp type and object size, these postural synergies are designed to generate new human-like grasp postures, that were not demonstrated by the human. Further, kinematic synergies of both arm and hand motions are described. Grasp synergy primitives are presented that allow the specific adaptation of synergy trajectories for the entire finger motion throughout the grasp.

In Chapter 4, an analysis of the grasp contact forces between the object and the human hand is detailed. Comprehensive static force synergies are presented taking into account severals subjects and a wide range of object shapes and weights. For the description of dynamic contact force patterns, two methods are proposed. Synergy trajectories in a static force synergy space describe the time-dependent contact force patterns as a series of static force synergy samples. In addition, a dynamic force synergy space is proposed, that incorporates the grasp progress in the synergy space by directly learning time-dependent contact force patterns.

The human-like grasps generated from grasp synergies are executed on a robotic prosthetic hand in Chapter 5. A library of human grasp strategies is defined, that comprises general and adaptable grasp trajectories learned from human demonstration. These can be applied in the semi-autonomous control of a prosthetic hand. This control provides autonomous grasp functionalities to release the user from the burden of fine-granular finger control, while still keeping the user in supervision. The semi-autonomous control combines the human grasp library with environmental sensing to provide object-specific, autonomous grasp suggestions. It reduces the workload for the user, as shown in a large-scale user study.

The Chapter 6 concludes the thesis and resumes the contributions in kinematic and force synergies as well as semi-autonomous grasp control. In addition, an outlook on future work is given.

CHAPTER 2

Fundamentals and Related Work

Understanding the human hand and strategies of human grasp control is crucial for the design and control of humanoid robotic and prosthetic hands. Further, intuitive human grasp strategies can provide valuable insights to simplify and improve the grasp control for both human-inspired, but also non-humanoid robotic grippers. Hence, the description and analysis of human grasping behavior has been of interest in research for decades. Overall, there are two main approaches used to represent human grasping behavior. On the one hand, conceptual grasp representations structure and classify grasps according to a set of criteria. Thereby, they allow the description of grasps that can be used for human grasp analysis or grasp objectives in robotic grasping. On the other hand, computational grasp representations strive for a generalized description of human grasps on control level. These can then be transferred to the kinematics of a humanoid robotic hand to learn robotic grasp control directly from human demonstration.

Having human-like grasping motions is of specific importance in the field of prosthetic grasping. In addition to the grasp success, the optical appearance also plays an important part here, since the prosthetic hand should look and behave optically unobtrusive and similar to its human counterpart. Grasp strategies learned from human demonstration are therefore an ideal approach for prosthetic applications since they can tackle both the successful grasping as well as a human-like appearance of the grasp motion. Such partially automated

grasp control can be provided by semi-autonomous prosthetic control that simplifies grasping for the user while still keeping the user in control of their prosthetic hand.

This chapter provides an overview over the different approaches towards conceptual and computational human grasp representations in literature. Subsequently, the field of grasp control for myoelectric prosthetic hands is discussed with an emphasize on semi-autonomous grasping.

2.1 Conceptual Grasp Representation

To describe and categorize human grasps on a conceptual level, observed grasps are abstracted into grasping taxonomies. Using observed grasp criteria, human grasps can be classified within a grasp taxonomy. Such a conceptual classification of human grasps can be performed based on a variety of characteristic criteria. Two fundamental grasp taxonomies have been defined in (Kamakura et al., 1980) and (Cutkosky, 1989). While Kamakura classifies grasps by the contact area covered between the hand and the object, Cutkosky focuses on the posture of hand and fingers in the grasp. The Kamakura Taxonomoy subdivides grasps in power, precision and intermediate grasp types with the adduction grip fixing an object between the sides of two fingers denoting an additional grasp type without thumb contact. Within these grasp categories, a more precise structure is proposed based on the grasp contact patterns. Cutkosky's grasp taxonomy also distinguishes power and precision grasps, but in addition it suggests a distinction between prehensile and non-prehensile grasps. Thereby, the platform grasp as additional, non-prehensile support grasp is introduced. By further categorising power and precision grasps in several circular and prismatic sub-categories, a total of 16 different grasp postures is described.

The GRASP Taxonomy in (Feix et al., 2016) provides a review of existing grasp taxonomies and combines the grasps described in the literature into one taxonomy. This results in a very precise distinction of human grasp postures into 33 different grasp types. It is structured based on the methodic description of opposing hand surfaces as *opposition types* proposed in (Iberall, 1997). They categorize grasp opposition based on two or three *virtual fingers* describing a combination of palm and fingers placed on opposing sides of the object. By these means, human grasps are divided into four opposition types involving the palm, finger pads, finger side or a third virtual finger. These virtual fingers

provide an abstract description of grasp posture characteristics independent of the shape and kinematics of a robotic hand. Besides the opposition type, Feix et al. consider the ad- and abduction of the thumb as well as a differentiation between power and precision grasps to structure the GRASP taxonomy. Applying these criteria, the taxonomy can be structured into 17 different grasp patterns.

There are only few taxonomies that consider not only the static grasp posture, but also motion and forces of the hand in a grasp. For object manipulation (Bullock et al., 2013b) defines a taxonomy describing time-varying hand-object relations. The contact with the object distinguishes between non-prehensile and prehensile grasps and also hand motions without object contact are considered. In addition, the manipulation strategies are classified according to global hand motion and motion between the object and the hand. The taxonomy lists 15 manipulation types describing different possible interactions of the hand with an object and the environment. Twelve of these manipulation types consider grasping by holding or manipulating an object. (Liu et al., 2014) builds a taxonomy conceptually describing dynamic human grasp behavior. It specifies 40 grasp types, that are not represented by the previous state of the art and serve a very specialized purpose like tying laces or scratching. Furthermore each grasp description is expanded by a force type, motion and force direction, the motion's flow and object-related characteristics like the weight, size and roughness of the object. The motion's flow is divided into three grades and measures whether the motion is executed in a controlled or rather casual manner. 20 different force types classify the intention of the applied force and the direction of both motion and force is described in the world coordinate system. While this taxonomy results in a comprising description of grasping actions, it also results in complex grasp categories depending on five individual parameters. It is therefore most suitable to get a precise annotation of observed grasps.

These conceptual grasp taxonomies can be used to structure and classify observed human grasp strategies. This allows the identification of grasps frequently used for a specific task or in a defined environment that can then be transferred to a robotic execution of the same task. Further, the determination of important grasp types that are frequently used by humans throughout their daily activities can provide a prioritization of grasping skills needed on a flexible, universal robot working in a human-centered environment. To this end, (Bullock et al., 2013a) provides the statistical frequency of grasp types by analyzing 31 hours of hand recordings taken in the daily life of two machinists and two housekeepers. The study evaluates all grasps performed with the subjects'

dominant right hand. For each subject ~ 4700 grasps are annotated and categorized according to the GRASP Taxonomy. From the 33 different grasp types recognized in the recordings, ten grasp types account for $71\,\%$ of the observed grasps. For housekeepers, more than half of all grasps are power grasps, while the machinists also use precision and intermediate grasps more frequently. A study on grasp frequency based on 180 videos of 43 subjects performing everyday activities is presented in (Vergara et al., 2014). The recorded scenes cover eight areas of the activities of daily living including household and care as well as mobility and provisioning. More than 1500 grasps with both hands are identified in the videos and categorized in nine grasp types based on the literature on occupational therapy. Overall, nearly half of all grasps are classified as pinch grasps. However, oblique palmar grasps are predominant in driving and transport and cylindrical and lumbrical grasps are frequently used in shopping. Interestingly, grasp type frequencies are similar for left and right hand as well as bimanual tasks.

Overall, grasp taxonomies are a tool to categorize human grasps into abstract classes of grasp types. This provides an architecture to describe structural grasp characteristics in a simple and general way and enables the analysis of human grasp strategies on a symbolic level. Thereby grasp taxonomies help in the definition of suitable grasp strategies learned from human demonstration for specific situations or the analysis of frequent grasp strategies in human everyday grasping.

2.2 Computational Grasp Representation

Opposed to conceptual grasp representations, computational grasp representations aim at a description of grasp strategies on the level of control characteristics. This may include hand muscle activations, angles or velocities of finger joints as well as grasp contact forces. Computational grasp representations strive to describe these control characteristics in a generalized and simplified manner to build a universally valid model of human hand control. Grasp synergies are a computational grasp representation frequently used in literature. They are originating from findings in neuroscience showing correlations between different muscle activations for grasping, as for example presented in (d'Avella et al., 2003). Such correlations can be exploited to simplify the representation of human grasp control by reducing its dimensionality. (Castellini and Van Der Smagt, 2013) suggests such a control based on muscle synergies

learned from *electromyographic* (EMG) measurements of the muscle activation signals and (Pei et al., 2019) shows the existence of correlations in *electroencephalographic* (EEG) signals during grasping.

Postural Grasp Synergies

Similarly, for the field of human hand posture analysis, Santello et al. did pioneer work by showing strong correlations between the joint angles of human hands throughout grasping a wide variety of imaginary objects presented in (Santello et al., 1998). By applying a *Principle Component Analysis* (PCA) on 15 joint angles of static human grasping postures, a postural synergy space is defined. For four out of five subjects, two synergies are sufficient to describe $80\,\%$ of the variance of all grasping postures. For the fifth subject, $80\,\%$ of the variance are represented by three synergies. $90\,\%$ of the overall variance are described by three synergies for three out of five subjects. For the other two subjects, four synergies are required to cover $90\,\%$ of the variance. Overall, this means that two to three postural synergies are sufficient to describe $80\,\%$ of the variance of grasping postures of a single subject. Due to the linear dimensionality reduction with the PCA, the postural synergy space is continuous. However, it is not structured with respect to the grasp type of the static grasp postures. A comparison of postural and muscular grasp synergies in (Weiss and Flanders, 2004) shows no direct correlation between both representations.

(Della Santina et al., 2017) analyzes postural grasp synergies with and without contact to an object or the environment in grasping with environmental exploitation. A change in grasp synergies for pre-grasp and contact phase is only measurable in higher order synergies. Further, (Jarque-Bou et al., 2020) derives a postural synergy space from a large and comprehensive dataset of human grasps executed by a large number of subjects on real objects. Similar to Santello et al. they apply a PCA for synergy definition. On the recorded 22-dimensional joint angle data, twelve synergies are needed to represent $80\,\%$ of the variance of the grasping data over all subjects. This number is significantly higher than the one reported by Santello et al., since it includes a higher number of subjects, considers more joint angles and is based on data from grasping physical instead of imaginary objects, thereby inducing more variance based on the object's shape.

All of these postural synergies are linearly defined and therefore capture only linear correlations within the hand pose. Further, the grasp representation in

the postural synergy space is not naturally structured according to the grasp characteristics used in conceptual grasp representations. This complicates a hand control based on postural synergies, since the choice of synergy parameters corresponding to a specific grasp type or hand aperture is not straightforward.

This thesis therefore strives to learn a non-linear, adaptable representation of postural synergies, that can capture non-linear joint correlations and provides an explicit representation of important grasp characteristics in the synergy space. For the first time, a postural synergy space is learned with a deep autoencoder network, exploiting the non-linearity and direct influence on the shape of the latent synergy space provided by this method. The non-linear, adaptable postural synergy representation developed in this thesis has been presented in a scientific publication in (Starke et al., 2020) and has been adopted and extended by (Dimou et al., 2021). A survey on research and applications in postural hand synergies is provided in (Santello et al., 2016).

To enable the control of robotic hands only based on postural synergies, the interaction of the hand with the environment needs to be modeled. Therefore, (Bicchi et al., 2011) introduces the model of soft synergies. It includes the interaction with the object into the control algorithm by introducing a repelling force field on the object surface. By these means, rigid postural synergies can be applied to control flexible grasps with a synergy-shaped posture that maximizes the contact surface between hand and object. The control method of soft synergies can also be used to predict and influence grasp forces for robotic hands with known dynamics, as shown in (Prattichizzo et al., 2010), (Gabiccini et al., 2011) and (Prattichizzo et al., 2013).

A mechanical implementation of postural synergies in an underactuated robotic hand was presented in (Brown and Asada, 2007). It was later enlarged in (Rosmarin and Asada, 2008) with a shape memory alloy array to adapt the synergy controlled hand posture to the object shape. A similar implementation was later presented in (Chen et al., 2015). Inspired by soft synergies, (Catalano et al., 2012) presents the concept of adaptive synergies that provides an adaptively underactuated implementation of postural synergies for robotic hands. The Pisa/IIT SoftHand from (Godfrey et al., 2013) is driven by a single motor implementing an adaptive postural synergy, as explained in (Catalano et al., 2014). (Chen et al., 2018) aims to design synergies for a robotic hand that can be implemented in hardware by an underactuated mechanism. Based on a set of desired grasps, mechanically realizable manifolds are defined, which optimize the desired grasp posture as well as grasp stability. A tendon-driven continuum

robot is proposed for synergy-based hand control in (Xu et al., 2019). The tendons actuating individual finger joints are composed into a continuum robotic structure at the wrist. By externally pulling or pushing the continuum actuation structure, the hand is closed and opened respectively. Bending the continuum robot causes the robotic hand to adopt different finger postures. A survey on humanoid robotic hands with a focus on underactuation and adaptive synergies is presented in (Piazza et al., 2019).

Kinematic Grasp Synergies

Beyond the final grasp posture, the entire grasping motion resulting in that posture is crucial for a successful, human-like grasp. The coordination of the finger closing motions shapes the position of the object in the hand and the final grasp posture. Between different fingers, motion dependencies have been shown in (Ingram et al., 2008). To explicitly consider this motion coordination of the fingers, kinematic synergies strive to describe the entire grasp motion trajectory over time in a low-dimensional synergy space. Different approaches have been presented in literature to consider the aspect of time in kinematic grasp synergies. A representation of hand motions by trajectories in a static postural synergy space has been proposed by Romero et al. in (Romero et al., 2013). They compare different linear and non-linear dimensionality reduction techniques to learn a static hand synergy space independent of time or grasp progress. Both PCA and *Gaussian Process Latent Variable Models* (GP-LVM) provide appropriate hand synergy spaces with the PCA resulting in a synergy space that is more smoothed with respect to the original hand postures. The grasp motion is then described as a timed trajectory in this static synergy space and multiple demonstrations are combined using Gaussian Mixture Regression.

(Kent et al., 2014) suggests an alternative approach reducing the dimensionality of the temporal aspect of a grasp motion. By approximating the trajectory of every joint angle with a polynomial function, the trajectory is reduced to the polynomial parameters. The space of temporally synchronized synergies thereby consists of the parameters of all joint polynomials to recalculate the joint trajectories. (Thomik et al., 2015) defines a set of characteristic eigenmotions of the hand that are used in different phases of the grasp motion. These eigenmotions are learned by a sparse movement decomposition based on short-time PCAs performed on time windows within the motion. By combing these eigenmotions, the grasp movement can be described, whereas usually only two

or three eigenmotions are active at the same time. (Konnaris et al., 2016) controls a robot hand based on such sparse eigenmotions from a motion dictionary learned on human activities of daily living. More specialized synergies exist for various specific tasks like the pegboard test in (Gonzalez et al., 2017) or periodical screwing motions in (Karnati et al., 2013).

All kinematic synergy descriptions focus on a generalization of either correlations between the different joint angles or the temporal grasp progress. The respective second characteristic is then directly deduced from a human grasp demonstration. Conversely, the generation of new, unseen grasp motions is restricted by the manual definition of the grasp characteristic not generalized by the kinematic synergies themselves. This means that the definition of kinematic synergies in a static synergy space requires the explicit definition of the trajectory path over grasp progress and temporally synchronized synergies are conversely limited to a specific grasping motion. Therefore, kinematic synergies in literature do not provide a full generalization of both joint coordination and timing of grasp motions. Hence, the derivation of robotic control strategies from these kinematic synergies requires additional knowledge on the grasp motion, that needs to be either derived from a human demonstration or handcrafted.

This thesis contributes to the generalization capabilities of kinematic synergy trajectories by introducing synergy primitives. Based on the method from (Romero et al., 2013), kinematic synergy trajectories are defined in a static synergy space. The static hand postures and their respective timing are then related using *via-point movement primitives* (VMPs) learned on the kinematic synergy trajectories. This methods captures the motion variability in human demonstrations and allows for the direct control of timing in motion execution. Thereby, human-like grasp motions can be generated from the synergy primitives at a desired speed using the motion timing learned from human demonstration.

While grasp synergies have been extensively studied with respect to the finger postures and grasp motion, little attention has been paid to the approach motion and hand pose. Synergies in wrist pose were individually assessed in (Casini et al., 2017) by performing a PCA on human wrist orientation for nine activities of daily living. One arm synergy parameter thereby describes $74\,\%$ of the overall variance of the three-dimensional wrist orientation. This thesis strives to further characterize the role of arm motion and hand pose in grasping. To this end the global motion of the hand is analyzed in conjunction with the finger motion and the foundation and merit of synergies in arm motion is considered.

To transfer grasp synergies to robotic hands, the concept of eigengrasps was developed in (Ciocarlie et al., 2007b) and later refined in (Ciocarlie et al., 2007a) and (Ciocarlie and Allen, 2009). For each hand an individual set of eigengrasps is defined manually or by analyzing the synergies resulting from teleoperated grasping. Human eigengrasps are defined by the synergy parameters of a human postural synergy space. The transfer of a human grasp demonstration to the robotic hand is then done by a mapping of contact points on both hands. Solving the optimization problem of contact point alignment yields a control strategy in the eigengrasp space of the robotic hand, that can be directly applied to the hand. (Wimböck et al., 2012) derives synergies for the DLR Hand by performing a dimensionality reduction on predefined grasp poses. The grasps are demonstrated beforehand by a human shaping the robotic hand in force controlled mode. A hand control derived from these robotic hand synergies thereby profits from the teleoperated human demonstrations of successful grasping postures. To perform different grasps on the Pisa/IIT Softhand actuated by one adaptive synergy, approach directions and environmental contacts are taken into account in (Della Santina et al., 2019). Nine different grasp strategies are designed based on human demonstration and the association of these grasp strategies with 20 everyday objects is learned. By these means an autonomous grasp architecture inspired by human grasp strategies is designed. (Monforte and Ficuciello, 2020) applies individual synergies for a humanoid hand and arm to perform different reaching motions demonstrated by humans. To improve the resulting grasps, the synergy control is combined with a reinforcement learning algorithm further refining the synergy parameters. Their combined approach shows better results compared with only synergy control. However, further improvement is needed to achieve reliable grasping.

Grasp Force Synergies

The second important grasp characteristic other than hand posture and motion are the human grasp contact forces. Grasp force analyses have been performed for different tasks. However, the description of grasp contact forces in the form of synergies has been considered only sparsely in literature. By using the soft synergy model presented in (Bicchi et al., 2011) combined with a dynamical model of the robotic hand, grasp forces have been determined in simulation in (Gabiccini et al., 2011). By these means, the authors in (Prattichizzo et al., 2010) and (Prattichizzo et al., 2013) analyze the merit of postural synergies for the position and force control of robotic hands. They show a direct correlation

between the number of applied postural synergies and the dimensionality of controllable internal forces.

Force synergies in human grasping were first analyzed by Santello and Soechting in (Santello and Soechting, 2000). They considered pinch grasps on a specifically designed sensor object measuring grasp forces on all five fingertips. The experiments showed correlations between different grasp contact forces and thereby proved the general existence of force synergies. Later experiments with the same sensor setup showed a correlation of force synergies to the center of mass, but no difference for handedness of the subjects, as explained in (Rearick and Santello, 2002). (De Souza et al., 2014) and (De Souza et al., 2015) describe human grasps based on opposition force primitives. These are extracted from the points of contact between hand and object and identify the parts of the hand, that apply opposing forces on the grasped object. The authors show, that grasp force opposition types are tightly connected to different grasp intentions. Thereby, they are used to categorize grasps with different manipulation goals for the same object.

The human grasp force in a power grasp on a cylindrical object under perturbations is characterised in (Naceri et al., 2014). (Marneweck et al., 2016) analyzes the force on the thumb and jointly over all opposing fingers in power grasps. The authors show that grasp forces and finger poses vary between trials, but are correlated with each other. Both thumb posture and grasp force are adapted based on the center of mass of the object, meaning that different grasp postures also require different contact force patterns. When grasping is constrained, the grasp force is also more restricted to the given posture, which can be seen in a change in activity in the sensorimotor cortex, as measured in (Parikh et al., 2019). With a high resolution tactile glove, (Sundaram et al., 2019) provides very detailed grasp force measurements of human grasp executions. The hand contact force patterns allow to identify 26 different grasped objects and to deduce information on the object's weight and shape.

Overall, the importance of the grasp force configuration for grasp success is strongly emphasized by the mentioned analyses on human grasp forces. Further, correlations between grasp forces have been identified in various grasping conditions. The idea of force synergies has been applied on controlled pinch grasps. However, there is no general analysis on synergies in human grasp force patterns spanning a larger variety of unconstrained human grasp postures.

This thesis presents the first static human force synergies learned by a PCA on human grasp contact forces for wide range of different power and precision

grasps. Using *Pearson's Correlation Coefficient* (PCC), correlations between different contact locations throughout the hand are analyzed over different grasp types. By these means, the validity of a general force synergy representation is proven. Further, two strategies for the representation of temporal force synergies are presented. Similar to the kinematic synergies in (Romero et al., 2013), a temporal force pattern is described as a timed trajectory in a static force synergy space. Additionally, an LSTM autoencoder network is trained to learn a novel latent synergy representation with an inherent encoding of time and grasp progress.

2.3 Prosthetic Grasp Control

Myoelectric prosthetic hands provide a replacement for a lost human limb. They are attached to the user's remaining forearm stump and include one or several motors driving the hand's grasping motions. The user can control their prosthetic hand using the forearm muscles meant to actuate the missing human hand. To this end, *electromyographic* (EMG) electrodes are attached to the stump to measure the muscle activations issued by the user. The grasp control of the prosthetic hand is directly driven by these measured muscle activations.

While myoelectric control relies on the same control input normally used for the able human hand, it is still limited and imperfect in the practical application. Commercial myoelectric prostheses are still strenuous to control, especially because of the limited number of EMG control inputs and their sensitivity to changing conditions due to temperature or sweat as demonstrated in (Schweitzer et al., 2018). Therefore, a literature review in (Biddiss and Chau, 2007) shows that the number of amputees, who reject their prosthesis or only wear it as a passive device is still very high. Improvements are needed in prosthetic control and sensory feedback for the user, but also in dexterity and weight of the prosthetic hand, as pointed out in (Cordella et al., 2016) and (Chadwell et al., 2016). Especially sensory feedback is completely missing in commercial hand prostheses and (Wijk and Carlsson, 2015) shows that this reduces the feeling of ownership of amputees regarding their prosthetic hand.

To simplify the control of myoelectric prosthetic hands and reduce the cognitive burden for the user, two different strategies are adopted in research. On the one hand, interpretation and quality of EMG signals are improved by enlarging the number of sensing electrodes and distinguishing different control commands

by multi-electrode decomposition. On the other hand, semi-autonomous control strategies enhance the user control with environmental sensor information to provide autonomous grasp functionalities. Semi-autonomous grasp control thereby reduces the general dependency on EMG control signals. It is therefore especially interesting for users that have difficulties in producing reliable muscle signals due to bad stump conditions.

Multi-electrode decomposition for prosthesis control is performed since a long time, for example in (Light et al., 2002). As shown in (Dalley et al., 2011) and (Fougner et al., 2012), it is able to distinguish between different grasp postures or motions. Recently, advances have been achieved in the repeatability of recognition algorithms, as shown in (Palermo et al., 2017). Further, other sensor modalities can be taken into account in multi-signal decomposition, e. g. IMU orientation data used in (Kyranou et al., 2016) and (Piazza et al., 2016) or *mechanomyography* (MMG) used in (Wilson and Vaidyanathan, 2017). Further methods in the field of pattern recognition and multi-electrode decomposition were presented e. g. in (Ortiz-Catalan et al., 2014), (Hahne et al., 2014), (Zhuang et al., 2019), (George et al., 2020), (Piazza et al., 2020) and (Paskett et al., 2021). A comprehensive overview of methods for multi-electrode decomposition is provided in (Segil et al., 2014) and (Ciancio et al., 2016).

Swain and Nightingale first presented a control for a prosthetic hand in (Swain and Nightingale, 1980), that was not only based on direct user input but provided different functionality based on the state of the prosthesis. This semi-autonomous grasping later emerged to allow sophisticated prosthesis control with a very limited number of user inputs. The partially autonomous hand control is defined based on environmental sensor information. At the same time, grasp control is kept under the supervision of the user. (Bennett et al., 2018) presents an autonomous wrist rotation combined with a manual grasp control. The wrist rotation is based on the forearm orientation measured by an IMU. A similar approach in (Volkmar et al., 2019) provides a semi-autonomous adaptation of the wrist orientation based on the orientation of the second able hand. This allows the coordinated interaction of both hands in bimanual tasks. (Gardner et al., 2015) performs a semi-autonomous selection of different grasp types based on object images from a camera and IMU information. The user input is given with MMG sensors. Objects are classified according to their shape and one of four different grasp types is chosen and suggested to the user. For the task of identifying objects and suggesting appropriate grasp types, several groups have presented neural networks for visual scene understanding, e. g. in (Ghazaei et al., 2015), (Degol et al., 2016) and (Ghazaei et al., 2017).

A sequential grasp control with autonomous grasp type and size suggestion is presented in (Došen et al., 2010) and (Došen and Popović, 2011). A camera and a distance sensor are placed on the back of the hand to estimate the shape and size of the object. Based on this object information, a grasp type and hand aperture are suggested to the user and can be accepted or adjusted manually. The semi-autonomous control is based on a state machine that sequentially defines the different grasp characteristics. This work has been continued in (Nobre Castro and Došen, 2022) using an RGBD camera mounted on the back of a prosthetic hand. Using the depth images processed on an external computer, the orientation, grasp type and hand aperture of the prosthetic hand are controlled autonomously. The user takes over control for the grasp closing motion, which is performed manually via a conventional EMG control. (Markovic et al., 2014) and (Markovic et al., 2015) rely on a stereo camera system and an IMU to infer information on the scene and the prosthesis' state for semi-autonomous grasp control. The user wears AR-glasses including the camera system, which are not only used to record the object, but also return information on the suggested grasp to the user. The presented semi-autonomous control includes the wrist orientation, grasp type and hand aperture. Based on the object's shape and the current hand orientation, a grasp configuration is suggested to the user and can be adjusted manually. In continuation (Mouchoux et al., 2021) provides an autonomous control of hand orientation, grasp type and grasp aperture. Unlike the previous approaches, all grasp characteristics are controlled simultaneously and are continually updated based on environmental information. Such information is gathered by a multimodal sensor setup including an IMU and an RGBD camera mounted on AR glasses worn by the subject. An infrared sensor included in the camera allows to track the prosthesis, which is equipped with retroreflective markers. A myoelectric control based on eight EMG electrodes allows the user to take over full control at any stage of the grasping process.

An autonomous control for grasp force and hand positioning is developed in (Cipriani et al., 2008). (Hansen et al., 2021) combines an autonomous grasp force control based on proximity and pressure sensing with a multi-electrode decomposition approach for hand preshaping and closing. A method to control a hand prosthesis only based on arm motions and without any need for EMG sensing is presented in (Gonzalez-Vargas et al., 2015). An electrocutaneous menu continuously offers different grasp suggestions, which can be chosen and executed by performing arm motions. Furthermore a range of input modalities for user control was tested including electrooculography presented in (Hao et al., 2013),

tongue control presented in (Buckley et al., 2011) and speech presented in (Jafarzadeh and Tadesse, 2019).

Overall, it has been widely shown that semi-autonomous grasp control is beneficial for prosthesis users by reducing the cognitive burden of the user and increasing the grasp speed and success. However, existing systems rely on external sensors mounted in the room or on the user. Sensor processing and control is also performed on external computing resources connected to the prosthetic hand. This allows for sophisticated processing strategies and capable control systems that are helpful to validate the general merit of semi-autonomous control strategies. However, the local and static setup limits the mobility of such systems. Further, existing control systems provide static grasp preshapes and a wrist orientation preceding the final grasp. Throughout the final grasping motion the fingers are closed in this fixed configuration. There are several approaches for simultaneous coordinated grasp control including all available degrees of freedom in the remote control of robotic arms, e. g. in (McMullen et al., 2014), (Zhuang et al., 2019) and (Shafti et al., 2019). However, such continuous coordinated control has not yet been applied to prosthetic hands. This discards the potential of coordinated finger motions and a simultaneous, correlated hand and finger motion including wrist rotation.

Therefore, this thesis develops a semi-autonomous control scheme that simultaneously drives all degrees of freedom of the prosthetic hand. It is the first semi-autonomous control based on grasping motions learned from human demonstration. The control scheme is applied on the KIT Prosthetic Hand described in (Weiner, Starke, Rader et al., 2022) and is evaluated in a use study with able-bodied subjects.

CHAPTER 3

Postural and Kinematic Synergies

To grasp objects safely with a humanoid robotic hand, all the degrees of freedom of the five fingers need to be coordinated in order to achieve a stable grasping posture. This requires the synchronization of up to 23 individual joints to accurately mimic the human hand kinematics (Sancho-Bru et al., 2003). Moreover, not only the final grasping posture is important for a successful grasp. The coordinated finger motion starting from the hand's resting configuration is vital for grasp success. The finger motion defines the position and order of contacts made between the hand and the object. A well-designed grasp motion needs to avoid undesired object movement and can even include purposeful object re-positioning to improve grasping.

The existence of synergies between the individual joint angles of the human hand is well established in grasping, manipulation and hand gestures, as presented in Chapter 2. Primarily linear postural synergies identified by a principal component analysis are described not only for the human hand (Santello et al., 1998), (Jarque-Bou et al., 2020) but also for a wide range of robotic hands and grippers (Ciocarlie et al., 2007b), (Wimböck et al., 2012). These postural synergies allow to simplify the grasp synthesis for complex humanoid hands by reducing the dimensionality of the hand's parameter space. Thereby, new grasps can be sampled from the low-dimensional space of postural synergies, which decreases computation complexity and leaves unnatural hand configurations and configurations unsuitable for grasping aside from the beginning.

However, for grasp control of a humanoid hand, a formal description is needed that covers not only the stable grasp posture, but also any hand motion required to achieve the final grasp. A hand synergy representation able to characterize the finger joint trajectories of entire grasping motions can be provided by a set of kinematic synergies. In addition to the general challenges of postural synergies, these require an association of time with the synergy representation. Ideally, timing should be considered in posture sampling to take advantage of the additional information on grasp progress and continuity.

Finally, a robotic hand must be able to cope with very different object shapes, weights and grasping tasks. Given a limited number of human grasping demonstrations, the hand control needs to be adapted to different situations and requirements. Therefore, a grasp synergy representation needs to be general and allow for the generation of synthetic, human-like grasps. This implies that the synergy space is well structured with respect to relevant grasp characteristics and thereby permits purposeful sampling of specific grasps. The generated grasps ought to be represented in a way that allows adaptation to changing environmental conditions like different object position or size.

In this chapter, a general grasp synergy representation for robotic hand control is presented. Adaptable postural synergies are described first, allowing the intuitive generation of human-like grasp postures. Based on this static postural synergies, kinematic synergies are described in a static synergy space. In addition, the arm trajectories complementing finger motions in grasping are considered. Finally, grasp synergy primitives are introduced as an adaptable representation of kinematic grasp synergies.

3.1 Postural Synergies

Postural synergies provide a low-dimensional representation of static grasp postures. They are derived based on an extensive study of human hand postures in different grasp types. A non-linear learning approach applying an autoencoder network is proposed to capture the synergies inherent in the human grasping data. Additionally, the approach allows structuring of the synergy space in an intuitive manner regarding the grasp type and object diameter. The resulting adaptable postural synergies are used to generate new, human-like grasps for robotic hands. They are evaluated on the human hand in simulation and are later applied to a hand prosthesis.

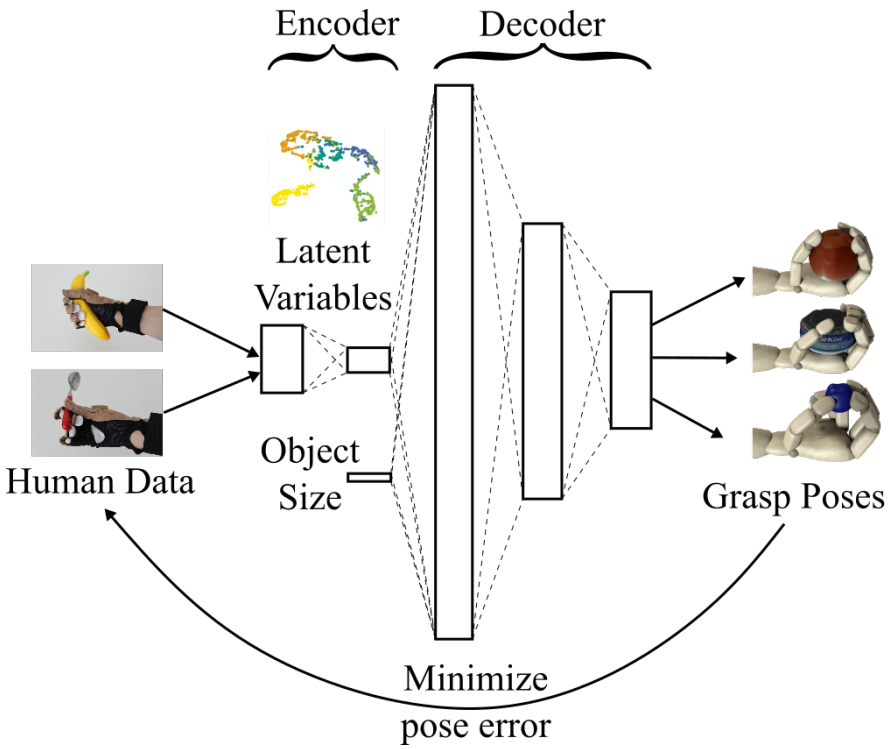

Figure 3.1: Architecture of the autoencoder to describe postural grasp synergies; the latent synergy space is complemented by the object size (Starke et al., 2020) ©2020 World Scientific Publishing

The work described in this section was presented in a conference and a journal publication (Starke et al., 2018, 2020). Graphs and images in this section are partially adapted from these publications.

3.1.1 Adaptable Synergy Description

Postural grasp synergies do not provide any distinction regarding grasp characteristics like the grasp type, as was shown in (Santello et al., 1998). In their work, the authors apply a linear PCA on the joint angles of human grasping postures to derive low-dimensional grasp representations. This limits the resulting synergy space to the representation of linear correlations between joint angles for a grasping posture. To address this limitation and account for non-linear correlations in joint angles, this thesis proposes a deep autoencoder network, that is trained with human grasping data. The human grasp posture is described by a vector of 16 dimensions denoting 16 joint angles of the human hand. The network learns a postural synergy space while taking into account meaningful grasp characteristics within the shape of the latent synergy space.

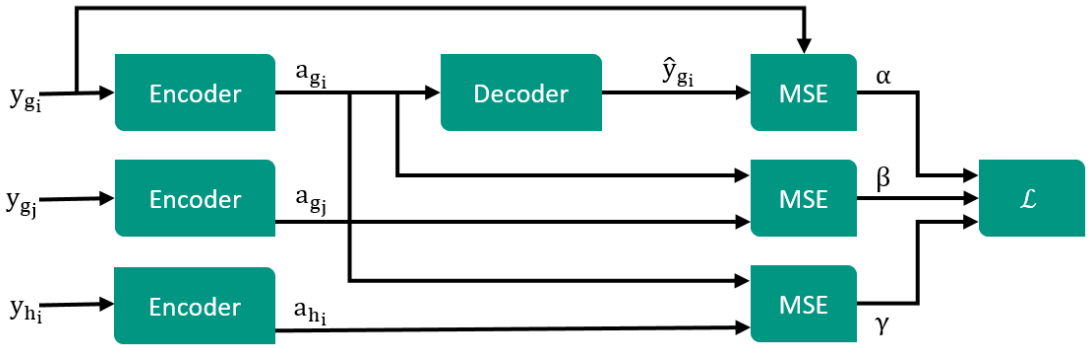

Figure 3.2: Loss function of the autoencoder for postural grasp synergies; the threefold execution of the encoder enhances clustering of grasp types in latent synergy space while preserving the replicability of grasps by the encoder (Starke et al., 2020) ©2020 World Scientific Publishing

The **network structure** is depicted in Fig. 3.1. The encoder has a classical triangular shape. Within two layers, the encoder reduces the input vector of 16 joint angles of the human grasping posture to three synergies. The diameter of the object is fed into the decoder as a scalar fourth input parameter in addition to the three synergy variables. The object diameter is normalized according to the size of the hand. To ensure a continuous synergy representation, a normally distributed noise is added to the latent variables before they are fed into the decoder. A reversed triangular structure is used for the decoder to allow the processing of the synergies, that are applied with the noise. All internal layers apply a hyperbolic tangent activation function. The output layer is used with a linear activation function.

To enhance the structure of the latent synergy space, a **threefold loss function** is applied, as shown in Fig. 3.2. The loss function consists of the following terms:

1. The first row shows the mean squared error between a real grasp posture $\mathbf{y}_{g_i}$ of the grasp type g and the corresponding decoded grasp posture $\widehat{\mathbf{y}}_{g_i}$, which is returned by the autoencoder. This classical reconstruction loss contributes with a weight of $\alpha = 1.0$ to the overall loss function.

2. In addition, the mean squared distance is calculated between two synergy representations $\mathbf{a}_{g_i}$ and $\mathbf{a}_{g_j}$, which correspond to the human grasp postures $\mathbf{y}_{g_i}$ and $\mathbf{y}_{g_j}$. g_i and g_j denote different demonstrations of the same grasp type g. This loss describes the distance between two grasps of the same grasp type in latent space and thereby enhances clustering of simi-

lar grasps. A weight of $\beta = 0.5$ is applied to keep the focus on the quality of the overall grasp representation.

3. To promote the separation of distinct grasps, a third loss term considers the mean squared distance between two synergy representations $\mathbf{a}_{g_i}$ and $\mathbf{a}_{h_i}$. g and h denote different grasp types. This distance between grasps of different grasp types in the synergy space is included in the loss function with a negative weighting of $\gamma = -0.15$. Thereby the clustering of grasp types in the synergy space is further enhanced.

As shown on the left of Fig. 3.2, the encoder is thus executed three times in parallel with the input postures $\mathbf{y}_{g_i}$, $\mathbf{y}_{g_j}$ and $\mathbf{y}_{h_i}$.

The autoencoder network is trained on 2250 human grasp postures described by 16 joint angles within the hand using an Adam optimizer. Hence, an input vector of 16 joint angles is fed into the encoder of the network. The grasping data is split into a training and test set by a proportion of $90\,\%$ to $10\,\%$. Since the amount of available data is quite large in terms of human grasping analyses, but small in terms of machine learning datasets, a large proportion of the grasp demonstrations is required for training. 10-fold cross validation is used to obviate the need for a separate validation set and the noise applied to the latent synergy space prevents over-fitting of learned grasps.

3.1.2 Static Grasp Posture Analysis

To learn the expressive postural grasp synergies, a static grasping study was performed comprising 2250 grasps from 15 subjects on 35 objects. The nine male and six female subjects aged $27.0\,\text{years} \pm 2.0\,\text{years}$ hand an average hand length from the wrist to the tip of the middle finger of $180.2\,\text{mm} \pm 16.9\,\text{mm}$. They were wearing a data glove (CyberGlove III, CyberGlove Systems) measuring 16 joint angles of the hand. The measured joint angles and their annotation are shown in Fig. 3.3. All subjects performed the grasping study with their dominant hand.

The study concentrates on five grasp types, each corresponding to one or two classes from the grasp taxonomy in (Cutkosky, 1989). These grasp types are namely *cylindrical* (1, 2), *spherical* (11, 13), *disk* (10, 12), *pinch* (8, 9) and *lateral* (16) grasps, with the numbers in brackets denoting the corresponding grasp classes according to Cutkosky's taxonomy. Comparing analyses of grasp type frequency in literature, these five grasp types are invariably within the eight most frequent postures for grasping according to (Bullock et al., 2013a) and

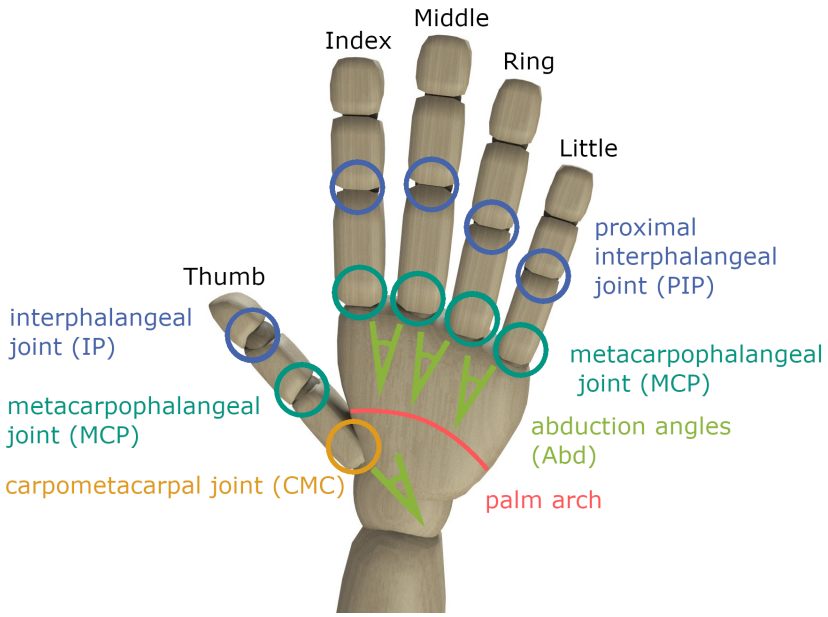

Figure 3.3: Annotation of the 16 joint angles measured in the static grasping study (Starke et al., 2020) ©2020 World Scientific Publishing

(Vergara et al., 2014). Exemplary grasps within each grasp type are depicted in Fig. 3.4.

The data glove for **joint angle measurement** was calibrated based on reference measurements of fixed joint angles achieved with wooden reference blocks. Joint angles were then calculated by linear interpolation between at least two reference measurements taken for each joint. In addition, a closed-chain motion was recorded with the tips of thumb and index finger pressed together. This calibration procedure was adapted from (Gracia-Ibáñez et al., 2017) according to the requirements and timeframe of the static grasping study.

During the **study procedure**, subjects were seated comfortably in front of a table. They were shown images from the taxonomy in (Cutkosky, 1989) depicting the classes included in the required grasp type. Then subjects were asked to perform the presented grasp on a single object three times. The same grasp was repeated on ten different objects placed one after the other on the table in front of the subject. The objects were chosen from a household and workshop environment and are a subset of the YCB Object Set (Calli et al., 2015) and the KIT Object Database (Kasper et al., 2012). The objects are shown in Fig. 3.5.

An **analysis of the joint angle data** from these static grasp recordings directly shows a correlation between the diameter of the grasped object and the finger flexion angles. As to be expected, the finger joint angles decrease with increas-

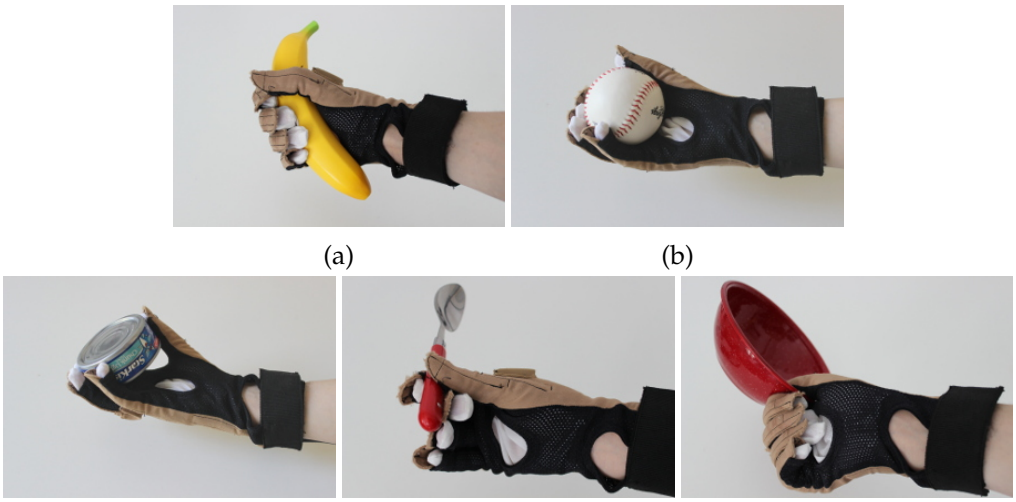

(a) (b) (c) (d) (e)

Figure 3.4: Grasp types applied in the static grasping study: cylindrical (a), spherical (b), disk (c), pinch (d) and lateral (e) grasps (Starke et al., 2020) ©2020 World Scientific Publishing

Figure 3.5: Objects used in the static grasping study

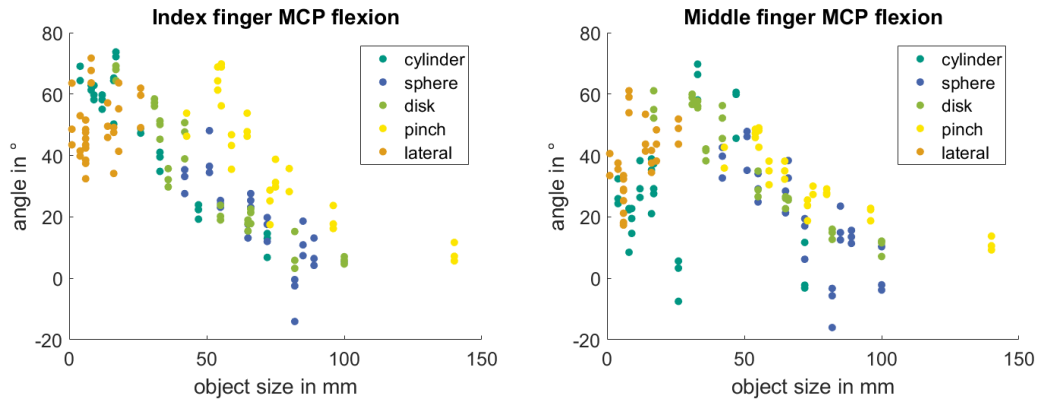

(a) (b)

Figure 3.6: Finger joint angles in relation to the object diameter for the metacarpophalangeal joints of index and middle finger (Starke et al., 2020) ©2020 World Scientific Publishing

ing objects size, as can be seen in Fig. 3.6. However, the hand size also influences the finger joint configuration for a given object size. Therefore, the grasping data was normalized according to the subject's hand length. The latent postural synergy space was then derived by training the synergy autoencoder with these human grasp postures.

3.1.3 Generation of Human-Like Grasps

The learned postural synergies can be used to represent demonstrated human grasp postures in a low-dimensional space by applying the encoder on the original joint angles. Besides, the decoder can also be applied to generate new, unseen grasp postures that are similar to the learned demonstrations and hence similar to human grasps. The desired grasp type and object size can be controlled separately in generation. Since the object diameter was fed to the decoder as a fourth, independent parameter, the object can be controlled directly with this input parameter. Since grasp types are clustered in the synergy space, the posture of a generated grasp can be deliberately influenced by targeted sampling from the latent synergy space. The center and expanse of each cluster mark the sampling area of the corresponding grasp type.

Grasp generation is done by sampling from the area populated by the respective grasp type in synergy space with the object diameter normalized to the length of the human hand model of the Master Motor Map (Mandery et al., 2016) scaled to a person of $1.70\,\mathrm{m}$ height. The grasps are applied in simulation

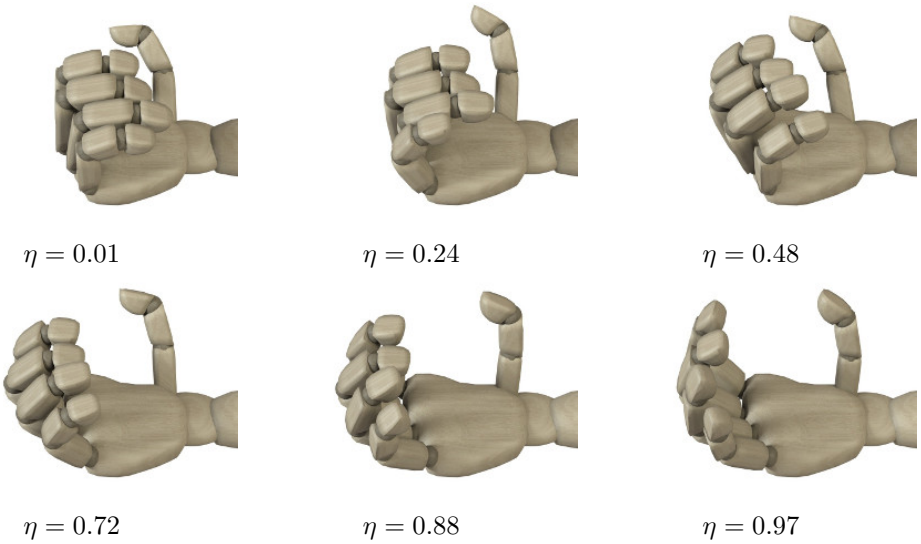

Figure 3.7: Cylinder grasps generated for different object diameters; the size parameter η describes the object diameter normalized with respect to the hand length (Starke et al., 2018) ©2018 IEEE

as soft synergies according to (Bicchi et al., 2011) to guarantee contact between the fingers and the object. The same, synergy-generated cylinder grasp for different object diameters can be seen in Fig. 3.7. Generated grasps for all five grasp types simulated on different objects are shown in Fig. 3.8. The shown objects were also used in the human demonstrations.

3.1.4 Evaluation

The approach is evaluated regarding 1) reproduction error, 2) clustering of grasp types and 3) generalization for the generation of unseen, human-like grasp postures. The linear postural synergies defined by a PCA with two synergy variables in (Santello et al., 1998) are considered as the baseline for comparison.

First and foremost the **reproduction error** of three variations of the presented autoencoder is considered. To allow a fair comparison with the results from Santello et al., an autoencoder with two latent synergy variables is trained with the structure and loss described in the previous section. Further, an autoencoder with two latent synergy variables and an additional decoder input for the object size is considered. And finally, the presented autoencoder with three latent synergy variables and the object size as fourth decoder input is included in the evaluation. The reproduction error for all grasp types is shown in Fig. 3.9.

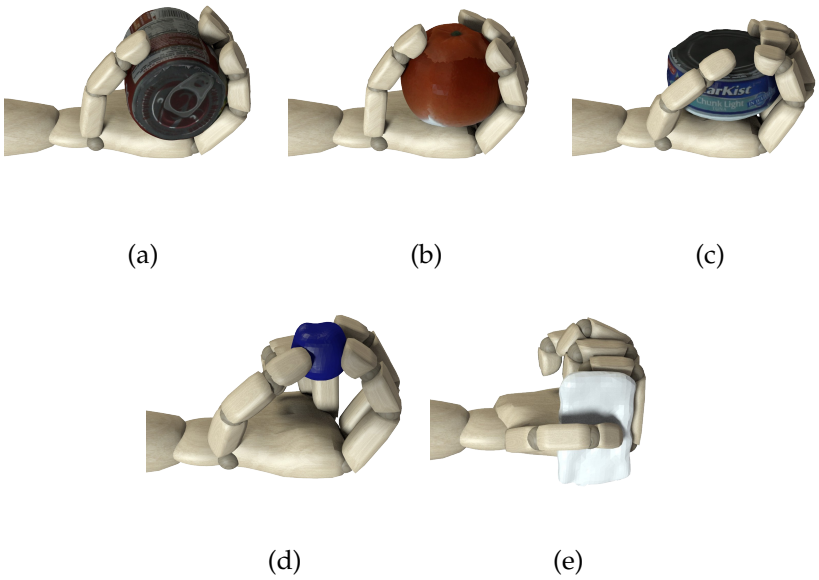

(a) (b) (c)

(d) (e)

Figure 3.8: Grasps generated from the postural synergy space with the decoder and executed in simulation; cylinder grasp on a tomato soup can (a), spherical grasp on an orange (b), disk grasp on a tuna can (c), tripod grasp on a toy block (d) and lateral grasp on a credit card (e) (Starke et al., 2020) ©2020 World Scientific Publishing

The two-dimensional autoencoder clearly outperforms the PCA-derived synergies in terms of reproduction accuracy. An additional boost of the synergy accuracy is achieved by adding the normalized object size as an additional parameter to the decoder. This allows the encoder to shift attention to the hand shape and focus less on the grasp aperture defined by the object. The reproduction error is thereby reduced by $26\,\%$ compared to the basic reference autoencoder. Enlarging the latent synergy space to three dimensions yields a relatively small improvement in reproduction error. However, this additional synergy variable facilitates the secondary goal of clustering grasp types in the synergy space, since it provides more flexibility for grasp representation and reorganization in the latent space. Because of the merit of a descriptive, structured synergy space in generation of novel grasp postures, this enlarged synergy space is applied in this work at the cost of a third synergy variable.

The resulting **structured synergy space** is depicted in Fig. 3.10 (a). For visualization purposes the three-dimensional synergy space is reduced to two dimensions by t-distributed stochastic neighbor embedding (t-SNE). The clustering of different grasp types can be clearly seen and Fig. 3.10 (b) shows a clear distance in mean synergy value between grasp types in three dimensions. The pinch

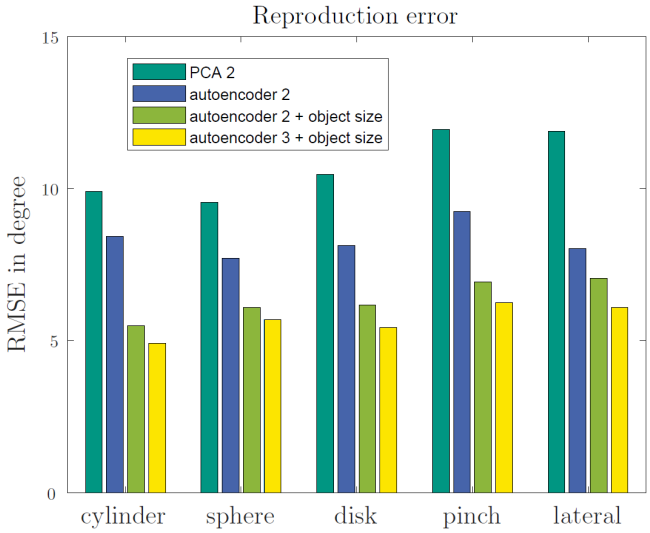

Figure 3.9: Reproduction error of three variations of the autoencoder synergies compared to the baseline approach using PCA (Starke et al., 2020) ©2020 World Scientific Publishing

grasp shows a significant cluster separation. The distance between the means of the pinch and the closest other cluster, being cylinder grasps, is $50\,\%$ of the size of the synergy space. The two cluster means of sphere and disk grasps are significantly closer with a distance of $25\,\%$ of the synergy space size. These two grasp types only differ in the adduction of fingers and therefore, both grasp types transition fluently in synergy space. This shows that the synergy space is able to descriptively represent different human grasp postures in a way that allows to interpret and control the grasp type directly using the synergy representation.

To assess the **generalization** of the postural synergy representation, human-like grasps generated from the decoder are evaluated. Grasps on 24 objects are generated and executed in simulation with the human hand models of the Master Motor Map (Mandery et al., 2016) as described in the previous section. The evaluation includes objects used in the human grasp demonstrations as well as objects unknown to the synergy network. Grasps are generated by the decoder by sampling from within one standard deviation around the cluster mean of the desired grasp type. Additionally, the normalized object diameter is provided to the decoder. The generated grasp is applied as a soft synergy according to (Bicchi et al., 2011), thereby allowing the hand to adapt to the complex, non-smooth surface of the object. Grasp are simulated in the grasp simulator Simox (Vahrenkamp et al., 2010). The grasp quality is evaluated with the ϵ-metric (Ferrari and Canny, 1992). To assess the robustness and stability of a grasp posture,

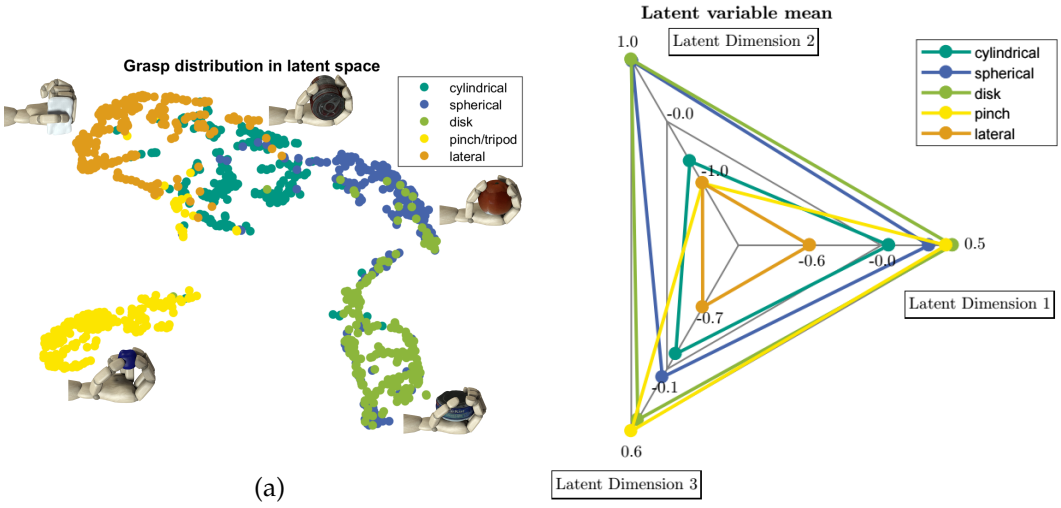

(a) (b)

Figure 3.10: Clustering of grasp types in synergy space; a two-dimensional representation of the synergy space generated by t-SNE (a) and the mean representation of each grasp type cluster in all three synergy dimensions (b) (Starke et al., 2018, 2020) ©2018 IEEE

the mean ϵ-metric is calculated over 50 hand poses with a deviation of $\pm 10\,\mathrm{mm}$ and $\pm 10^{\circ}$ (Weisz and Allen, 2012).

Due to the stiff palm of the human hand model, contact points between the object and the palm cannot be considered appropriately in the given simulation. Therefore, the grasp quality of lateral grasps cannot be adequately assessed. The grasp quality evaluation is hence restricted to the four grasp types cylinder, sphere, disk and pinch/tripod. Fig. 3.11b shows the mean ϵ quality for these four grasp types. It can be seen that all power grasp types achieve a grasp quality in the range of 0.3 to 0.5. However, the pinch/tripod grasps show a significantly lower grasp quality of 0.05 to 0.2. These precision grasps rely on only two or three contact points, which makes them far more sensitive to perturbations in the object pose. The wide range of perturbations applied to calculate the mean ϵ-metric therefore significantly reduces the overall quality for these precision grasps. A comparison of cylinder grasps is shown in Fig. 3.11a on known objects included in the human demonstrations and similar objects the autoencoder was not trained on. There is no significant difference observed in the grasp quality on similar objects compared to the ones included in the training examples. Instead, the object size impacts the overall grasp quality with larger objects like a soup can or a coffee can yielding better results than thin objects like a spoon or a banana. Altogether all generated grasps yield an ade-

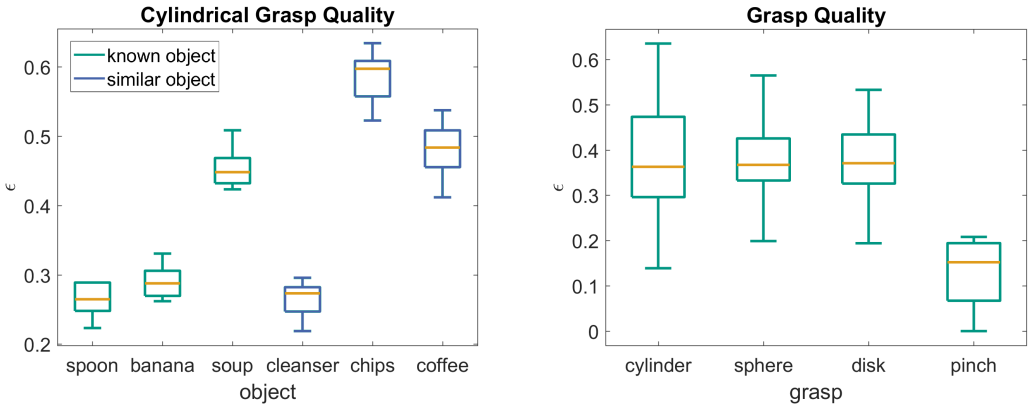

(a) (b)

Figure 3.11: ϵ-metric of grasps generated from the postural synergies; cylinder grasp quality of objects known from the training examples and unseen similar objects (a) and grasp quality on different grasp types with known objects (b) (Starke et al., 2020) ©2020 World Scientific Publishing

quate grasp quality, thereby proving the capability of the decoder to generate feasible grasp postures.

3.2 Kinematic Synergies

To achieve a desired grasp posture, the alignment of finger closure is important. The timing of the closing trajectories of individual finger joints determines the coordination of fingers throughout the grasp execution. This finger coordination can severely influence grasp success. Ideally, a good coordination ensures that fingers simultaneously wrap around the object to grasp it. A sub-optimal coordination however, might cause the object to be pushed out of the hand, if antagonistic fingers are not closed simultaneously. For small or thin objects, even more complex finger movements are needed to pick an object up from a table surface and push it into the hand. Therefore, a grasp representation should also consider the finger joint angle trajectories during the entire grasping process. In addition, the reaching motion of the arm also complements the grasping action. While it is affected mostly by the global hand and object positions, the timing of reaching and grasping overlap and a reorientation of the hand pose can be used as a means of adjusting a grasp posture throughout its formation.

Due to the importance of both finger and arm movement throughout the grasping process, this thesis analyzes both characteristics in human grasp demon-

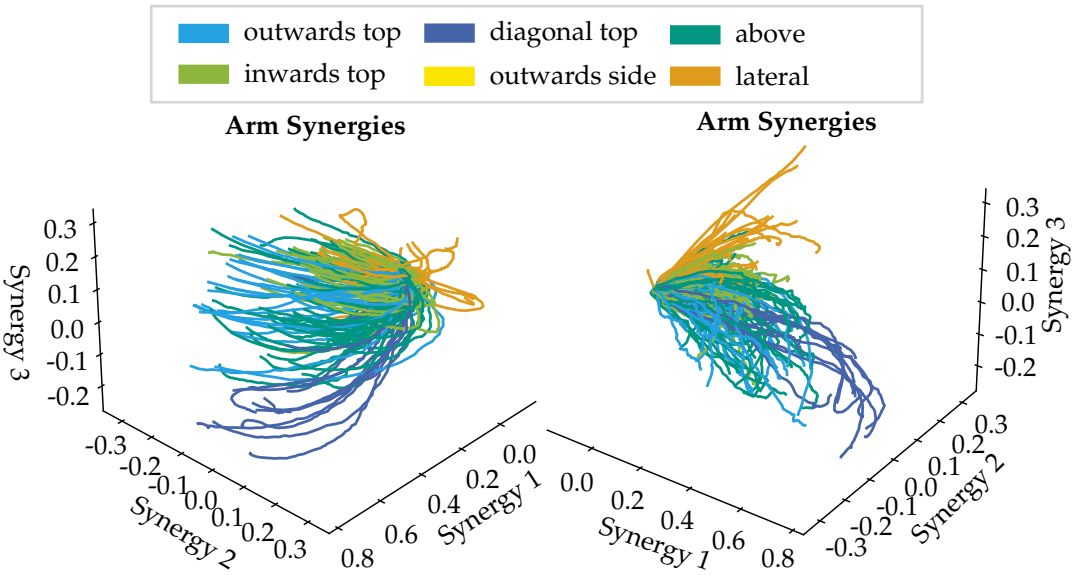

Figure 3.12: Approach trajectories in the arm synergy space shown from two different angles; grasps with different approach directions are clearly structured with a smooth transition

strations. Correlations of the hand pose trajectory resulting from the arm's reaching motion are analyzed with respect to different grasp characteristics. Finally, kinematic synergies inspired by Romero et al. are explained (Romero et al., 2013), which lay the basis for the adaptable synergy primitives presented in this work.

3.2.1 Arm Trajectories in Grasping

An analysis of the human arm motion is performed based on the absolute position and orientation of the hand. The hand pose in space is described by a three-dimensional Cartesian position and a quaternion rotation. From these seven dimensions, a lower-dimensional synergy space is derived by a PCA. Both Cartesian positions as well as rotation quaternions are normalized separately to the range of positions and orientations observed in the kinematic grasping study. The synergy space is calculated over all individual hand poses disregarding the time dimension. While two synergy dimensions already account for $81.6\,\%$ of the overall variance of the static hand pose data, a third synergy further improves the structure of the synergy space. Arm synergy trajectories are represented by a series of static arm synergy configurations over time, as shown in Fig. 3.12.

The arm synergies are analyzed regarding the **representation of meaningful grasp characteristics**. Both the arm trajectories as well as their synergy representation do not differ significantly for varying grasp types. This is to be expected, since the categorization of grasp types in grasp taxonomies like (Cutkosky, 1989), (Kamakura et al., 1980) or (Feix et al., 2016) is focused on the hand shape and finger placement. Instead, the arm synergy space shows a structuring of arm trajectories with respect to the approach direction of the grasp. As visible in Fig. 3.12, the synergy trajectories of different approach directions unfold into dissimilar directions of the arm synergy space. The final hand poses in the grasps thereby form a continuous spectrum evolving from grasp motions approaching from above with the elbow rotated outwards to a sideways approach motion grasping the object from the back. Similar to the approach directions, also their synergy representations vary continuously. The transition from a top to a side approach direction is most clearly marked and can be seen by a less populated gap between the top grasps in blue and green as well as the side grasps in orange and yellow in Fig. 3.12.

3.2.2 Kinematic Grasp Synergies

Throughout grasping the trajectories of individual finger joints as well as the timing of joint closure need to be considered. We consider 22 joints $j_1, j_2, ..., j_{22}$ within the human hand according to the MMM hand model (Mandery et al., 2016). This results in a 22-dimensional vector of joint angles $\mathbf{j}_g = (j_1, j_2, ..., j_{22})$ for a grasp g. The grasping motion is therefore described by a joint trajectory $\mathbf{j}_g(t)$ with $t \in [0, T]$. Hence $\mathbf{j}_g(t = 0)$ denotes the relaxed hand posture and $\mathbf{j}_g(t = T)$ denotes the posture of the final stable grasp. Applying the methodology proposed by Romero et al. a set of kinematic synergies is calculated from these joint trajectories (Romero et al., 2013). A PCA is trained on all joint configurations $\mathbf{j}_{g,t}$ from the kinematic grasp recordings regardless of grasp progress and time $t \in [0, T]$. This results in a static postural synergy space $\mathcal{S}$ learned from hand postures throughout all stages of the grasping motion.

By again including the time information, the hand trajectory in grasping can be described as a **kinematic synergy trajectory** in synergy space. This means that a postural synergy configuration $\mathbf{s}_{g,t}$ is calculated for every joint posture $\mathbf{j}_{g,t}$ by performing the transformation into the synergy space $\mathcal{S}$. A grasp trajectory in synergy space is defined as a timed series of postural synergy configurations with $\mathbf{s}_g(t) = (\mathbf{s}_{g,0}, \mathbf{s}_{g,1}, ..., \mathbf{s}_{g,T})$. Six synergies are needed to represent $80\,\%$ of the variance within the 22 joint angles of the human hand posture, hence $\mathcal{S} \subset \mathbb{R}^6$.

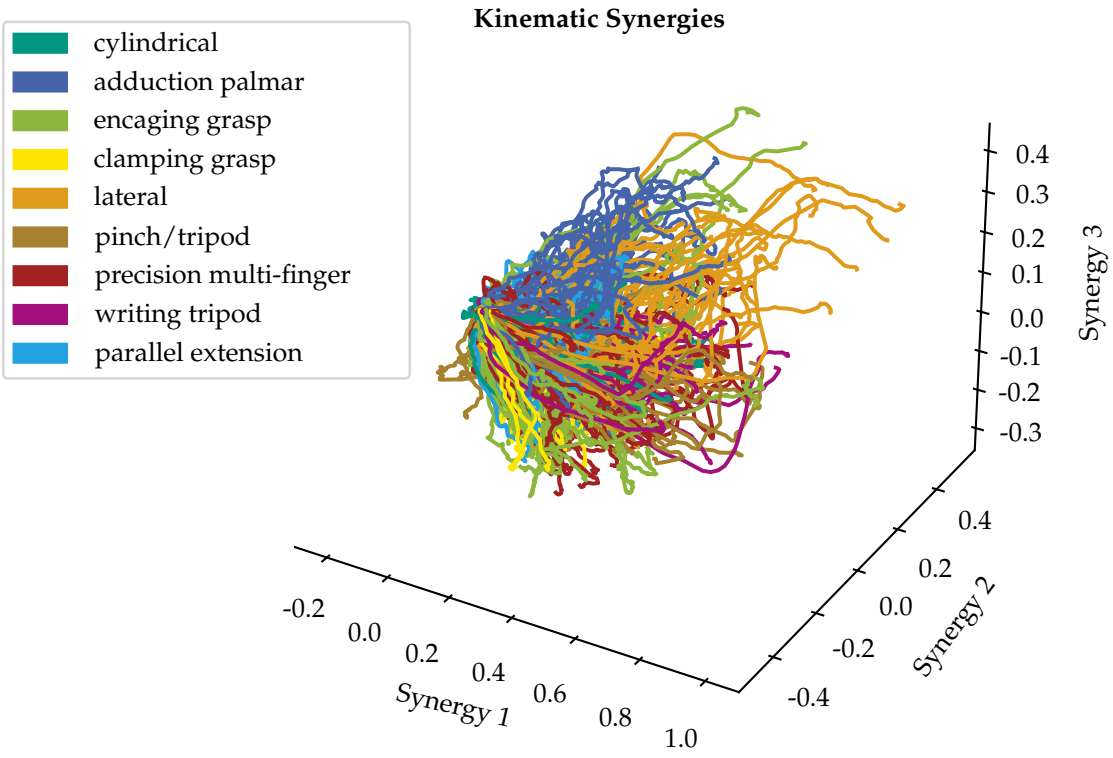

Figure 3.13: Kinematic grasp synergies described in a static synergy space and marked according to grouped grasp types

Table 3.1: Grasp categories subsuming several grasp types with similar grasp characteristics from the GRASP taxonomy

category	grasp types (Feix et al., 2016)
cylindrical	*large diameter, small diameter, medium wrap, power disk, power sphere*
adduction palmar	*index finger extension, adducted thumb, light tool, fixed hook, palmar*
encaging grasp	*ring, sphere 3 finger, extension type, sphere 4 finger, distal type*
clamping grasp	*adduction grip, tripod variation*
lateral	*lateral, stick, ventral, lateral tripod*
pinch/tripod	*palmar pinch, tip pinch, inferior pincer, prismatic 2 finger, tripod*
precision multi-finger	*prismatic 3 finger, quadpod, prismatic 4 finger, precision disk, precision sphere*
writing tripod	*writing tripod*
parallel extension	*parallel extension*

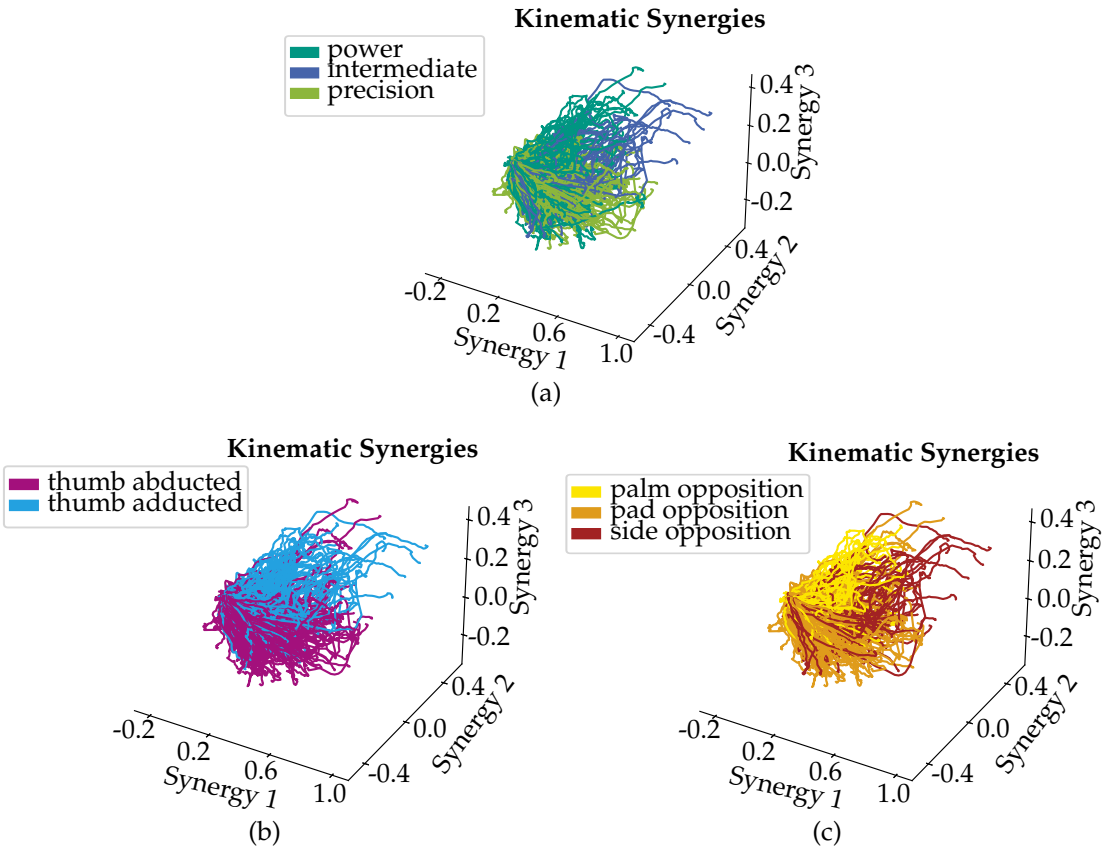

Figure 3.14: Structure of the kinematic synergy space based on the fundamental grasp categories power, precision and intermediate grasps (a), the position of the thumb (b) and the grasp opposition type (c)

Fig. 3.13 shows human grasp trajectories of different grasp types in the first three dimensions of the kinematic synergy space. For visualization purposes, related grasp types from the GRASP taxonomy (Feix et al., 2016) are clustered according to the categories listed in Table 3.1. While lateral grasps and adduction palmar grasps are localized in a confined subspace of the static synergy space, there is no strict clustering of grasp types. However, Fig. 3.14 shows that the structure of the static synergy space is defined mostly by thumb circumvention and the grasp's opposition type. The latter distinguishes between pad opposition with opposing fingers, palm opposition with the palm opposing one or several fingers and side opposition with at least one finger opposing a plane perpendicular to the palm (Iberall, 1997).

Additionally, a combination of both arm and hand movement into the same **hand-arm synergy space** is investigated. A parameter set is compiled from the seven-dimensional pose of the hand, comprised of the position and the quaternion rotation, and the 22 DoF of the finger joints. Global hand position and

orientation as well as finger joint angles are normalized according to their corresponding range of motion throughout the entire dataset. The entire grasping process is considered beginning with the start of the arm motion until the final grasp is reached and the finger joints are not moving any more. A static synergy space is then learned similar to the kinematic synergies by a PCA trained on all static arm and hand configurations regardless of grasp progress or grasp type. However, the resulting synergy space focuses almost exclusively on the hand posture and discards most information covering the arm motion. Given the significantly higher dimensionality of the hand posture with 22 DoF compared with the global hand pose with 7 DoF, the synergies are encouraged to focus on the hand posture. A more elaborate method of synergy extraction would therefore be needed to overcome the difference in dimensionality and also the changing focus from arm to finger movement over the course of the grasping progress. The concept of grasp synergies combining hand and arm motion is not further pursued in this thesis.

3.2.3 Human Grasp Trajectories

To study continuous human grasp motions both for the arm and the hand, a study of human grasp kinematics is performed. The human kinematic synergies are then analyzed on these human grasping motions. The study comprises 15 subjects grasping 30 different objects. The three female and twelve male subjects had a hand length of $188\,\mathrm{mm} \pm 15\,\mathrm{mm}$ measured from the wrist to the tip of the middle finger. All grasp types from the GRASP taxonomy (Feix et al., 2016) are demonstrated on at least one object by at least six subjects. Objects are chosen to accommodate the particular grasp type in a way the object might also be used in daily life. In addition, complex object geometries are chosen whenever reasonable. The objects used in the kinematic grasping study are shown in Fig. 3.15.

Throughout the **study procedure**, subjects were standing comfortably in front of a table, that was adjusted to be at waist height. Colored markings on the table indicated the starting pose for both hands and the object. Before each trial, the grasp type was shown to the subjects on a picture using a different object than the one presented in the study. Subjects started with both hands flat on the table, grasped the object with the demonstrated grasp type with their right hand, lifted it and placed it back to the table. Finally, subjects put their right hand back flat to the table. Each combination of grasp type and object was recorded three times per subject resulting in a total of 2736 recorded grasps.

Figure 3.15: Objects used in the kinematic grasping study

A comprising **sensor setup** was used for data recording. The hand and finger motions were recorded with a marker-based motion capture system (VICON Vero, Vicon Motion Systems) as well as a data glove (CyberGlove III, CyberGlove Systems). The data glove was calibrated as described with the grasp posture analysis in subsection 3.1.2. In addition, intermediate poses for each degree of freedom of the thumb base joint were recorded and a linear crossgain was calculated to correct the interference between these joint angles in the measurements. For the marker-based measurement, an additional glove was worn over the data glove with optical markers attached to every finger segment. The marker setup on the hand is shown in Fig. 3.16. Furthermore, the human wrist and lower arm are markered as well, thereby also measuring the hand's pose. The object pose is also tracked. Markers on the objects are positioned to minimize the interference with the fingers during grasping.

Given defined hand and object positions in the kinematic grasping study, the arm movements are analyzed focused on the characteristics of object shape, grasp type and approach direction. The arm trajectories of all subjects on all objects used in the study are normalized with respect to the hand's position in the beginning of the reaching movement. In addition, grasp recordings are normalized with the grasp progress over time. The motion of the arm is considered throughout the entire approach and grasp phases beginning with the hand placed motionless on the table until the fingers have performed the static, stable grasp. The later phases of manipulation involving the lifting and placing of the object are not considered. Kinematic synergies for the arm and the

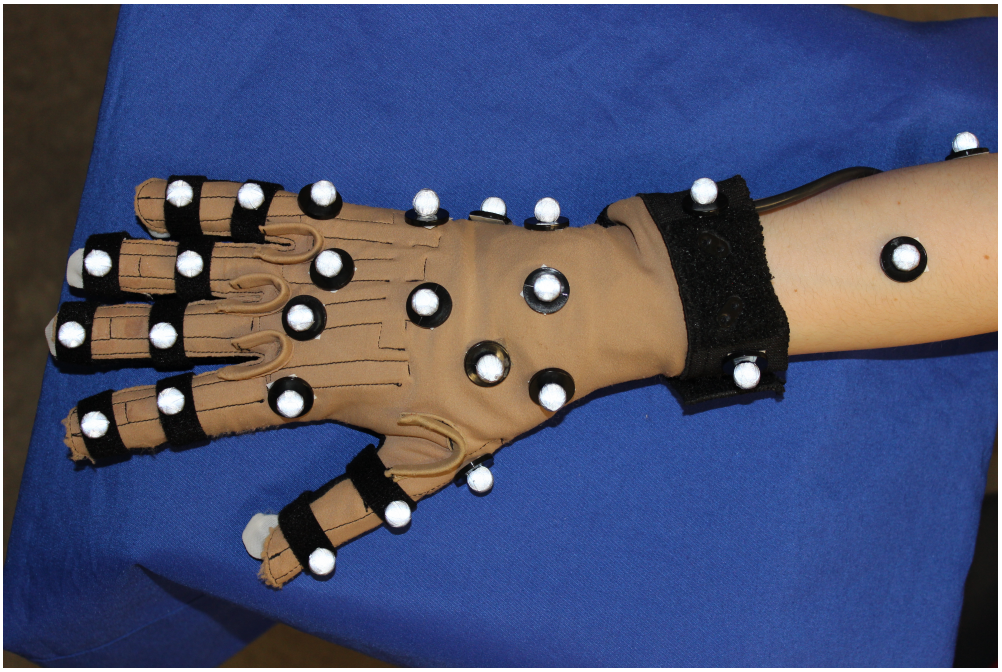

Figure 3.16: Marker configuration on the hand for the marker-based motion capture

hand are derived separately from the human grasp motions of this kinematic grasping study.

3.2.4 Evaluation

The **kinematic arm synergies** are evaluated regarding the variance explained with respect to the original grasping data as well as the grasp reproduction error. Fig. 3.17 (a) shows the explained variance for an increasing number of synergies in the seven-dimensional space of the hand pose. Two synergies are enough to represent more than $80\,\%$ of the overall variance of the hand pose throughout grasping. Four synergies are needed to ensure a representation of over $90\,\%$ of the variance. As explained previously, three synergies are used to enable a better propagation of grasps with different approach directions in synergy space. These three-dimensional synergies have a reproduction error of $2.6\,\%$ of the overall data range. Fig. 3.17 (b) shows that the reproduction of hand orientation is slightly better than for the hand position.

For the **kinematic grasping synergies**, explained variance and grasp reproduction error are depicted in Fig. 3.18 and Fig. 3.19. Six synergies are needed to represent $80\,\%$ of the overall variance and eight synergies account for $90\,\%$ of the variance. With six synergies, the synergy reproduction of kinematic grasp trajectories yields an average error of $1.9\,\%$ of the overall joint angle range. The

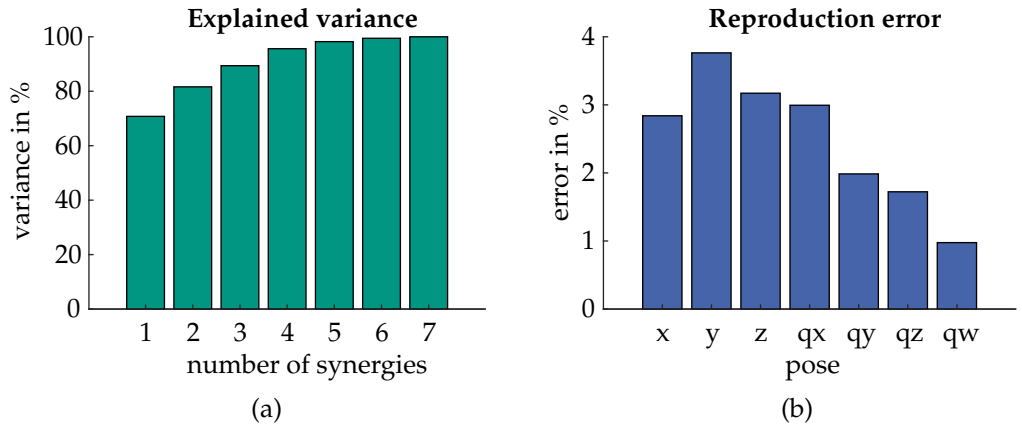

Figure 3.17: Arm synergy characteristics regarding the explained variance for a varying number of synergies (a) and the reproduction error of arm movements for grasping from synergy space (b)

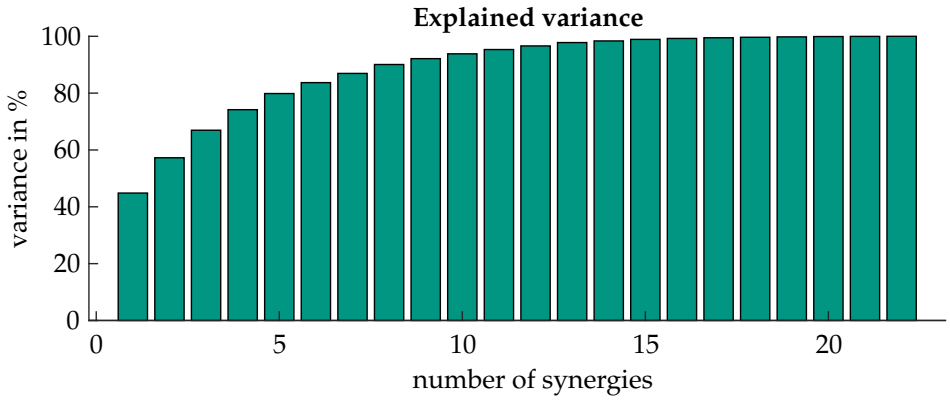

Figure 3.18: Explained variance of the kinematic grasp synergies

reproduction quality is particularly high for the thumb abduction (TAbd) and the carpometacarpal joint of the ring finger (RCMC). The latter has a very low range of motion of $5°$ compared to the other joints. Thereby there is less variation in the RCMC, which causes a palmar arch, and it is simpler to replicate for the synergies. The highest error is observed in the proximal and distal interphalangeal joints of index, middle and little finger, namely IPIP, MDIP, LPIP and LDIP joints. Overall, both arm synergies and kinematic grasp synergies are able to represent the human grasp trajectories of arm and hand with three and six synergy variables respectively. Human grasp trajectories can be reconstructed from both synergy spaces with an error below $4\,\%$ of the overall grasp range. The synergies thereby adequately reflect the human grasping behavior taking into account both the approach direction and the grasp motion.

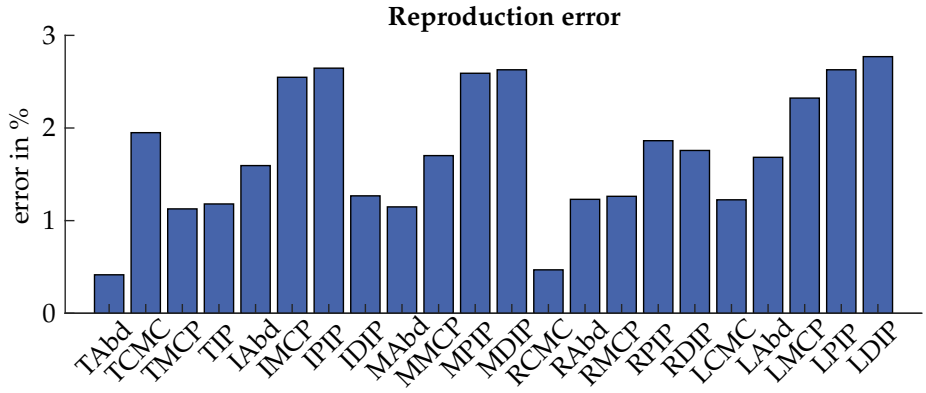

Figure 3.19: Reproduction error of the kinematic grasp synergies for each joint angle of the joints for abduction (Abd), carpometacarpal (CMC), metacarpophalangeal (MCP) and proximal and distal interphalangeal joints (PIP, DIP, IP) and for the five fingers thumb (T), index (I), middle (M), ring (R) and little finger (L)

3.3 Grasp Synergy Primitives

For the application of robotic hand control, grasp synergies do not only need to represent human grasp trajectories, but also need to be adaptable according to varying environmental constraints and different robotic hand kinematics. To this end, it is desirable to separate the inherent human grasping motion from execution-specific details as for example the finger adaptation imposed by the object's shape. Therefore, a library of movement primitives is defined in the kinematic synergy space. These primitives of different human grasping motions encode the motion-inherent synergy trajectory, while at the same time being adaptable in terms of time and desired known synergy configurations at any point throughout the trajectory.

3.3.1 Synergy Primitives

Dynamic movement primitives (DMPs) (Ijspeert et al., 2002) are widely used in learning from demonstration to describe adaptable motions for robotic arms. DMPs allow for the adaptation of the start and goal point of a primitive motion, thereby flexibly adapting it to changing environmental conditions, e. g. different object placement. In addition, the speed of the motion primitive can be adapted to achieve a faster or slower execution. *Probabilistic movement primitives* (ProMPs) (Paraschos et al., 2013) take the variance in human motions into account. ProMPs can be trained on several human demonstrations and provide

a mean trajectory as well as a probabilistic description of the valid variation at each point of the motion trajectory. This work uses *via-point movement primitives* (VMPs) (Zhou et al., 2019), which describe a motion trajectory as

$$y(x) = h(x) + f(x). \tag{3.1}$$

The elementary trajectory $h(x)$ represents the direct path from the start to the goal position of the motion. The shape of the motion is encoded by

$$f(x) = \boldsymbol{\Psi}(x)^T \boldsymbol{w} + \epsilon(f), \tag{3.2}$$

with the weighting $\boldsymbol{w}$ applied on the radial basis kernels $\boldsymbol{\Psi}(x)$ and the noise $\epsilon(f)$.

VMPs combine the approaches of DMPs and ProMPs to achieve a flexible, probabilistic motion description with extrapolation capabilities. In addition, VMPs allow to constrain the motion to via-points along the trajectory, that need to be passed throughout the motion execution. By these means VMPs allow a more precise adaptation of the primitive motion. In contrast to ProMPs, VMPs allow for motion extrapolation and can therefore also handle via-points placed outside of the area covered by the seen demonstrations.

The goal of this section is a general, flexible description of human grasping motions, that can be easily adapted to different environmental requirements and desired grasp characteristics. Therefore, a **library of synergy VMPs** is computed from the kinematic synergy trajectories. One such synergy primitive is defined for each grasp type within the GRASP taxonomy. Kinematic synergy trajectories are derived as described in subsection 3.2.2. A VMP is subsequently trained on the kinematic synergy trajectories of all demonstrations of the same grasp type. Hence, the resulting synergy primitive learns from demonstrations of all 15 subjects and is thereby presented with a wide range of functional, yet individually varying grasp motions.

The synergy primitives of all grasp types from the GRASP taxonomy grouped according to Table 3.1 are shown in Fig. 3.20. While the first synergy mainly describes the progress in finger closure throughout the grasp, the synergy structure of different grasp types is covered by the second and third synergy as well as the synergies four to six not shown in Fig. 3.20. These synergy primitives represent an average grasping motion from the respective grasp type.

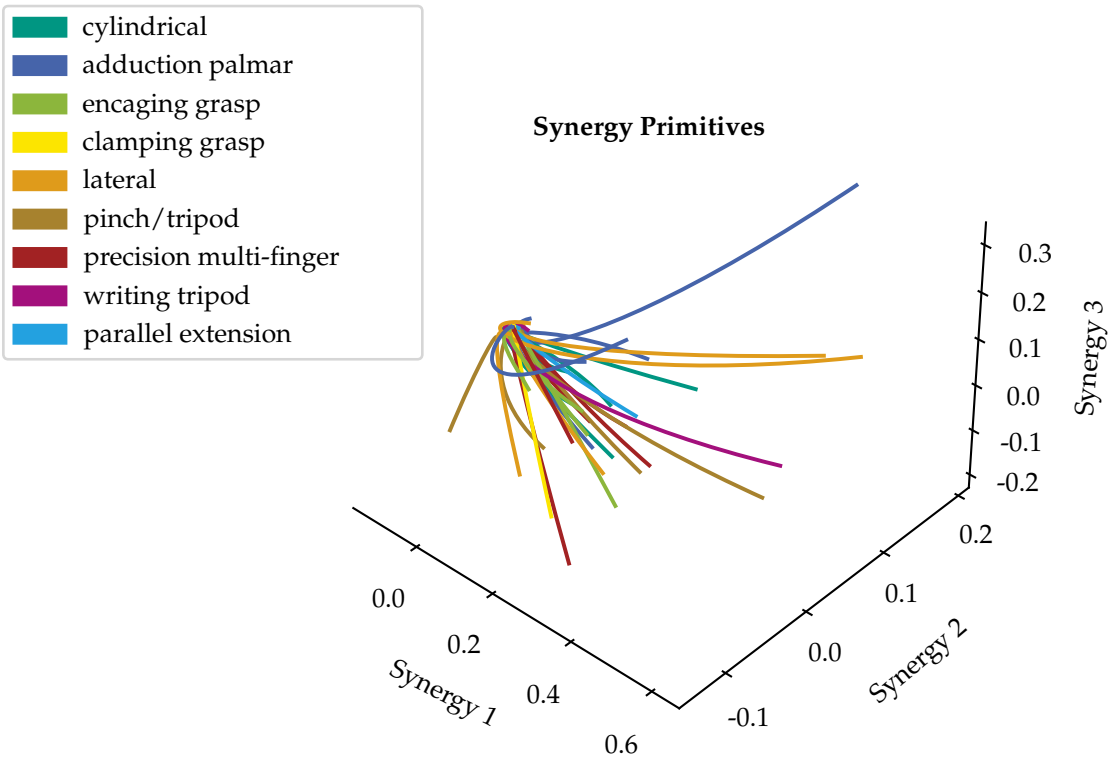

Figure 3.20: Synergy primitives for different grasps within the nine grasp type categories in the static synergy space

3.3.2 Adaptable Grasp Generation

Using the learned synergy primitives, grasps of a given type can be adapted to different environmental conditions and the grasp motion can be varied both in time and space. The probabilistic VMP representation allows a variance of the grasp motion for the same object shape and grasp position according to the variations seen in human demonstrations. By adjusting the goal of the synergy primitive trajectory, the final grasp pose can be influenced. Both the grip aperture as well as the proportional joint angle configuration of the grasp can be adapted. This allows the synergy primitive to adapt to different object sizes and surface shapes. The grasping motion can be influenced by via-points defined along the trajectory, thereby forcing the hand closing motion to pass through these via-points. An onset of the grasp different from a flat hand position can be accounted for by adapting the start of the synergy primitive.

By these means, the human-learned synergy primitives can be applied to generate grasps for different environmental conditions, varying e. g. the object size and shape, the grasp position on the object surface as well as the grasping motions shape and velocity. Several kinematic synergy trajectories for large diam-

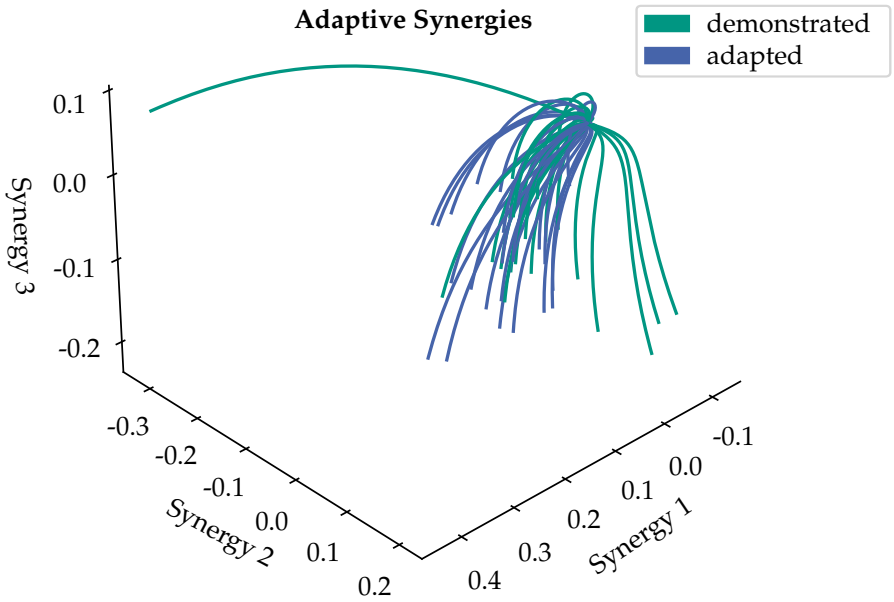

Figure 3.21: Synergy trajectories for large diameter power grasps generated for grasp postures demonstrated by humans as well as artificially adapted grasp postures

eter power grasps are shown in Fig. 3.21. All trajectories are generated based on the synergy primitive for large diameter grasps. Different grasp trajectories are generated by changing the goal of the primitive to a grasp pose demonstrated by a human subject or adapted artificially within the range of human grasp postures.

3.3.3 Evaluation

The kinematic synergy primitives are evaluated regarding the reproduction error for known motions as well as the specificity of the synergy primitives in representing human grasp types. The synergy primitives represent a generalization of human demonstrations by a small number of elements in a motion primitive library. To assess the additional cost in accuracy for the individual motion demonstration within this generalized representation, the **reproduction error** of human motion demonstrations is considered. Fig. 3.22 shows the error of both the kinematic synergy representation as well as the synergy primitives in comparison. The synergy primitives are defined in the kinematic synergy space and therefore include the error arising from the synergy representation. Hence, the overall error of the synergy primitives described in the kinematic synergy space of $3.08\,\%$ is higher than for the direct representation of a spe-

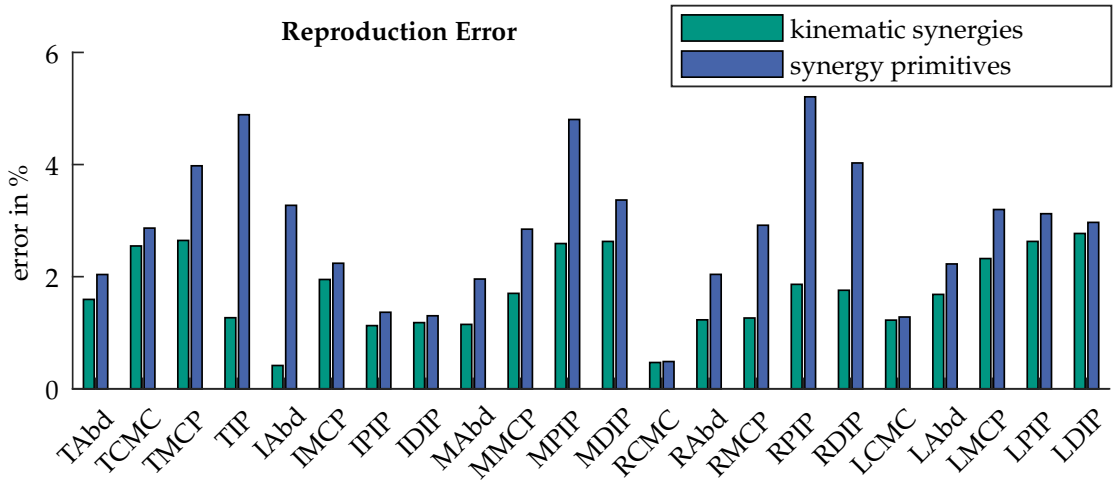

Figure 3.22: Reproduction error of the kinematic synergy description and the motion generation based on the synergy primitives, both shown for the different finger joint angles

cific demonstrated motion in the same kinematic synergy space with an error of $1.86\,\%$.

In many finger joints, the increase in reproduction error due to the synergy primitive representation is very low, i. e. for all carpometacarpal joints, but also for the index flexion joints as well as the thumb abduction joint. However, a significant increase in reproduction error is notable in some specific joints, especially the thumb interphalangeal joint, the index abduction joint and the ring finger interphalangeal joints. This indicates, that these joints show a high variance within each grasp type. The reported error is calculated based on the mean trajectory of the respective synergy primitive with start and end point of the motion adapted to the demonstrated human reference trajectory. For joint angles with a high variance over different demonstrations, this mean synergy primitive does not reproduce every possible joint angle trajectory. Since the variance of the demonstrated data is covered in the synergy primitive as well, it would still be possible to reproduce the different trajectories of the original demonstrations by setting via-points or exploiting the primitive's variance, given the full knowledge of the desired human trajectory.

In addition, a comparative evaluation was performed to prove the **specificity of the synergy primitives** by a classification of grasp types. Given the assumption that a significant divergence exists between primitives of different grasp types and that each synergy primitive $\overline{s}_g$ is representative for its specific grasp type g. For this assumption to hold, the synergy primitive $\overline{s}_g$ should be able to describe hand trajectories from its own grasp type g more accurately than any

other synergy primitive $\overline{s}_{h \neq g}$. Therefore, for each demonstrated grasp, trajectories with start and end point tailored to the demonstration are generated by each synergy primitive. The evaluation of the representation error with respect to the demonstrated trajectory shows, that the corresponding synergy primitive $\overline{s}_g$ always provides the best grasp representation over all demonstrations of its grasp type g. This shows that synergy primitives are specific towards the grasp type they are trained on and can capture the unique characteristics of this grasp type.

3.4 Summary and Conclusion

This chapter presented methods for the descriptive representation of postural and kinematic human grasp synergies. These synergies describe the joint angles of the human hand in grasping. Thereby, the grasp synergies characterize human grasping postures and motions and hence provide a methodical description of human grasp strategies. This thesis expands existing human grasp synergies in three main aspects:

- A postural grasp synergy space is connected to meaningful grasp characteristics. Thereby, the postural grasp synergies can be used for the generation of specific grasp postures for robotic hand control.
- The motion of arm and fingers in approaching and grasping the object is considered. The approaching motion of the hand in preparation of the grasp is thereby taken into account.
- Kinematic synergy trajectories observed from human demonstration are generalized. Such generalized synergy primitives allow to control and alter grasping motions for robotic hands based on kinematic synergies.

A deep autoencoder is trained to represent **descriptive postural synergies** in its latent space. Unlike a principal component analysis the autoencoder is able to capture also non-linear correlations between joint angles. In addition, the design of the loss function enforces a clustering of different grasp types in the latent synergy space. The size of the object is considered as additional parameter. The decoder can be applied to generate novel grasps with specific characteristics from the postural synergy space.

To consider arm motions during grasping, **kinematic arm synergies** are learned by a PCA. These describe the global pose of the hand in a lower-dimensional

synergy space. The arm synergies are analyzed with respect to different grasp characteristics.

Synergy primitives are learned from kinematic synergy trajectories of the same grasp type. The synergy primitives are described by Via-Point Movement Primitives capturing the specific behavior as well as the variance of the kinematic synergy trajectories from human demonstration. Thereby, the synergy primitives can be altered in a controlled way with respect to start-, end- and via-points of the trajectory as well as the timing of the motion execution. This allows the adaptation of kinematic grasp synergies for the application on robotic hands.

The **evaluation** shows a low reproduction error for grasps demonstrated by the human in all synergy representations - namely the descriptive postural synergies, the arm synergies and the kinematic synergies. The generalization in synergy primitives increases the error of simple reproduction, but allows the adaptation of a single synergy primitive to a range of kinematic synergy trajectories of the same grasp type. The generalization for the generation of novel, human-like grasps is additionally analyzed for the descriptive postural synergies. Novel, generated grasps have a similar grasp quality compared to grasps demonstrated by a human.

CHAPTER 4

Grasp Force Synergies

In addition to the arm motion and finger posture, the forces applied on the object are also very important for a stable grasp. The number and distribution of contact points throughout the hand influences the grasp stability and determines, whether a grasp can withstand external disturbances. The equilibrium of forces applied at the different contact points influences the stable grasping posture. Deliberate variations of the grasp force distribution can initiate changes of the grasping posture by in-hand manipulation, while unwanted disturbances of the grasp force equilibrium can break grasp stability and at its worst lead to grasp failure. Therefore, grasp contact forces are considered as the second pillar for successful grasp description and generation in this thesis.

Different to grasp postures however, there is little analysis on grasp forces in unconstrained human grasping over different grasp types and objects. The importance of grasp forces is widely recognized and there are thorough analyses on forces for specific grasp characteristics, as described in Section 2.2. Only recently, technology allows for spatially comprehensive and less-restrictive force measurement within human hands. This enables the comprehensive analysis of grasp contact forces (De Souza et al., 2015; Sundaram et al., 2019).

A common observation of all research done in human grasp force analysis is the importance of the coordination of grasp contact forces. Therefore, it seems natural to consider a synergy space used as a comprehensive general description of grasp forces. In this work, grasp forces are studied in human handover

tasks on a large variety of object shapes and weights. These grasp forces are analyzed and significant correlations between different grasp contact points are found. In addition, grasp contact patterns can be directly correlated to different grasp types and hence the kinematic posture of the hand. Inspired by the grasp force correlation, novel *static force synergies* are defined, that describe the contact force configurations for stable grasps. In a second step, two representations are proposed to describe the contact force patterns over the time of the entire grasping process. For the first time, these *dynamic force synergies* allow the representation of grasp forces from the first contact between the hand and the object until the final, stable grasp in a comprehensive synergy space. The two representations apply 1) synergy trajectories evolving over time in a static synergy space and 2) a dynamic synergy space that learns a notion of time within the synergy description. The work described in this section was presented in two conference publications (Starke et al., 2019, 2021). Graphs and images in this section are partially adapted from these publications.

4.1 Grasp Force Analysis

To understand the underlying principles of force distribution in human grasping, a study of human grasping and handover actions is performed. The grasp forces recorded throughout intuitive and unconstrained human grasping are analyzed regarding the force correlation between different contact points. In addition, grasp forces in the two different settings of the study, namely grasping from a table and grasping an object presented by another person, are compared. Finally, force contact patterns are analyzed with respect to the hand posture and grasp type.

4.1.1 Human Handover Study

Human grasp contact forces can only be considered in a comprising manner by taking into account all varieties of grasps, that can be observed in everyday life. However, most grasp studies measuring interaction forces with the object are limited to specific object shapes or grasp contact points due to the placement of force sensors. In this work, an extensive human grasping study is performed in cooperation with the École Polytechnique Fédérale de Lausanne (EPFL), that captures a wide variety of grasps spontaneously performed by the subjects.

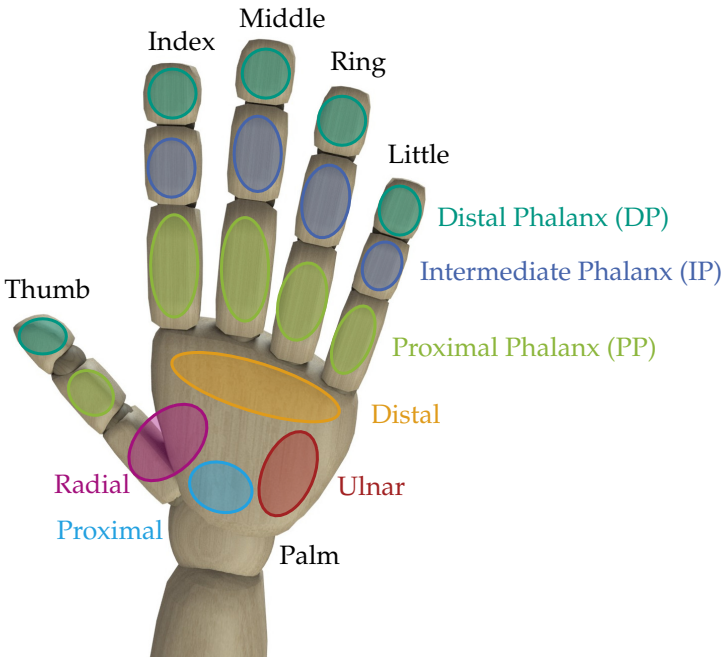

Figure 4.1: Placement of the 18 pressure sensors recording contact forces within the human hand

The **measurement system** is set up to measure all aspects of the grasping process. To measure grasp contact forces within the entire human hand, a Grip System (Tekscan Inc., USA) is attached to a data glove on the palmar side of the hand. It covers the palm as well as the fingers with 18 flexible pressure sensor pads, as shown in Fig. 4.1. Thereby, the normal forces at these 18 contact locations are measured, forming an 18-dimensional normal force vector $\mathbf{f}$. In order to record the corresponding hand posture, the grip system is attached to a data glove (CyberGlove III, Cyber Glove Systems LLC, USA) which is worn by the subject and measures finger joint angles in addition to the forces acquired by the grip system. The subject's arm motion is recorded using three optical markers at the wrist, elbow and shoulder which are tracked by an optical motion capture system (Optitrack, Natural Point Inc., USA). In addition, the scene is recorded by two RGBD cameras placed behind each subject and an RGB camera placed above the table. Two egocentric cameras are fixed to each subject's head. Finally, some of the subjects wear an eye-tracking system. The image data from the cameras is not used in this thesis, but it enhances the dataset for a wider range of applications in human grasp analysis.

The handover grasping study was performed by eight **subjects** executing the study tasks in pairs. All of the seven male and one female subjects considered their right hand as the dominant one. Subjects stood comfortably at two oppo-

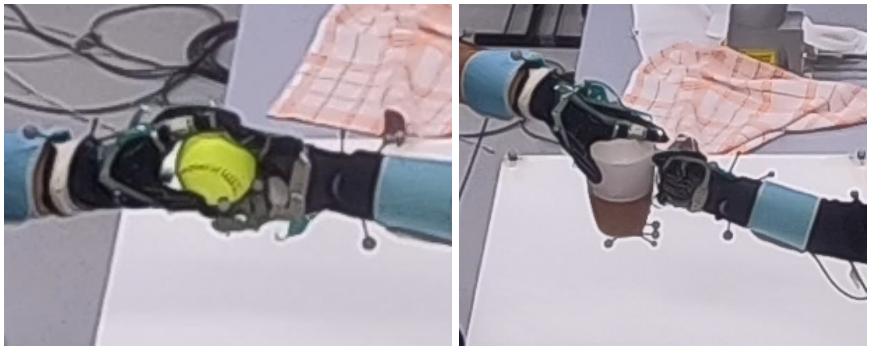

(a) (b)

Figure 4.2: Two handover actions with a softball (a) and a pitcher (b) performed in the human handover study (Starke et al., 2019) ©2019 IEEE

site sides of a table, thereby facing each other. The object was placed on the table between the two subjects. One subject, in the following denoted as the *presenter*, took the object from the table and handed it over to the second subject. This second subject, further on denoted as the *receiver*, took the object from the presenter's hand and placed it back on the table. The placing position was freely chosen by the receiver and in the subsequent run the presenter took the object directly from that placing position. The presenter performed the handover with their right hand, while the receiver used their left hand. However, it has been shown in (Rearick and Santello, 2002), that hand dominance has no influence on simple grasping tasks. The setup of the human handover study is shown in Fig. 4.2.

The **study procedure** included subjects handing over 14 household and workshop objects. The objects were chosen from the KIT Object Database (Kasper et al., 2012) and the YCB Object Set (Calli et al., 2015) and the set was enlarged with several custom objects. All utilized objects are listed in Table 4.1. A number of containers were used with different filling levels, thereby varying the weight of an object while keeping the same object shape. For several tools, the task was performed with two different strategies. In a handover task, the objects were handed over by the presenter directly after grasping them from the table. In a tool use task, the presenter grasped the object from the table, used it several times for its usual purpose (i. e. hammering with the hammer or writing with the pen) and finally handed the object over to the receiver. Each task was performed subsequently at least four times by the same pair of participants. Subjects were asked to grasp the objects naturally and vary their grasp posture throughout the repetitions. There were no restrictions of the grasp type or direction by the experimenter.

Table 4.1: Object characteristics (Starke et al., 2019) ©2019 IEEE

Object	Configurations	Weight	Object Set
Bowl	E / F	163 g / 297 g	YCB
Brush	HO / TU	75 g	KIT
Champagne Glass	E / HF / F	31 g / 71 g / 138 g	
Clear Plastic Cup	E / HF / F	18 g / 82 g / 142 g	KIT
Hammer	HO / TU	796 g	KIT
Mug	E / HF / F	107 g / 278 g / 423 g	YCB
Pasta Box	E / HF / F	46 g / 324 g / 497 g	
Pen	HO / TU	16 g	YCB
Pitcher	E / HF	125 g / 715 g	KIT
Plate	E	87 g	KIT
Red Plastic Cup	E / HF / F	27 g / 225 g / 389 g	
Screwdriver	HO / TU	159 g	KIT
Softball	HO	138 g	YCB
Wineglass	E / HF / F	151 g / 207 g / 277 g	

E: empty HF: half full F: full
HO: handover TU: tool use

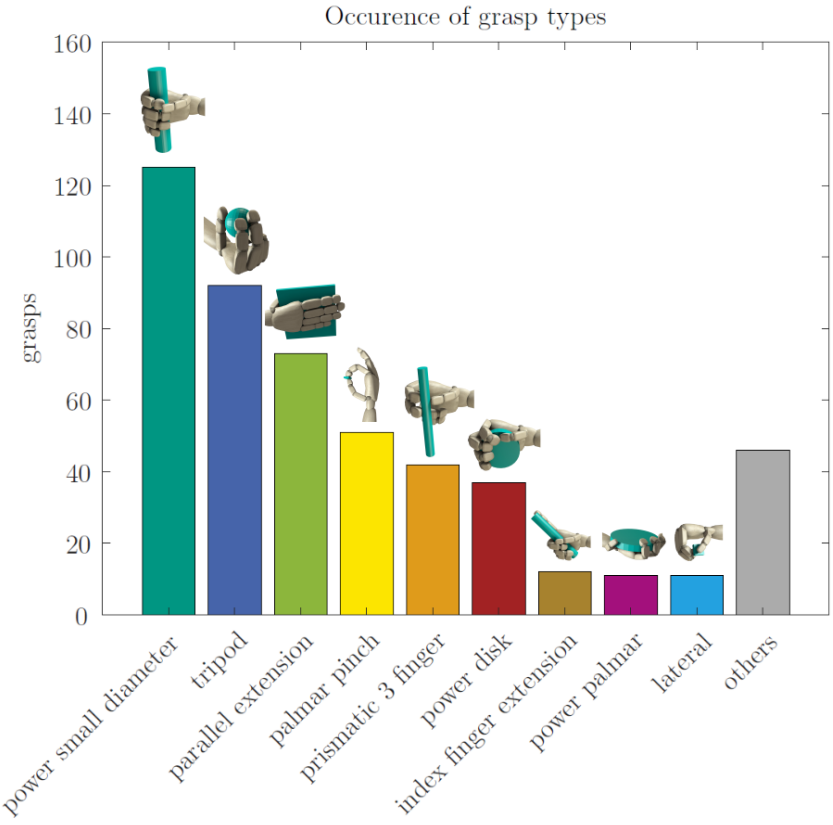

Figure 4.3: Distribution and frequency of the grasp types demonstrated in the human handover study; in total 16 grasp types were used by the subjects (Starke et al., 2019) ©2019 IEEE

Grasp classification of the 466 recorded grasps is performed according to the GRASP Taxonomy (Feix et al., 2016). Overall 16 different grasp types were demonstrated by the subjects. Six grasp types were recorded in more than 30 demonstrations, as shown in Fig. 4.3. The label *others* in this figure summarizes the grasp types *adduction grip*, *middle palmar pinch*, *tripod variation*, *power sphere*, *power large diameter*, *little palmar pinch* and *fixed hook*. In the following, all recorded grasps will be used to describe the force synergy spaces. For evaluation purposes however, only the six most frequent grasp types are used, to ensure the representative status of the evaluation data. As an exemplary case, the *lateral* grasp type is considered in addition due to its exceptionally strong thumb adduction.

Table 4.2: Grasp contact patterns (adapted from (Starke et al., 2019) ©2019 IEEE)

	power small diameter	tripod	parallel extension	palmar pinch	prismatic 3 finger	power disk	lateral
thumb DP	●	●	●	●	●	●	●
thumb PP	○	○	○	○	○	○	○
index DP	●	●	●	●	●	●	●
index MP	●	●	●	○	●	○	●
index PP	●	○	○	○	○	○	○
middle DP	●	●	●	○	●	●	○
middle MP	●	○	○	○	○	○	○
middle PP	○	○	○	○	○	○	●
ring DP	●	○	●	○	●	●	○
ring MP	●	○	○	○	○	○	●
ring PP	●	○	○	○	○	○	●
little DP	●	○	○	○	○	○	○
little MP	○	○	○	○	○	○	○
little PP	○	○	○	○	○	○	○
palm distal	○	○	○	○	○	○	○
palm radial	○	○	○	○	○	○	○
palm ulnar	○	○	○	○	○	○	○
palm proximal	○	○	○	○	○	○	○

4.1.2 Correlations in Human Grasp Forces

The human grasp normal forces recorded in the handover study are analyzed regarding their amount and distribution. For the analysis of grasp contact distribution, a binary contact label is defined based on the continuous normal force at the respective contact point. Any location with a measured contact force $> 1\,\mathrm{N}$ is considered as a grasp contact point. Table 4.2 shows the grasp contact points for different grasp types. All grasp types except for *parallel extension* and *prismatic 3 finger* exhibit a unique grasp contact pattern, thereby allowing the distinction of different grasp types. The precision grasps *parallel extension* and *prismatic 3 finger* differ mostly in the kinematic hand posture as well as the usage of the little finger. In the handover study, the force configurations of these two grasps transition fluently. While the little finger is not involved at all in *prismatic 3 finger* grasps, its contribution to the parallel extension grasps is measurable, but still small and therefore below the aforementioned threshold of $1\,\mathrm{N}$. Therefore, a distinction of these two grasp types is not possible only with the grasp contact pattern, but needs to be additionally based on the grasp posture.

Overall it can be seen that the power grasps like *power small diameter* have a high number of different contact points compared to precision grasps like *tripod* or *palmar pinch*. The *lateral* grasp type exhibits a number of contact points along the middle and ring finger, that cannot be directly attributed to the expected grasp posture. These are likely caused by contacts between the fingers and the palm, as all four fingers are closed to support the object held between thumb and index finger.

The **correlation of grasp forces** at different contact locations is analyzed by applying *Pearson's correlation coefficient* (PCC) on the continuous normal forces of static grasps, as shown in Fig. 4.4. Most notably, the thumb force does not exhibit any significant correlations with respect to any other part of the hand. This is to be expected as the thumb usually counteracts an opposing virtual finger being represented by either the palm or a varying number of other fingers. Therefore, the number of contact points opposing the thumb's force is varying depending on grasp type and posture and no general correlation exists over the entire range of human grasps.

Within the fingers and the palm, a consistent correlation is demonstrated by Fig. 4.4. Most notable correlations can be seen between the palm and the index and middle finger respectively. The proximal phalanges of index and middle finger show a PCC of 0.84 and 0.86 with respect to the distal area of the palm.

Interestingly, no correlation can be seen with the proximal phalanx of the little finger as well as the radial part of the palm with respect to any other part of the hand. The radial part of the palm is situated directly below the thumb and is integrated into the kinematic chain of the thumb, containing the metacarpal bone of the thumb. Therefore, it contributes to the opposing force of the thumb and adapts according to the grasp's posture, as explained above. The little finger is only used in a small number of grasps and proximal finger phalanges only make contact with the object in the case of power grasps. Therefore, few human demonstrations show a significant contact force at the lower little finger in general.

In accordance with existing analyses on specific grasp types or objects (Rearick and Santello, 2002; Naceri et al., 2014; Marneweck et al., 2016), correlations between normal forces at different grasp contact locations could be shown for the general grasping study considered in this work. Such correlations thereby exist not only for specific grasp postures, but also over the entire range of human

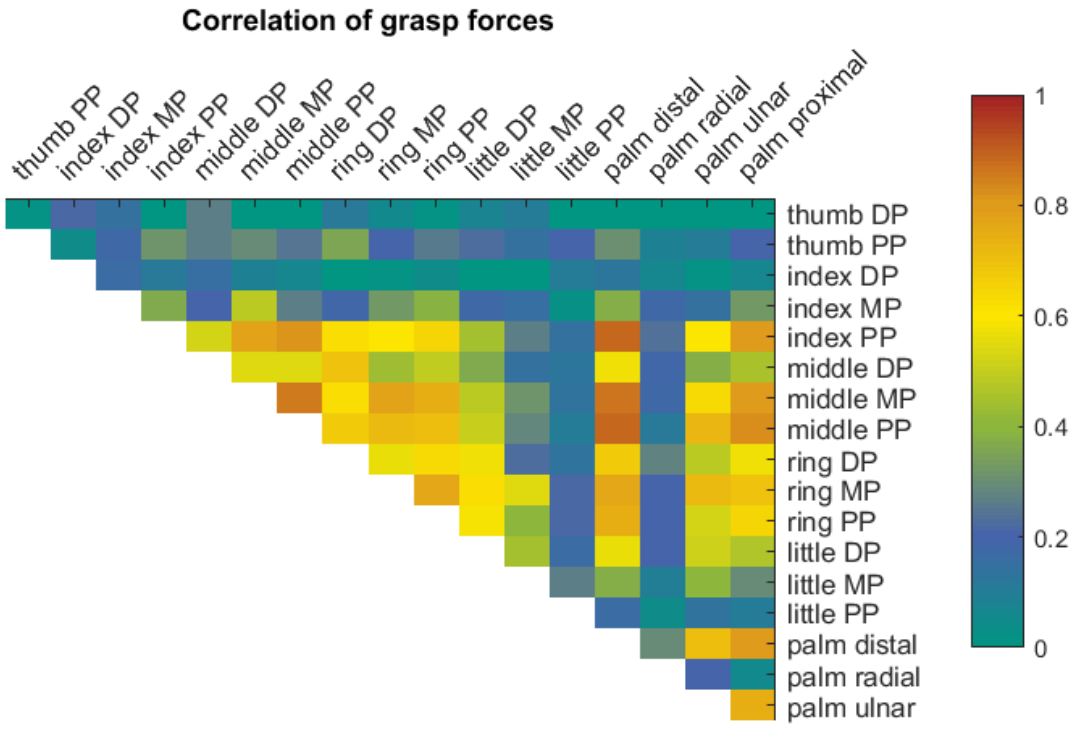

Figure 4.4: Correlation between grasp forces at different contact locations throughout the hand over all demonstrated human grasps, calculated by Pearson's correlation coefficient (Starke et al., 2019), warmer colors denote higher correlation between joints, a high correlation can be seen between the fingers and the palm while the thumb force does not exhibit any correlation with the forces at other contact points ©2019 IEEE

grasping. These findings motivate the description of grasping forces within a lower-dimensional force synergy space.

4.2 Static Force Synergies

The general correlations observed over normal contact forces throughout a wide range of human grasps prove the existence of force synergies similar to the postural synergies for hand kinematics. Therefore, this thesis presents a novel description of force synergies in general and unconstrained human grasping, i. e. covering a wide range of different grasp types and objects. For the first time a synergy space describing static human grasping forces is derived and analyzed.

4.2.1 Force Synergy Description

Given a human grasp $\mathbf{g}$ with a number of n grasp contact points $c_1, c_2, ..., c_n$. Each grasp contact point c_i is associated with a normal force f_i excerted on the grasped object. The static grasp force can thereby be described by an n-dimensional vector $\mathbf{f}_g = (f_1, f_2, ..., f_n)$. The human handover study described in Section 4.1 measures grasp contact forces at 18 different contact locations and thereby the dimensionality of the grasp force will be $\mathbf{f}_g \in \mathbb{R}^{n=18}$ in the following. This work aims to derive a synergy space $\mathcal{S} \subset \mathbb{R}^k$ that encompasses the description of grasp forces $\mathbf{f}_g$ by force synergies $\mathbf{s}_g = (s_1, s_2, ..., s_k)$. The dimensionality of this static force synergy space shall be lower than for the original static grasp force patterns, i. e. $k < n$.

Similar to the postural synergies by Santello et al., a PCA is performed on all force patterns $\mathbf{f}_g$, to describe this synergy space $\mathcal{S}$ (Santello et al., 1998). This yields the transformation

$$\mathbf{s}_g = \mathbf{W} \cdot \mathbf{f}_g \,, \tag{4.1}$$

with $\mathbf{W}$ being the weight matrix defined by the PCA. As shown in Fig. 4.5, eight synergy parameters can describe over $90\,\%$ of the variance of human grasp force patterns. Therefore, the static force synergy space is defined as $\mathcal{S} \subset \mathbb{R}^{k=8}$.

The grasp force patterns for different grasp types in the **force synergy space** can be seen in Fig. 4.6. It shows the eight-dimensional synergy space projected into two dimensions by *t-Distributed Stochastic Neighbour Embedding* (tSNE). For specific grasp types, e. g. *power small diameter* or *palmar pinch*, a clustering of

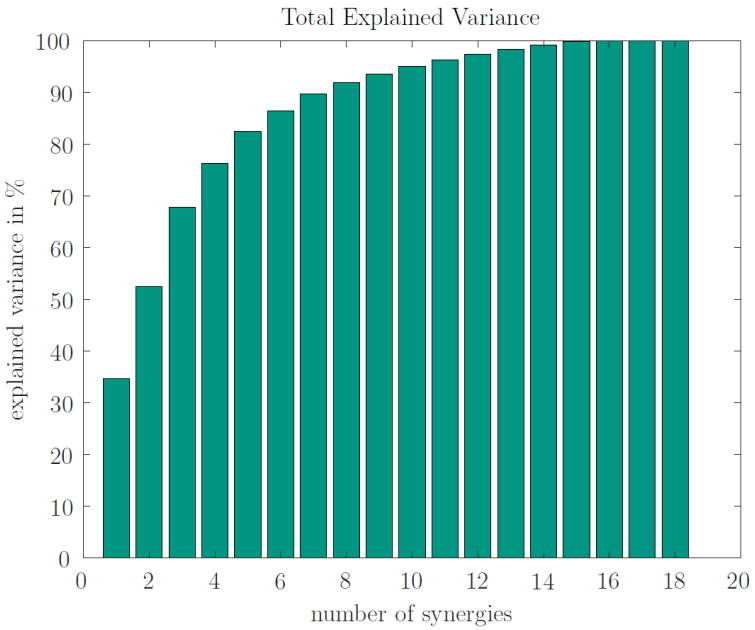

Figure 4.5: Overall explained variance over the number of linear static force synergies (Starke et al., 2019), eight synergies can describe over 90 % of the total variance of the grasp ©2019 IEEE

force synergies can be seen. However, similar to the linear postural synergy space (Santello et al., 1998), there is no clear structure of the grasps in the static force synergy space with respect to the grasp type.

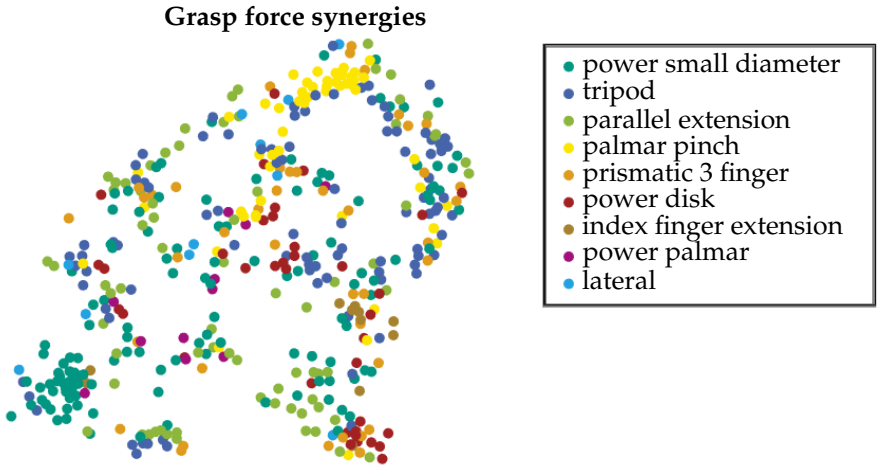

Figure 4.6: Distribution of grasps in the static force synergy space; the eight-dimensional space is projected to two dimensions by tSNE (Starke et al., 2019) ©2019 IEEE

4.2.2 Analysis and Evaluation

Based on the normal contact forces, the discriminability of grasp types can be measured with a numerical index similar to the *sensorimotor efficiency index* for hand postures (Santello et al., 1998). On average the contact forces can transmit $93.9\,\%$ of all possible information. This demonstrates the suitability of grasp contact forces to discriminate and classify different grasp types in human grasping.

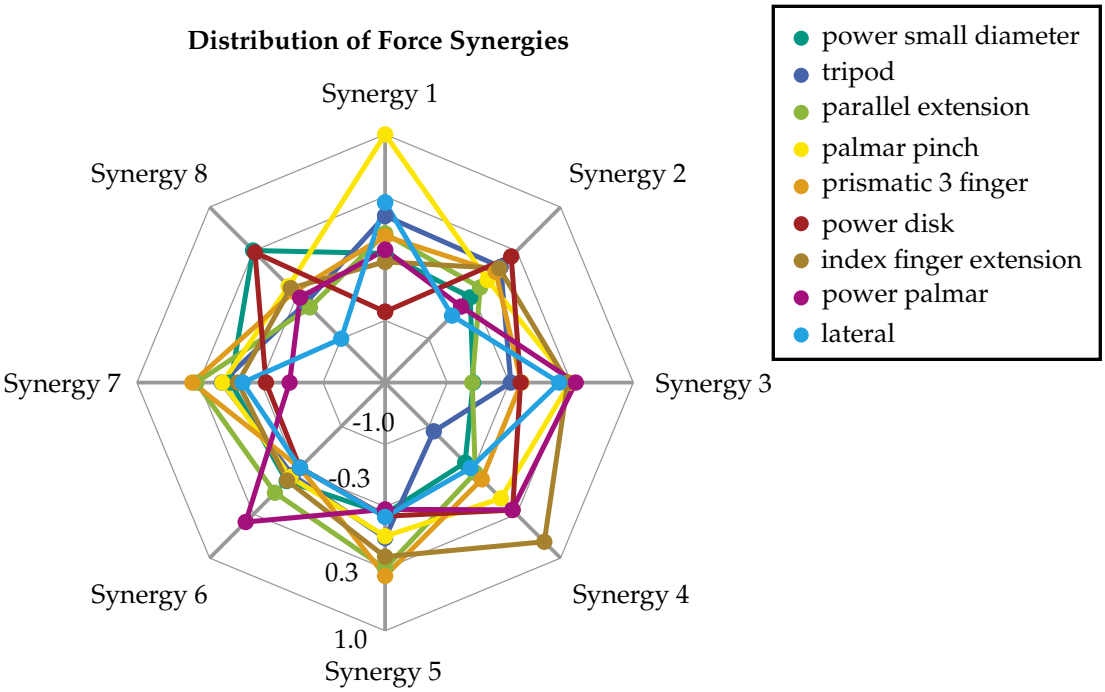

Figure 4.7: Mean force synergies of different grasp types (Starke et al., 2019), the plot shows a notable distinction between grasp types in the first synergy with 1.00 for palmar pinch and -0.91 for power disk and in the fourth synergy with 0.75 for index finger extension and -0.93 for tripod grasps ©2019 IEEE

Further, the **mean synergy representation** of each grasp type is shown in Fig. 4.7. A clear differentiation of grasp types can be seen in the first and fourth synergy. In accordance with the direct observations in synergy space, the distribution of grasp types is rather homogeneous. Similar to the postural hand synergies, a more explicit structure of the static force synergy space requires a synergy extraction strategy, that explicitly fosters the separation of grasp types.

Two exemplary **grasp force configurations** are shown in Fig. 4.8. Human grasp demonstrations of a power *small diameter grasp* on a hammer and a *tripod* grasp on a pen yield the depicted grasp force configurations and corresponding synergy representations. For these two exemplary grasps, differences in synergy

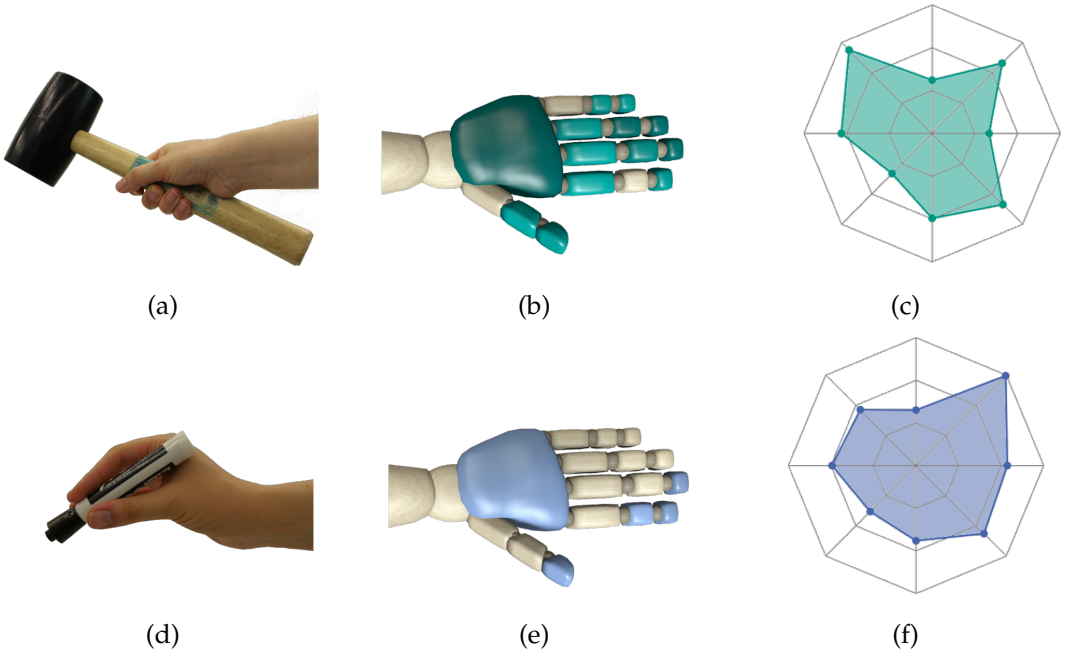

(a) (b) (c)

(d) (e) (f)

Figure 4.8: Exemplary human grasp demonstrations, the corresponding normal force configurations with darker colored parts applying a larger normal force on the object and their respective representation in the force synergy space; power small diameter grasp on a hammer (a) with the corresponding force configuration (b) and synergy representation (c) as well as a tripod grasp on a pen (d) with its force configuration (e) and synergy representation (f) respectively (adapted from (Starke et al., 2019) ©2019 IEEE)

representation can be clearly seen. Also, expected characteristics of both grasp types can be found in the grasp force configuration. While the power grasp shows a wide force distribution with almost all finger segments in direct contact with the object, the tripod grasp reflects the expected grasp contacts at the tips of thumb, index and middle finger. The static force synergy space allows to represent these distinct features of both grasps in a low-dimensional space, that preserves meaningful force characteristics while taking into account general correlations between grasp contact forces. With these force synergies, the complexity of force control for humanoid robotic hands can be reduced.

4.3 Time-Dependent Force Synergies

The quality of a grasp is not only influenced by its static posture and configuration of contact forces. In addition, the motion and interacting forces applied by the hand throughout the grasping action are contributing significantly to the final grasp. The interaction of contact forces throughout the grasp execution

shape the final grasp posture. Furthermore, the balanced increase of counteracting forces is crucial for grasp success. An imbalanced force configuration throughout the grasp execution may lead to undesired object motions or even grasp failure due to the object being pushed out of the hand.

Therefore, this work considers the entire grasping process with the **evolution of normal grasp force patterns** from the first contact to the stable grasp. Instead of a static normal force pattern $\mathbf{f}_{g,T}$, this requires the consideration of a temporal force pattern $\mathbf{f}_g(t)$ for $t \in [0, T]$ with T being the time the final grasp is achieved. Based on the correlations found within static force patterns, this work aims at defining temporal force synergies $\mathbf{s}_g(t)$ that represent the entire temporal progression of the normal force pattern $\mathbf{f}_g(t)$ throughout the grasping process.

Towards this goal, **two synergy representations** are presented. Firstly, a static synergy space is learned by applying the method used in Section 4.2. Temporal force sequences can then be represented as temporal trajectories within this static synergy space. Secondly, a dynamic synergy space is learned based on entire temporal force sequences. By these means, the force synergies directly take the progression of the contact forces into account. Both approaches are evaluated regarding their reproduction and generation capabilities.

4.3.1 Static Force Synergy Space

As presented in Section 4.2, a static force synergy space $\mathcal{S}$ can be described by eight synergy parameters learned by a PCA. Inspired by Romero et al., this static force synergy space can be exploited for the representation of temporal normal force patterns $\mathbf{f}_g(t)$ by describing them as a chronology of time-independent force synergies $\mathbf{s}_g(t) = (\mathbf{s}_{g,0}, ..., \mathbf{s}_{g,T})$ (Romero et al., 2013). Hence, the static synergy space $\mathcal{S}$ is retrained on all force patterns within the human demonstrations of the handover study regardless of their grasp type or timing within the grasping process. By these means, the shape of the synergy space is adapted to represent not only possible stable grasp force configurations, but also any grasp force patterns observed throughout the grasping process that leads to this final grasp configuration. The force synergy trajectories in the first three dimensions of the static synergy space $\mathcal{S}$ are shown in Fig. 4.9. All synergy trajectories start in a mutual point representing $\mathbf{f}_g(0) = \mathbf{0}N$ right before the initial contact between the hand and the object is made. From there on, synergy trajectories evolve into different directions of the synergy space depending

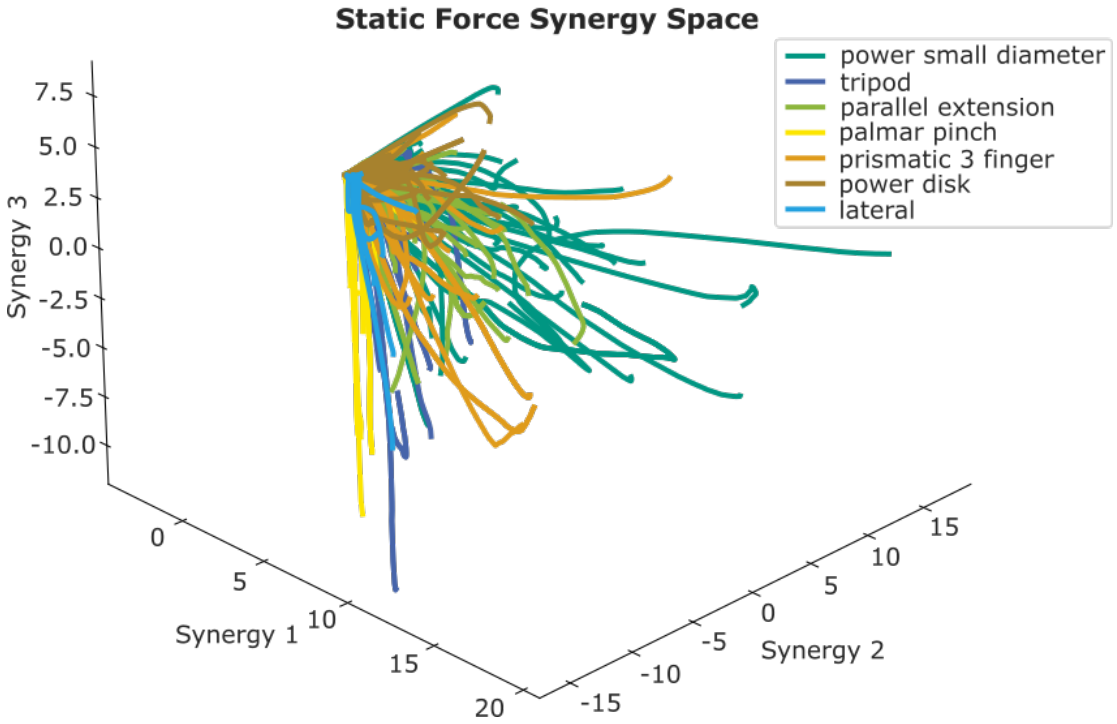

Figure 4.9: Force synergy trajectories of different grasp types in the first three dimensions of the eight-dimensional linear force synergy space (Starke et al., 2021), all synergy trajectories start at the same point marking no contact force, from there, synergy trajectories evolve into different directions of the force synergy space depending on their grasp contact configurations ©2021 IEEE

on their grasp force configuration. Interestingly, a differentiation of grasp types can be seen in the force synergy space. The directions of the synergy trajectories opening a spectrum from embracing power grasps to fine-granular precision grasps vary mainly in the first and third synergy.

To **generalize synergy trajectories** for different grasp types, a *Gaussian Mixture Regression* (GMR) is performed on several demonstrations of the same grasp type. For each grasp type, five *Gaussian Mixture Models* (GMM) are learned using expectation maximization on all demonstrated force synergy configurations. The initialization of the GMMs is performed by k-means clustering. Based on these Gaussians, the GMR yields an expectation $\mathbf{E}_g(t)$ as well as a corresponding variance $\mathbf{var}_g(t)$ for the synergy trajectory of each grasp type g.

The **grasp generation** of new, human-like temporal grasp force patterns can then be performed by using the synergy expectation $\mathbf{E}_g(t)$, which represents an

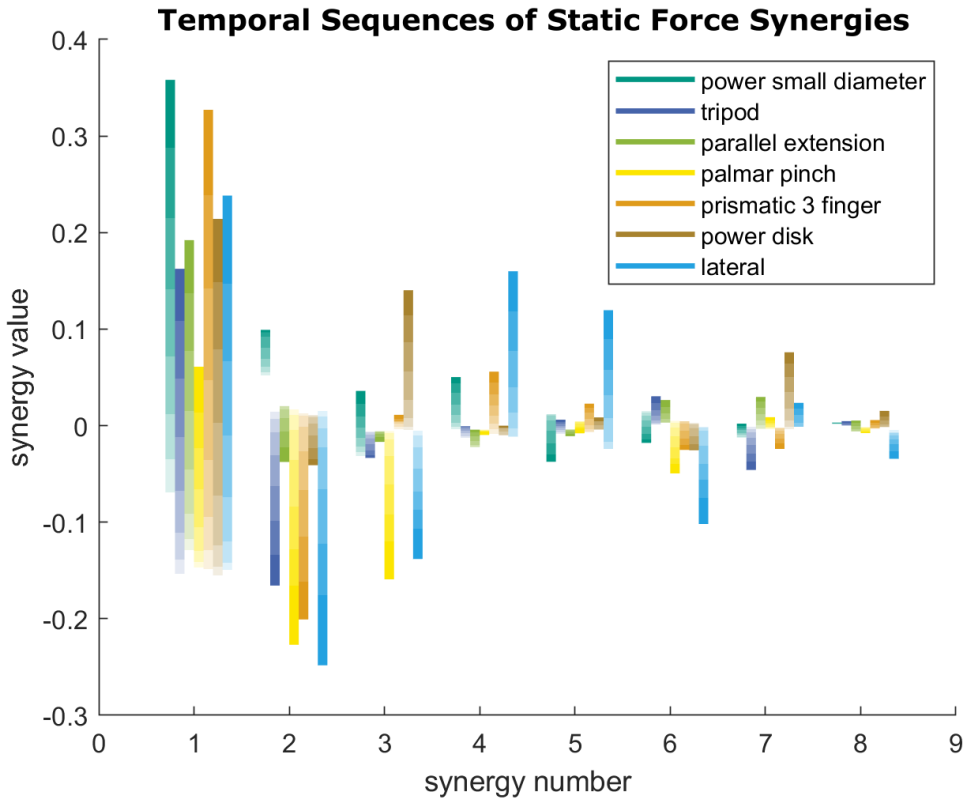

Figure 4.10: Average synergy trajectories in the static synergy space for each grasp type calculated by GMR; force synergy variables for the different grasp types are represented as bars, the temporal evolution of synergy variables is depicted by an continually increasing coloring within each bar (Starke et al., 2021) ©2021 IEEE

average force synergy trajectory of the desired grasp type. To cover the entire variety of human grasp force demonstrations, the synergy variance $\mathbf{var}_g(t)$ provides the range for adaptions with respect to the average force synergy trajectory that still result in valid, human-like temporal grasp force patterns. The average force synergy trajectories for different grasp types are shown in Fig. 4.10. It can be seen that the synergy trajectories of different grasp types evolve into distinct directions in synergy space. In the first synergy variable, the amplitude of the final grasp force is especially high for power grasps like the *power small diameter*. In the third to seventh synergy, synergy directions vary notably between grasp types. These findings match the qualitative observations for the trajectories in the static synergy space in Fig. 4.9.

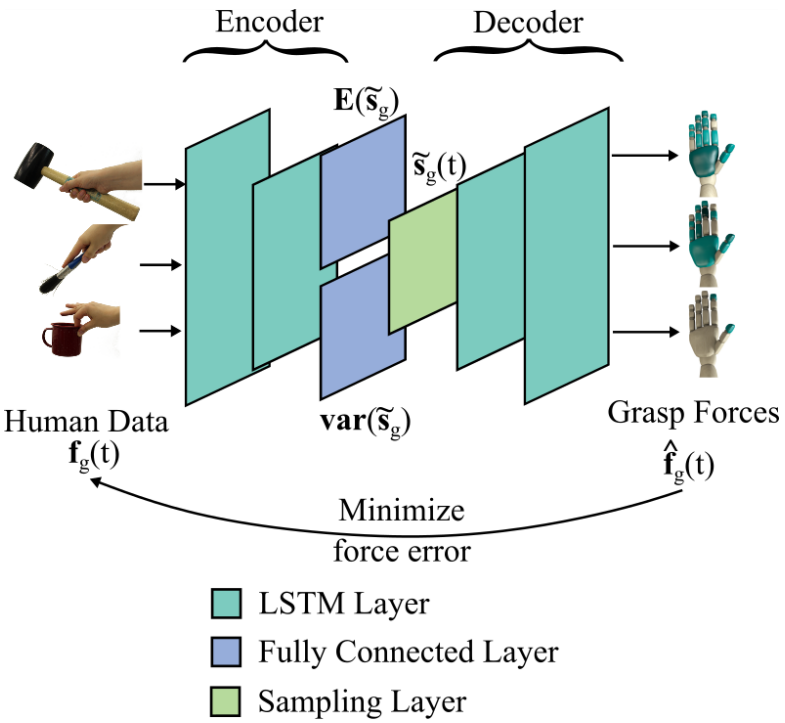

Figure 4.11: Structure of the LSTM autoencoder to represent the dynamic force synergy space; entire sequences of temporal force patterns are fed into an LSTM-encoder, synergy mean and variance are represented in two parallel fully connected layers, temporal force patterns are reproduced by an LSTM-decoder (Starke et al., 2021) ©2021 IEEE

4.3.2 Dynamic Force Synergy Space

While the static force synergy space can be used to represent time-dependent trajectories of human grasp forces, it has no notion of time by itself. This means that the consistency of a synergy trajectory over time is not inherently guaranteed, but needs to be ensured by an operator throughout the generation of new, human-like synergy trajectories for robotic hand control. Therefore, a second, dynamic synergy space is defined, that encodes the time-dependent grasp progress directly in the force synergies.

To this end, the **methodology** of a recurrent neural network is applied. It is trained to represent entire temporal sequences of human grasp force patterns. The structure of an *long short-term memory* (LSTM) autoencoder allows a nonlinear reduction of the dimensionality of the contact force patterns while considering the temporal relation of the forces evolving over the entire grasping process. The structure of the LSTM autoencoder network is shown in Fig. 4.11. Entire normalized temporal human grasp normal force patterns $\mathbf{f}_g(t)$ are fed into the encoder. Hence, the input of the network is a matrix denoting the 18-

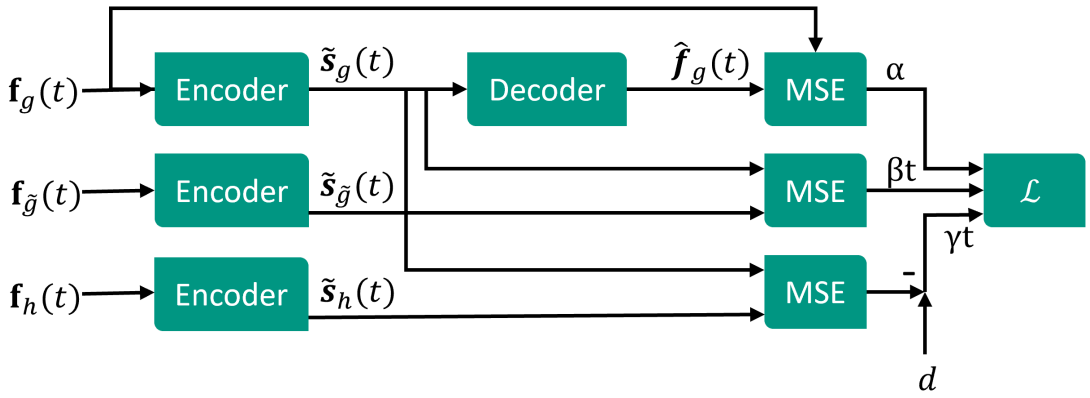

Figure 4.12: Loss function to train the dynamic force synergy space; the encoder is executed threefold to encourage both a good grasp representation and a clustering of grasp types in synergy space (Starke et al., 2021) ©2021 IEEE

dimensional vectors of the 18 scalar normal forces within a grasp configuration. The second dimension of the input matrix represents the grasp progress and is defined by concatenating static normal force vectors over every time step of the grasping motion. The encoder network consists of two LSTM-layers with a width of 18 and 13 variables, respectively. To ensure the consistent validity of the synergy space, the LSTM-encoder is followed by two parallel fully connected layers describing the expectation $\mathbf{E}(\widetilde{\mathbf{s}}_g)$ and logarithmic variance $\mathbf{var}_{log}(\widetilde{\mathbf{s}}_g)$ of the demonstration in the dynamic synergy space $\widetilde{\mathcal{S}}$. A sample $\widetilde{\mathbf{s}}_g(t)$ is drawn from this synergy space by

$$\widetilde{\mathbf{s}}_g(t) = \mathbf{E}(\widetilde{\mathbf{s}}_g(t)) + \epsilon \cdot e^{0.5\mathbf{var}_{log}(\widetilde{\mathbf{s}}_g(t))}, \tag{4.2}$$

with ϵ being a random number with a mean of 0.0 and a standard deviation of 1.0. $\mathbf{E}(\widetilde{\mathbf{s}}_g)$ thereby represents the dynamic force synergy space projecting the mean synergy trajectories of the human temporal grasp force patterns. $\mathbf{var}_{log}(\widetilde{\mathbf{s}}_g)$ describes the feasible variation of synergy trajectories that is still attributed to the same human demonstration. The dynamic synergy space $\widetilde{\mathcal{S}}$ has eight dimensions. The synergy sample $\widetilde{\mathbf{s}}_g(t)$ is fed into the decoder consisting of two LSTM-layers with 13 and 18 dimensions respectively. The network outputs the reconstructed temporal grasp force pattern $\widehat{\mathbf{f}}_g(t)$.

A **contrastive loss function** is applied to structure the dynamic synergy space in a meaningful way. This allows to control the grasp type when generating human-like grasps by sampling directly from the synergy space. The loss function is shown in Fig. 4.12. The encoder is run three times in parallel with a temporal force pattern $\mathbf{f}_g(t)$ of grasp type g, a reference sample $\mathbf{f}_{\tilde{g}}(t)$ of the same

grasp type and a second reference $\mathbf{f}_h(t)$ of a different grasp type h. The loss is thereby structured into three parts.

1. A general reproduction loss between the original and reproduced temporal force patterns $\mathbf{f}_g(t)$ and $\widehat{\mathbf{f}}_g(t)$ ensures that meaningful temporal force patterns can be generated from the dynamic synergy space.
2. In addition, a second term minimizes the distance between two synergy patterns originating from the same grasp type.
3. A separation between synergy patterns belonging to different grasp types is promoted by the third loss term, that approximates the squared distance in synergy space to a desired threshold $d = 0.15$.

Altogether this enforces a clustering of grasp types in the synergy space, similar to the approach used for the adaptable postural grasp synergies in Section 3.1. Temporal force patterns all start similarly with $\mathbf{f}(0) = \mathbf{0}$ right before contact between the hand and the object is established and only evolve into different force configurations over the grasp progress. Therefore, the separation of grasp types can only be preformed at later stages of the grasping process. To achieve this, both parts of the contrastive loss are weighted with the relative grasp time t, thereby continually increasing the amount of separation that is enforced over the progress of the grasp. The overall loss function is then given by

$$\begin{aligned}\mathcal{L} = \alpha \cdot \text{MSE}(\mathbf{f}_g(t), \widehat{\mathbf{f}}_g(t)) + \beta \cdot t \cdot \text{MSE}(\widetilde{\mathbf{s}}_g(t), \widetilde{\mathbf{s}}_{\widetilde{g}}(t)) \\ + \gamma(d - t \cdot \text{MSE}(\widetilde{\mathbf{s}}_g(t), \widetilde{\mathbf{s}}_h(t)))\,,\end{aligned} \tag{4.3}$$

with $\text{MSE}(\cdot)$ being the mean squared error function and the weighting parameters $\alpha = 1.0$, $\beta = 0.05$ and $\gamma = 0.005$. $\widetilde{\mathbf{s}}(t)$ denotes a synergy trajectory in the latent dynamic synergy space $\widetilde{\mathcal{S}}$.

For **network training**, the human grasp force demonstrations were split into training, validation and test motions by $90\,\%$, $10\,\%$ and $10\,\%$ respectively. The network is trained using an Adam optimizer with a learning rate of 10^{-3} and gradient scaling with a norm of 0.5. Pretraining is preformed applying only the reproduction loss for 1500 epochs, before training with the entire loss function for another 1500 epochs.

The first three dimensions of the learned **dynamic synergy space** are shown in Fig. 4.13. Synergy trajectories start from a mutual point marked in red, that represents the unloaded hand without grasp contacts. From there on, the synergy trajectories evolve into the entire synergy space, with the temporal progress depicted by increasingly solid lines in Fig. 4.13. The synergy trajectories of dif-

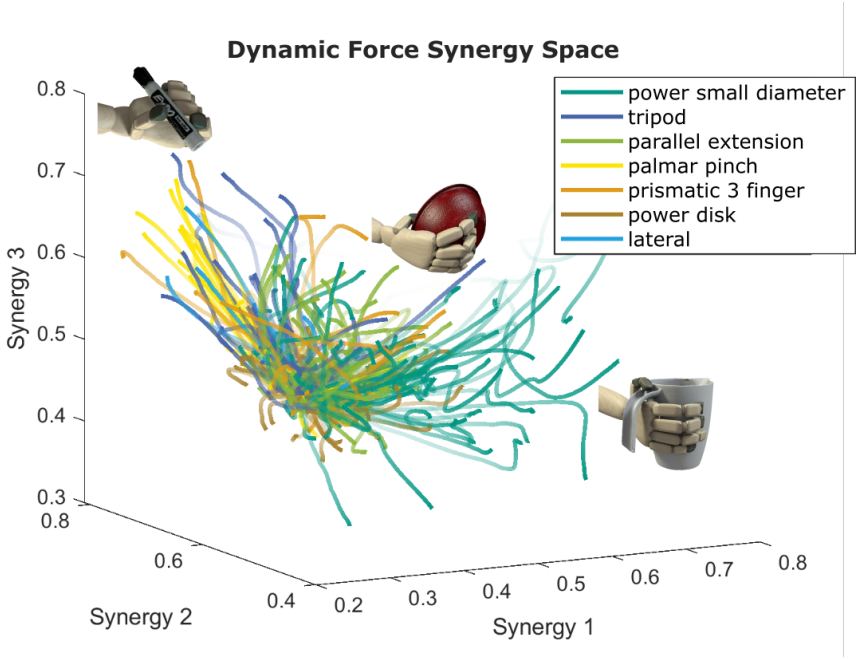

Figure 4.13: First three dimensions of the dynamic force synergy space, synergy trajectories are depicted with increasingly solid color throughout the grasp process (adapted from (Starke et al., 2021) ©2021 IEEE)

ferent grasp types evolve into different directions of the synergy space. A clear separation is also notable in the mean synergy trajectories of the different grasp types shown in Fig. 4.14. In comparison to trajectories in the static synergy space, synergy parameters in the dynamic synergy space vary less over time. Instead, a separation of grasp types can be seen early on over all synergy variables. Simultaneously, the inherent notion of time embedded into the dynamic synergy space reduces the necessity to encode the overall grasp progression into the synergy variables. By these means, the grasp progress does not need to be considered explicitly in the dynamic synergy space, but the same synergy configuration can generate a valid grasp force pattern for a timed series of momentary grasp forces.

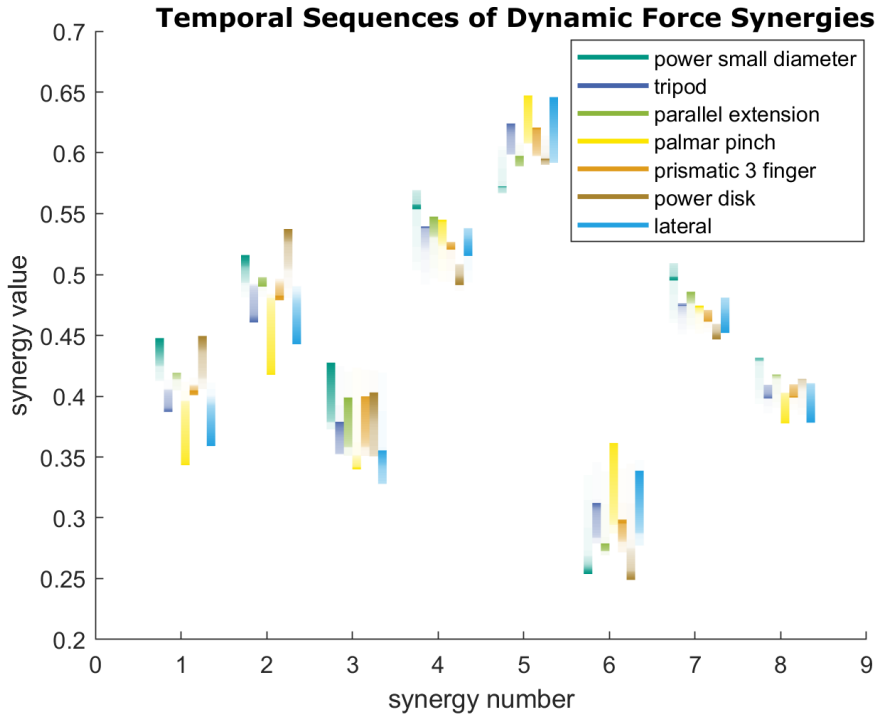

Figure 4.14: Evolution of the mean synergies of different grasp types throughout the grasp process, evolution over time is depicted by an increasingly solid bar color (Starke et al., 2021) ©2021 IEEE

4.3.3 Generation of Human-Like Grasp Forces

To control humanoid robotic or prosthetic hands in grasping a large variety of different, possibly unknown objects, grasp normal force patterns should be directly generated based on the presented force synergies without the need to specifically record a human demonstration under exactly similar conditions. Similar to the adaptive postural and kinematic synergies, force synergies are therefore shaped to allow a simple definition of the grasp's characteristics and temporal progress for the artificial generation of grasp force configurations from synergy space. By feeding the decoder with an artificially sampled synergy configuration, new, human-like temporal grasp force patterns can be generated from the dynamic force synergy space. This is shown for four generated grasps of different grasp types in Fig. 4.15. Similarly, a trajectory can be defined in the static synergy space to achieve a newly generated grasp normal force pattern for a humanoid hand.

For the **grasp generation from the static synergy space**, the temporal progress of the grasp has to be considered manually for the static synergy space, an artificially generated synergy trajectory should be defined within the expected vari-

ance of the desired grasp type's human demonstrations. By these means, the resulting temporal grasp force pattern is ensured to be meaningful. To choose a grasp type for the dynamic synergies, it is sufficient to position the trajectory within the associated area of the clustered synergy space. Two temporal force patterns generated from the static and dynamic synergy spaces as well as comparable human demonstrations of palmar pinch grasps are shown in Fig. 4.16. Both generated trajectories show a focus on normal forces at the thumb and

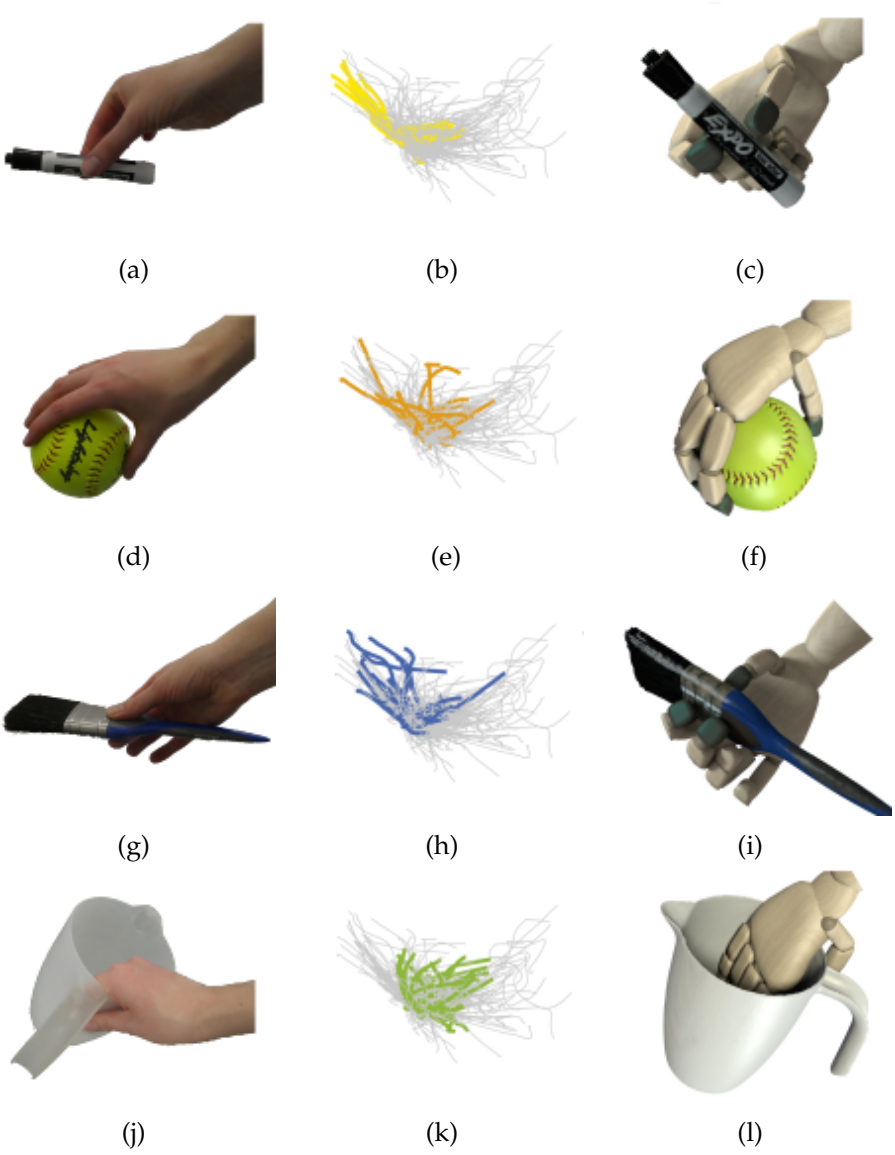

Figure 4.15: Application of the dynamic force synergies for four different grasps, a human demonstration of a palmar pinch (a), a prismatic 3-finger grasp (d), a tripod grasp (g) and a parallel extension grasp (j) are shown together with corresponding trajectories in synergy space (b, e, h, k) and generated, human-like grasp force patterns (c, f, i, l), force contact points are highlighted in green (adapted from (Starke et al., 2021) ©2021 IEEE)

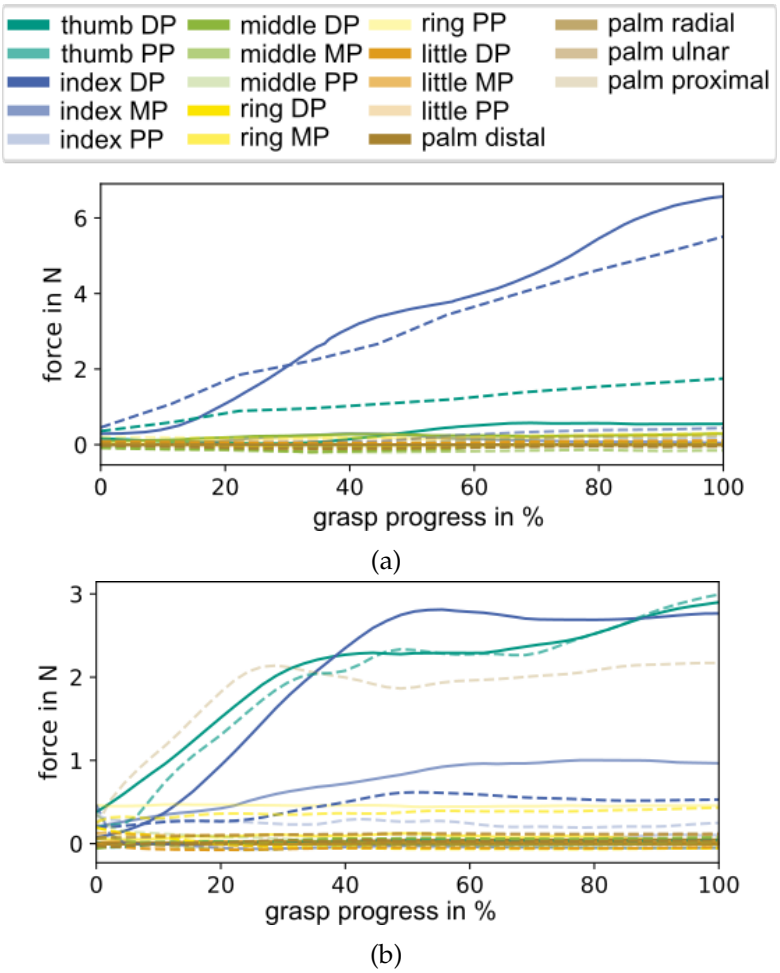

Figure 4.16: Human-like temporal force patterns of palmar pinch grasps generated from the static (a) and dynamic (b) synergy spaces, both depicted in dashed lines, solid lines show an exemplary human demonstration of the same grasp type (Starke et al., 2021) ©2021 IEEE

index finger, as expected in a palmar pinch grasp. The proximal palmar force generated by the dynamic synergy space is situated at the ball of the thumb, thereby contributing to the force applied by the thumb. The examples generated from both synergy spaces show plausible, human-like grasps while notably varying from the given human observations. Fig. 4.17 shows the final grasp force configurations of three different grasps generated from the dynamic force synergy space. Grasp contact forces are visualized using the Master Motor Map's model of the human hand (Mandery et al., 2016) with contact locations marked in red.

(a) (b) (c)

Figure 4.17: Grasp force configurations generated from the dynamic synergy space for a parallel extension grasp (a), a palmar pinch (b) and a power small diameter grasp (c), visualized on a simulated human hand with normal force contact areas highlighted in red (Starke et al., 2021) ©2021 IEEE

4.3.4 Evaluation

Both force synergy spaces are evaluated regarding their ability to represent temporal grasp force patterns demonstrated by humans. Further, the grasp quality of generated grasp normal force configurations from the dynamic force synergies is assessed.

To evaluate the validity of both force synergy representations, all human demonstrations from the handover study are mapped into synergy space. The **reproduction error** caused by the retrieval of temporal force patterns from the synergy trajectories is shown in Fig. 4.18. Over all grasps, the reproduction error in the static synergy space amounts to $0.32\,\mathrm{N}$ being $0.98\,\%$ of the maximum grasp force of $32.4\,\mathrm{N}$. For the dynamic force synergies, a reproduction error of $1.99\,\%$ or $0.65\,\mathrm{N}$ is measured on the data of the test set. As depicted in Fig. 4.18, the reproduction error between different grasp types varies equally for both synergy representations. Precision grasps like the tripod and palmar pinch are very well defined in the distribution of contact points and the relation of forces applied to the object. Therefore, they exhibit particularly low reproduction errors. In contrast, power grasps require a higher number of contact points. Hence, the variance within grasp forces is naturally higher for power grasps, as force coordination depends on the task and object shape. Overall, the static synergy space has a lower reproduction error for grasp force patterns observed from human demonstration, while both synergy representations prove to be generally able to represent human grasp force patterns.

To analyze the validity of grasps represented in the dynamic synergy space, their grasp quality is assessed in **grasp simulation**. To this end, the final grasp

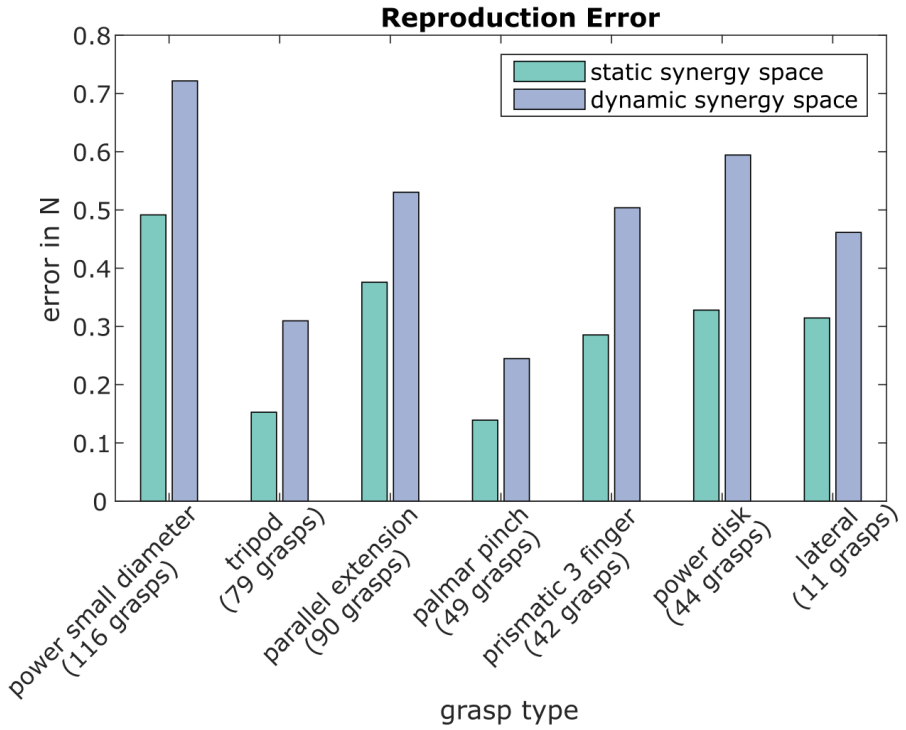

Figure 4.18: Reproduction error of grasp force patterns from human demonstration for both synergy representations and different grasp types (Starke et al., 2021) ©2021 IEEE

normal force patterns $\mathbf{f}(T)$ from the dynamic synergies $\widetilde{\mathbf{s}}(T)$ are simulated on the hand of the model of the Master Motor Map (Mandery et al., 2016) in the grasp simulator Simox (Vahrenkamp et al., 2010). In total, 75 grasps on nine different objects used in the human handover study are simulated. To apply the force patterns, kinematic hand postures and the relative positioning of the hand with respect to the object are directly taken from the human grasp recordings. Hand postures are optimized with respect to the defined grasp contact points to compensate inaccuracies in the recorded postural human data. Optimization is performed by gradually closing the fingers until grasp contact is established. Further, the hand's position and orientation relative to the object is gradually varied. Among all valid grasps, which achieve the correct contact points, the best grasp quality is chosen. The same hand pose and grasp posture is applied to evaluate both the grasp forces from human demonstration as well as the synergy-generated forces. Therefore, an objective comparison of both grasp force patterns is achieved.

The **grasp quality** is measured with the metric ϵ (Ferrari and Canny, 1992). The resulting grasp quality for different grasp types is shown in Fig. 4.19. Overall, the grasp quality of synergy-generated grasps with $\epsilon = 0.338$ is similar to the

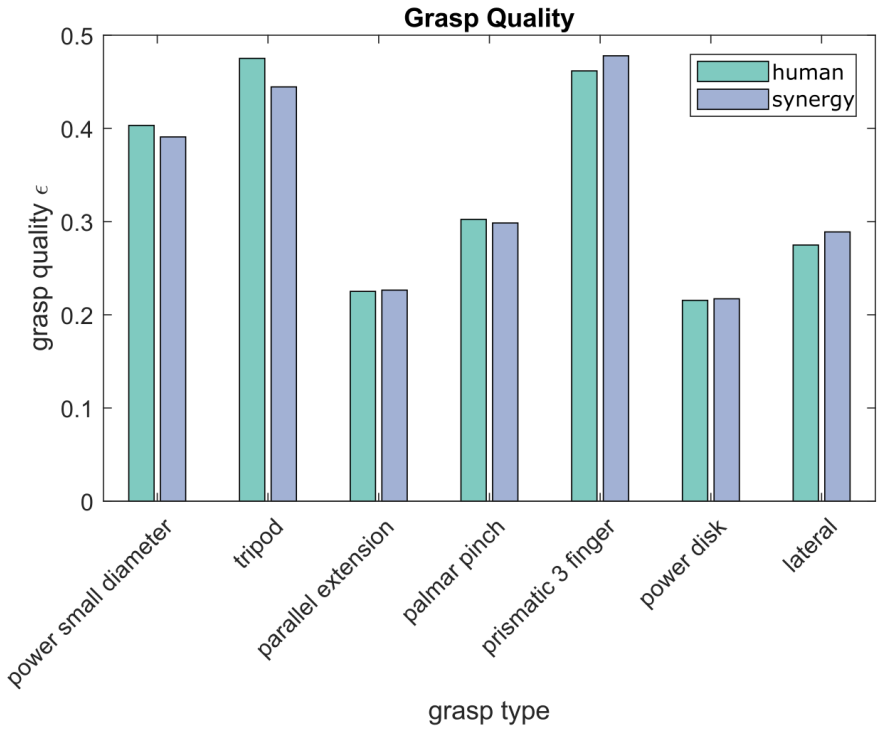

Figure 4.19: ϵ-quality of grasp force configurations demonstrated by humans and generated from the dynamic force synergy space (Starke et al., 2021) ©2021 IEEE

quality of human-demonstrated grasps with $\epsilon = 0.337$. Also considering different grasp types separately, there is no significant difference between human-demonstrated and syergy-generated, human-like grasps in terms of the grasp quality. However, there are notable differences in quality between the distinct grasp types. The tripod grasps and prismatic three finger grasps generally yield a higher grasp quality than the parallel extension grasp or power disc grasp for both human-demonstrated and synergy-generated grasps. These differences in grasp quality are caused by the high influence of the number of contact points on the ϵ-quality. In addition, the grasp quality is calculated assuming only point contact, which significantly simplifies the contribution of the palm in power grasps.

Overall, two novel synergy spaces are presented, that are able to represent and generate human-learned temporal contact force patterns in grasping. The static synergy space has a lower reproduction error than the dynamic synergy space. Therefore, trajectories in static synergy space are the preferable method to encode and represent human grasp demonstrations. However, the static synergy space has no inherent notion of time and the generation of new force patterns therefore requires hand-crafted synergy trajectories ensuring the feasi-

bility of the designed force progression. A comparison of grasp quality for human demonstrations and grasps generated by the dynamic synergies proves the functionality of the dynamic synergy space. Therefore, the dynamic synergies are preferable for the generation of new, human-like fore patterns due its inherent encoding of temporal grasp progress.

4.4 Summary and Conclusion

This chapter presented a thorough analysis of human grasp contact forces over a wide range of grasp types and objects. Based on correlations found in human grasping, static grasp force synergies are introduced. For the representation of temporally changing human grasp force patterns throughout the entire process of grasping, two methods for the description of time-dependent force synergies are presented. Besides the description of human grasps, these force synergies can also be applied in the control of human-like robotic hands. This thesis expands existing analysis and repesentation of human grasp forces in three main aspects:

- Correlations between grasp normal forces at different contact points are shown over a wide range of different grasp types. Human subjects in the grasp recordings could grasp spontaneously without any restrictions from the operator or the measurement setup regarding the grasp type and hand positioning.
- Static grasp force synergies are defined based on the correlations in human contact force patterns. These force synergies describe 18 grasp contact forces in an eight-dimensional synergy space.
- Two novel methods are proposed for the description of temporal force patterns. Time-dependent trajectories in a static synergy space allow an accurate, low-dimensional representation of temporal force patterns. A dynamic synergy space with an inherent notion of time allows the generation of new, human-like temporal grasp force patterns from the synergy space.

Correlations in human grasp contact force patterns have been shown in an open analysis of human grasping. Different from similar analyses in related works, this correlation analysis is not restricted to specific grasp types or special, sensorized objects. Instead, correlations can be proven in general over a wide range of spontaneous, unconstrained grasping actions.

Static grasp force synergies are defined based on the found force correlations. Similar to the basic postural synergies (Santello et al., 1998), the force synergies are learned by a PCA applied on human static grasp force patterns of stable grasps. The resulting synergy space describes 18 contact forces in eight dimensions.

Time-dependent force synergies are presented to describe entire temporal force patterns up to the final static grasp. Based on methodology used for kinematic synergies Romero et al. (2013), temporal force patterns are described as time-dependent trajectories in a static force synergy space, that has no notion of time by itself. In a second approach, a dynamic synergy space is learned from entire temporal force patterns by an LSTM-autoencoder. It encodes the temporal progression of grasp forces in the synergy space and additionally enforces a clustering of grasp types.

The **evaluation** shows that grasp types can be classified based on their static grasp force pattern and hence are relevant for the distribution of grasp contact forces. The structure of the eight-dimensional static force synergy spacehowever, does not show any clustering of grasp types. Even so, the static synergy space is able to accurately represent human grasp force patterns. Similarly, also temporal force patterns can be represented by a static synergy space with an error of less than $1\,\%$ of the maximum grasp force. The dynamic synergy space allows for a direct encoding of grasp progress and can be used to generate new, human-like temporal force patterns that result in a grasp quality similar to human-demonstrated grasps.

CHAPTER 5

Semi-Autonomous Grasping

The grasp synergies in this work enable a simplified, human-like control for humanoid hands. Such control is applied on robotic prosthetic hands, which combine the requirements of versatile, human-like grasping and simple, yet reliable grasp control. This chapter presents three contributions of this thesis.

1. The postural synergies are applied on the female KIT Prosthetic Hand (Weiner, Starke, Rader et al., 2022; Weiner, Starke et al., 2018) to grasp objects from daily life. While this robotic prosthesis simplifies grasp control by mechanical intelligence using an adaptively underactuated mechanism to drive the four fingers, the synergy-based control considers the coordination of thumb and fingers within the grasp to enhance grasp stability. Further, the object size is considered in the synergy-based generation of human-like grasps, enabling customized, object-specific grasp apertures.
2. A human grasp library is defined based on human grasp demonstrations, that allows the transfer of human grasping motions onto humanoid robotic or prosthetic hands. This includes the generalization and adaptation of robotic grasp trajectories based on different object characteristics. A fingertip trajectory mapping is applied to transfer human power grasp trajectories to a prosthetic hand. Complemented by a trajectory of the hand orientation, which is also extracted from human demonstration, a database of human grasps on a wide variety of object shapes and sizes is

defined, including different approach directions of the hand. The grasps in the human grasp database can be adapted with respect to the final grasp aperture. In addition, an object database is defined, which provides information on shape and fragility characteristics of objects of daily life.

3. A novel semi-autonomous prosthetic control is designed based on continuous human grasp trajectories. It aims at simplifying prosthetic control for the user by automating parts of the grasping process. Thereby, the number and frequency of control signals directly issued by the user is reduced, while keeping the user in control of the prosthesis. In comparison to the state of the art, this is the first semi-autonomous control that does not only provide static preshape and grasp postures, but a continuous and coordinated control of the hand closing motion as well as the wrist orientation. This allows a seamless coordination of all DoF of the prosthetic hand throughout the entire grasp execution. A user study proves the intuitiveness of the human-learned semi-autonomous grasp control, while users still feel in control of their prosthetic hand.

The work described in this section was presented in a journal publication ((Starke, Weiner et al., 2022)). Graphs and images are partially adapted from this publication.

5.1 Myoelectric Hand Prostheses

Prosthetic hands provide a replacement for a missing or lost human limb to independently master daily life. Very simple, cosmetic prostheses cannot perform any grasping motions and only provide an optical replacement of the missing hand. Movable prosthetic hands, that are able to partially replace the human hand's grasping abilities can be either driven by muscle power or or be electrically powered. Body-powered prosthesis harness remaining human motion capabilities, usually by the shoulder, to actuate the hand's grasping motion over mechanical or hydraulic force transmission as for example presented in (Smit et al., 2015). These body-powered prostheses provide a direct and robust, but less intuitive control applying a motion coupling between the hand and other parts of the human body.

In contrast, **myoelectric prosthetic hands** are driven by electric motors with a power supply directly integrated into the prosthetic shaft. The user does not need to power the prosthetic motion, but merely needs to control the hand with the use of myoelectric muscle signals measured on the muscles of the remaining

stump. (Belter et al., 2013) gives an overview of commercial myoelectric hand prostheses and (Piazza et al., 2020) presents a survey of humanoid robotic and prosthetic hands in research. Myoelectric prostheses are controlled by the muscles originally actuating the human hand, with the aim of an intuitive control interface. However, the robust generation and detection of control signals is difficult due to changing stump conditions including temperature variations and sweat. In addition, arm muscles can degenerate after the loss of the limb or might be affected by injuries or deformity themselves. Therefore, the bandwidth of myoelectric control signals is very limited in commercial prosthetics and varies significantly among prosthesis users. Meanwhile, the kinematics and grasp functionality of prosthetic hands become increasingly versatile. Consequently, the necessity for simple, yet reliable control of highly complex systems arises. Therefore, prosthetic research focuses on adaptivity and automation of prosthetic mechatronics as well as advanced myoelectric signal decoding to provide simple control for the increasingly complex prostheses.

The **KIT Prosthetic Hand** (Weiner, Starke et al., 2018; Weiner, Starke, Rader et al., 2022) is used as a platform for the human-learned grasp control presented in this work. This prosthesis aims to implement grasping intelligence in hardware as well as provide sensorization and computing power for intelligent grasp control. The hand is designed to be personalizable in size and functionality and has been built in two different versions with the size of an average male and female hand. The prosthetic hand can be connected to a self-experience shaft to be worn below a person's able hand. This allows the evaluation of prosthetic grasp control with able-bodied subjects. The mechanics of hand and self-experience shaft are shown in Fig. 5.1.

The **actuation** of the prosthesis consists of two motors driving the fingers (blue) and the thumb (red) individually. The wrist pronation and supination is driven by a third motor (green) integrated into the self-experience shaft. While thumb and wrist rotation are directly actuated, the four fingers are driven by a single motor over an adaptive underactuation mechanism. The mechanism distributes the force evenly over all four fingers and allows the continuation of the closing motion even if individual fingers are blocked. By these means, the fingers mechanically adapt to the object's shape without any software control.

Further, the prosthesis features a **sensor setup** including an inertial measurement unit (IMU), a distance sensor and a camera for environmental perception as well as a high-performance embedded system for resource-aware intelligent scene understanding and grasp control. The components for sensing and com-

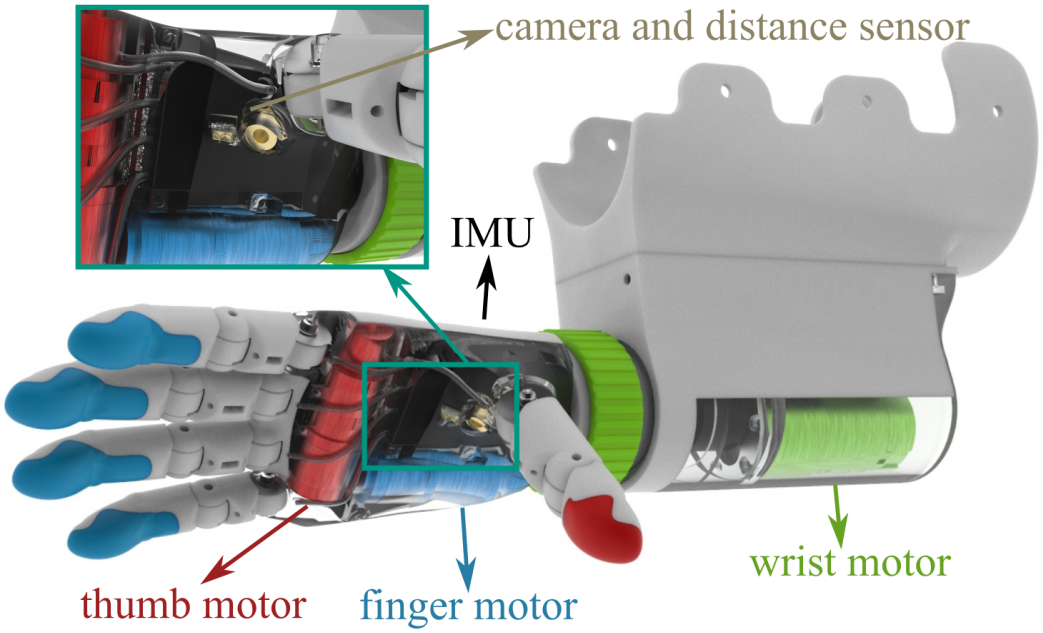

Figure 5.1: Actuation and sensorization of the KIT Prosthetic Hand, each degree of freedom is marked by one color (Starke, Weiner et al., 2022) © CC BY 4.0

putation are embedded into the palm. A display on the back of the hand can provide feedback to the user of the prosthesis.

5.2 Grasp Synergy Mapping and Control

To easily control human-like grasping, grasps generated by the adaptable postural synergies from Section 3.1 are applied on the KIT Prosthetic Hand. Due to the fixed thumb opposition of the prosthesis, only four of the five learned grasp types can be considered. These four grasp types are *cylinder* grasps, *spherical* grasps, *disk* grasps and *pinch/tripod* grasps. *Lateral* grasps, that require thumb adduction, are therefore excluded. Further, the prosthesis control is focused on power grasps due to the joint underactuation of all four fingers. While precision grasps cannot be directly executed, they can still occur when only some of the fingers get in contact with a small object. Therefore, *pinch/tripod* grasps are considered, but evaluated separately since the prosthesis does not allow the accurate implementation of these grasps. For each grasp type, grasps on all ten objects used in the static grasping study (subsection 3.1.2) are generated from the adaptable postural synergy space. Further, grasps on three novel household objects from the KIT Object Database (Kasper et al., 2012) and the YCB Object Set (Calli et al., 2015) are generated, that were not used in training of the synergy network. These additional objects are the coke bottle, fizzy tablets

and canned meat for the cylinder grasp, the pear, strawberry and plum for the sphere grasps, the chips, water glass and powdered sugar for the disk grasps and the bandaid package, rusk and green soup for the pinch grasps. The diameters of all new objects are within the range of the demonstrations of the static grasping study.

For **pose and motion mapping** from the generated, 16-dimensional hand configurations onto the two *degrees of actuation* (DoA) of the prosthesis, mutually actuated joints are summarized. The thumb motor is actuated according to the mean joint angle of the thumb CMC, MCP and IP joints. The average of the MCP and PIP joint angles of index, middle, ring and little finger is applied on the finger motor. All abduction angles and the palm arch are discarded, since these joints are fixed for the prosthetic hand. The desired joint angles for thumb and fingers are transferred to the position of the respective motor by calculating the relative joint angle with respect to the fingers full range of motion. This relative joint angle closure is then mapped to the relative motor position with respect to the range between the fully opened and fully closed hand state. The postural synergies only provide a static grasp posture. This target position is approached using a cascaded position and velocity control with a PI-controller for the position and a P-controller for the velocity. The controller gains are experimentally tuned to $K_P = 0.5$ and $K_I = 10^{-6}$ for the position control and $K_P = 100$ for the velocity control. The velocity controller is further capped at $4.25\frac{\text{turns}}{\text{s}}$ for the thumb and $6,37\frac{\text{turns}}{\text{s}}$ for the fingers.

The **postural synergies** are evaluated on the prosthetic hand regarding the grasp success and quality. The prosthesis is worn by the experimenter using the self-experience shaft. Objects are placed one by one on a table at chest height for the standing experimenter. Grasp commands are issued with a smartphone that is connected to the prosthesis via bluetooth. Grasp execution and motor control are computed directly on the embedded system integrated into the prosthetic hand. The objects are grasped from the table with the hand positioned manually in the direction promoting the desired grasp direction and type. Inspired by the YCB Gripper Assessment Protocol by (Calli et al., 2015), objects are lifted and held for $3\,\text{s}$, then rotated by $90°$ and held for another $3\,\text{s}$. Rotation is performed in the most critical direction, i. e. for a side grasp, the hand is rotated into a top grasp with the open fingers held downwards and for a top grasp, the hand is rotated sideways into a side grasp. If the object can be grasped and lifted from the table, one point is given. Another point is added for lifting the object without any motion within the hand. If the object stays within the hand, another point is scored and a last point is given for rotating the hand without

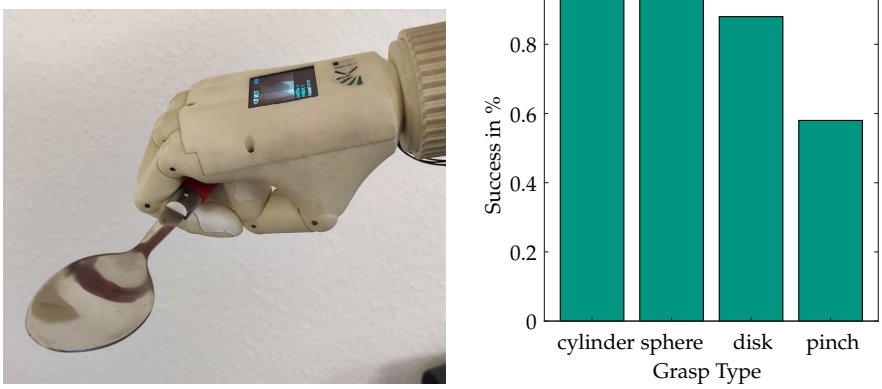

(a) (b)

Figure 5.2: Cylindrical power grasp on a spoon generated by from the postural synergies (a) and grasp success of synergy-generated human-like grasps (b)

any motion of the object within the hand. In total, four points can be achieved per grasped object.

Overall, a **grasp success rate** of $84.9\,\%$ (177 points out of 208) is achieved by the evaluated grasp control learned based on the postural synergies. An example of a cylindrical power grasp generated from the postural synergies and executed on the prosthetic hand is shown in Fig. 5.2 a). As can be seen in Fig. 5.2 b), the grasp success rate is significantly lower for pinch grasps, since these are applied on smaller, more difficult objects and cannot be directly executed with the underactuated prosthetic hand. For power grasps of the cylinder, sphere and disk grasp types, a success rate of $94.0\,\%$ (147 points out of 156) is achieved. This shows, that functional human-like grasps can be generated from the postural grasp synergies and can be applied in the grasp control of robotic prosthetic hands.

5.3 Human Grasp Database

A continuous and coordinated grasp motion is important both for fast and successful grasp execution as well as human-like, predictable grasping behavior. This implies the simultaneous control of all degrees of actuation of a robotic prosthesis. Commercially applied sequential control schemes control grasp characteristics like the wrist orientation, hand preshape defining the grasp type and the hand closing motion in an ordered sequence of isolated actions (Farina et al., 2014). This slows down the grasping process and visibly isolates its different

parts, since the prosthesis stops all motion when switching from one control phase to the next. In addition, such sequential control does not use the potential emerging from the coordinated interplay of motions in different joints for grasp success. Especially for thin or hard to reach objects, it might be beneficial to continuously rotate the hand throughout the finger closing to slide the fingers between the object and an environmental surface, e. g. from the supporting table, as has been done for a robotic hand in (Della Santina et al., 2019). To achieve such coordinated, continuous grasp motions, timed simultaneous control of all degrees of actuation of the prosthetic hand needs to be achieved.

To this end, a human grasp **database** is built. 510 grasps were demonstrated by five subjects on 29 different household and workshop objects. The objects are chosen to span a wide variety of sizes and shapes including cylindrical and spherical objects, boxes, handles and specific shape variations like a banana, a pear or a bowl. Subjects wear a sensorized glove measuring the finger joint angles (CyberGlove III, Cyber Glove Systems Inc.) and an IMU at the back of the hand to measure the wrist orientation. By these means, the human grasp recordings include all DoF present in the prosthetic hand. Subjects were seated comfortably in front of a table and the objects were placed one by one on top of the table. All objects were grasped from the top and the side if their size allowed both approach directions. For flat or spherical objects, only a top grasp was demonstrated. Fig. 5.3 shows two exemplary human grasp demonstrations. All human grasp recordings are available on the KIT Whole Body Human Motion Database by (Mandery et al., 2016) [1].

To use these human grasp demonstrations for the control of the prosthetic hand, the grasps are generalized and transferred to the prosthesis kinematics. In a second step, grasp motions are segmented into a pregrasp and grasp phase to be applied within an interactive semi-autonomous grasp control. These human-learned grasp strategies for prosthetic hand control form a human grasp database as the first part of a human-learned, semi-autonomous grasp control for prosthetic hands.

5.3.1 Grasp Generalization

The recorded set of human grasp demonstrations for a single object and approach direction need to be generalized and transferred to the prosthetic hand. The latter is done by an endpoint mapping, similar to the approaches by (Ek-

[1] `https://motion-database.humanoids.kit.edu/`

(a) (b)

Figure 5.3: Grasps demonstrated by a human on a banana (a) and the handle of a pitcher (b)

vall and Kragic, 2004) and (Peer et al., 2008). The method applied for grasp generalization and transfer is listed in Alg. 1 for the example of the finger trajectory. The thumb and wrist trajectories are generated in a similar way. For the finger motion, the human middle finger trajectory serves as demonstration for the mapping. In the recorded power grasps, the middle finger forms the central of the second virtual finger, as defined by (Iberall, 1997), and is therefore representative for all four fingers controlled by the underactuated mechanism in the prosthetic hand. Hence, the fingertip trajectories of the middle finger $\mathbf{p}_i(t)$ are given for all subjects i over the time of the entire grasping process $t \in [0, T]$ ending with the final grasp posture at time T. In addition, the length of the middle finger l_i of each subject i is required to normalize the fingertip trajectories with respect to the hand dimensions. Both parameters are summarized in a tuple $H_o := (\mathbf{p}_i(t), l_i)$ for each object o and all subjects i. In addition, the fingertip closing trajectory of the prosthetic hand $\mathbf{p}_{prosthesis}(t)$ is extracted from a video recording of the hand closing at constant speed.

A **normalization** of all human grasp trajectories over the finger length is performed in Alg. 1 Line 4. Further, grasp motions are also normalized over the execution time in Alg. 1 Line 9. By finding the average over all human demonstrations in Alg. 1 Line 12, a generalized human grasp trajectory is calculated. The points of this generalized human trajectory are mapped to the prosthesis by finding the closest point that lies on the prosthesis trajectory and is therefore reachable for the prosthetic hand in Alg. 1 Line 15. Finally, the resulting human-learned trajectory for the prosthetic hand $\mathbf{p}_{mapped}(t)$ is stored in the human grasp database.

Algorithm 1 Fingertip Trajectory Mapping (Starke, Weiner et al., 2022) © CC BY 4.0

Require: $H_{obj}, \mathbf{p}_{prosthesis}(t)$

$P_{obj} := \emptyset$
$t_{max} := 0$
for all $(\mathbf{p}_i(t), l_i) \in H_{obj}$ **do**
    $P_{obj} = P_{obj} \cup \text{NORMALIZE LENGTH}(\mathbf{p}_i(t), l_i)$
    $t_{max} = \text{MAX}\ (t_{max}, \text{LENGTH}(\mathbf{p}_i(t)))$
end
$\widehat{P}_{obj} = \emptyset$
for all $\tilde{\mathbf{p}}_i(t) \in P_{obj}$ **do**
    $\widehat{P}_{obj} = \widehat{P}_{obj} \cup \text{NORMALIZE TIME}(\tilde{\mathbf{p}}_i(t), t_{max})$
end
for $\tau := 0$ to t_{max} **do**
    $\mathbf{p}_{mean}(\tau) := \frac{1}{|\widehat{P}_{obj}|} \cdot \sum_{\widehat{\mathbf{p}}_i(t) \in \widehat{P}_{obj}} \widehat{\mathbf{p}}_i(\tau)$
end
for all τ **do**
    $\mathbf{p}_{mapped}(\tau) :=$ NEAREST NEIGHBOUR$(\mathbf{p}_{mean}(\tau), \mathbf{p}_{prosthesis}(t))$
end
return $\mathbf{p}_{mapped}(t)$

The grasp in the database consist of **simultaneous and coordinated motions** of thumb, fingers and wrist orientation over the entire grasping process. Fig. 5.4 shows a generalized, human-learned grasp trajectory on the handle of a pitcher from the human grasp database. By these means, the potential of hand reorientation throughout the finger closing is exploited. The corresponding prosthesis motor trajectories for the same grasp are also shown in Fig. 5.4. This representation clearly shows that both finger and wrist start moving simultaneously early on in the grasping motion. The wrist motion only stops after the fingers are more than halfway closed. Further, it can be seen that the fingers close with a varying speed, thereby achieving a different grasping behavior than using a conventional constant-velocity control.

A **temporal alignment** with the user's reaching motion needs to be enabled within the continuous human-learned grasp motions to apply them in prosthetic grasp control. To this end, a segmentation in pregrasp and final grasping motion is performed in a pre-processing step. This provides the user with a pregrasp motion to help aligning the grasp, but allows to pause the grasp in a preshaping state, if the user has not yet finished approaching the object. To find the correct segmentation time t_{seg}, the velocities of the tip of the fingers

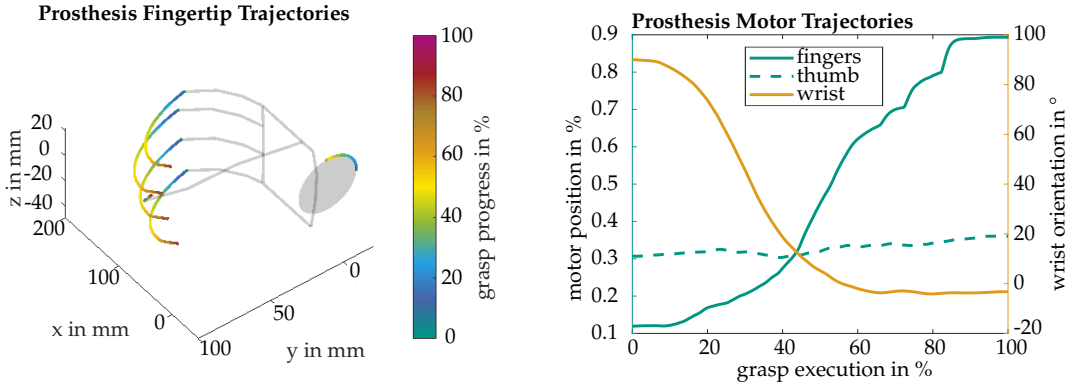

(a) (b)

Figure 5.4: Grasping motion on the handle of a pitcher learned from human demonstration, it shows the temporal progress of finger and wrist motions (a) as well as the corresponding motor trajectories on the prosthetic hand (b) (Starke, Weiner et al., 2022) © CC BY 4.0

Algorithm 2 Pregrasp Segmentation

Require: $v_{fingers}(t), v_{thumb}(t), v_{wrist}(t), v_{thresh}$
1: **if** $\text{MAX}(v_{wrist}(t)) > v_{thresh}$ **then**
2: $t_{max_w} :=$ *find* τ *where* $v_{wrist}(\tau) = \text{MAX}(v_{wrist}(t))$
3: $t_{seg} :=$ *find minimal* τ *where* $\tau > t_{max_w}$ *and* $v_{wrist}(\tau) \leq 0$
4: **else**
5: $v_{hand}(t) = \dfrac{v_{fingers}(t) + v_{thumb}(t)}{2}$
6: $t_{max_h} :=$ *find* τ *where* $v_{hand}(\tau) = \text{MAX}(v_{hand}(t))$
7: $t_{v=0} :=$ *find maximal* τ *where* $\tau < t_{max_h}$ *and* $v_{hand}(\tau) \leq 0$
8: $t_{seg} := t_{v=0} + 0.2(t_{max_h} - t_{v=0})$
9: **end**
10: **return** t_{seg}

$v_{fingers}(t)$, the tip of the thumb $v_{thumb}(t)$ and the angular velocity of the wrist $v_{wrist}(t)$ are considered. The outline of the applied segmentation is illustrated in Alg. 2. One highly important goal of the pregrasp motion is to have a correct orientation of the palm towards the object. Hence the wrist orientation needs to be set according to the approach direction of the hand within the pregrasp. To ensure this, the segmentation time is mainly determined by the wrist velocity. In case of top grasps, first the timestep t_{max_w} with the maximum wrist velocity is determined in Alg. 2 Line 2. The segmentation time t_{seg} is chosen as the first point in time where the wrist stops after t_{max_w} in Alg. 2 Line 3.

In the case of a side grasp, however, the wrist does not need to be reoriented significantly and its velocity does not exceed v_{thresh}. The wrist velocity is therefore not a sensible measure of grasp progress in this case. To nevertheless segment

the grasp motion, finger closure is considered. For preshaping, the fingers need to adopt the shape of the object to enhance the predictability of the grasping process that follows and ease the hand-to-object positioning for the user. At the same time it is crucial that the fingers are still opened wide enough to be moved around the object without touching it. The segmentation in these cases, is based on the finger and thumb motion trajectory, stopping the pregrasp motion at $20\,\%$ of the time before the maximal closing velocity is reached, as shown in Alg. 2 Line 8. Thereby, the hand closing motion is kept mostly within the final grasp trajectory.

Altogether, the human grasp database provides human-learned grasping motion on a variety of common objects. Grasp motions are transferred to the prosthesis kinematics based on several demonstrations from different human subjects. The grasp in the database include a continuous and simultaneous motion of the wrist and fingers of the prosthesis. Coordinated motor trajectories for the preshape and grasp phase of these grasp motions learned from human demonstration can therefore be queried from the database for the control of the prosthetic hand.

5.4 Prosthetic Grasping

Myoelectric prosthetic hands provide a functional replacement for a missing human limb, that is internally powered and does not rely on the user's force, as opposed to body-powered prostheses. Hand actuation is driven electrically with the motors and battery for power supply directly integrated into the prosthetic hand and shaft. The user can control the motion of such myoelectric prosthetic hands using the muscles in their remaining forearm stump, that were originally driving the strings of the human fingers. Commercial myoelectric hands most commonly rely on two *electromyographic* (EMG) electrodes, that measure the activation of the main flexor and extensor muscle strands along the forearm (Farina et al., 2014). In research, multi-electrode setups covering a wider range of muscles and monitoring points along the forearm, as well as partially automated grasp control are applied to simplify the control task for the user. A comprehensive overview of this field of research is given in Chapter 2.

The field of **semi-autonomous grasp control** strives to partially automate the grasping process and thereby reduce the amount of control needed based on direct user inputs. At the same time, the user should still keep in control of their

prosthetic device and should be able to manually influence the grasping process at any time. By these means, the dependency on direct, reliably measured user inputs is reduced without taking the control away from the user. This is especially helpful for users with bad stump conditions or a poorly fitting socket, who have difficulties in producing accurate muscular control signals.

In this thesis, **continuous grasp motions**, that are learned from human demonstration, are used to provide an automatic low-level control of the correlated finger and wrist motion throughout a grasp on the KIT Prosthetic Hand. Complemented by environmental information and high-level user commands, a semi-autonomous grasp control is developed that enables fluent grasp motions with only two direct user inputs. The semi-autonomous control scheme is evaluated in a user study in comparison with a conventional EMG control. Results show that the semi-autonomous control reduces the physical and mental demand for the user while allowing faster and more intuitive grasping. It is the first semi-autonomous control scheme that provides a continuous, coordinated grasp motion of wrist and fingers directly learned from human demonstration.

5.4.1 Semi-Autonomous Control

The semi-autonomous grasp control combines knowledge gained by proprioceptive and environmental sensing with continuous grasp strategies learned from human demonstration to simplify grasp control for the user. It has been developed in joint work of several researchers, the contribution of this thesis is the autonomous grasp execution learned from human demonstration, that is supervised by the user. A graphical representation of the incorporation of human-learned grasps into this prosthetic control is shown in Fig. 5.5. The procedure of the semi-autonomous control scheme is presented in Fig. 5.6. A diagram of the control architecture is shown in Fig. 5.7.

The **general idea** of our semi-autonomous control is to enhance the user's control input with the human grasp database and environmental sensor information. Both the sensing capability as well as the database are locally implemented on the prosthetic hand without any dependency on external computing power or resources. To **start** the semi-autonomous control, the user takes an image of the object to be grasped using the camera integrated into the palm of the prosthetic hand. The image recording and subsequent recognition of the object is triggered by a single EMG signal from the user. The object recognition

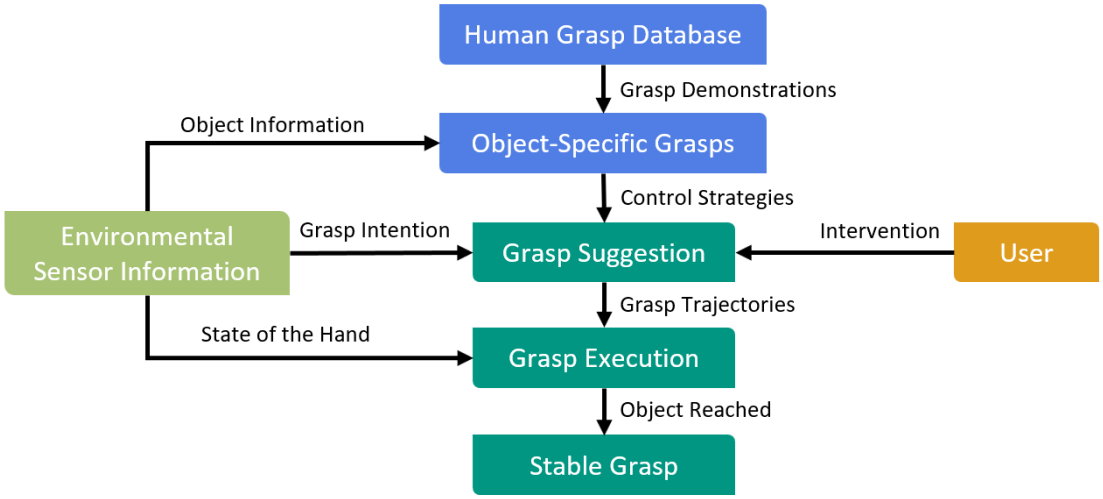

Figure 5.5: Procedure of the interactive prosthetic control based on human-learned grasping motions from the human grasp database

is performed by a neural network directly running on the processing system within the prosthetic hand (Hundhausen et al., 2019). After the object is recognized, specific object information is retrieved from an object database including the object class, the fragility and weight of the object. Based on the determined object class, available human demonstrations of object specific grasps are queried.

For **grasp suggestion**, one of the available grasps is picked based on the user intention. With an IMU the hand orientation is measured allowing to draw a conclusion on the grasp approach direction (top or side) intended by the user. A

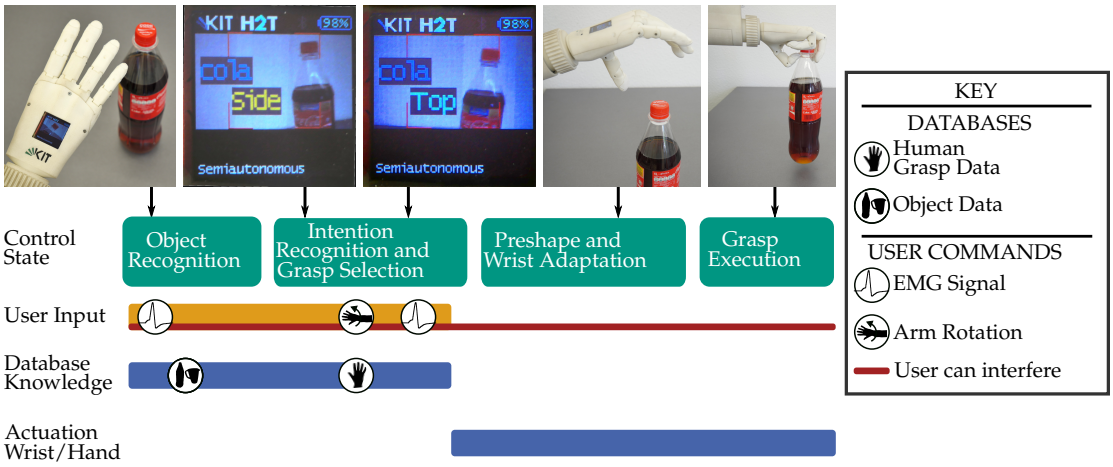

Figure 5.6: Flowchart of the semi-autonomous control depicting the different control states, user control inputs, the knowledge queried from databases and the hand's motion (adapted from (Starke, Weiner et al., 2022) © CC BY 4.0)

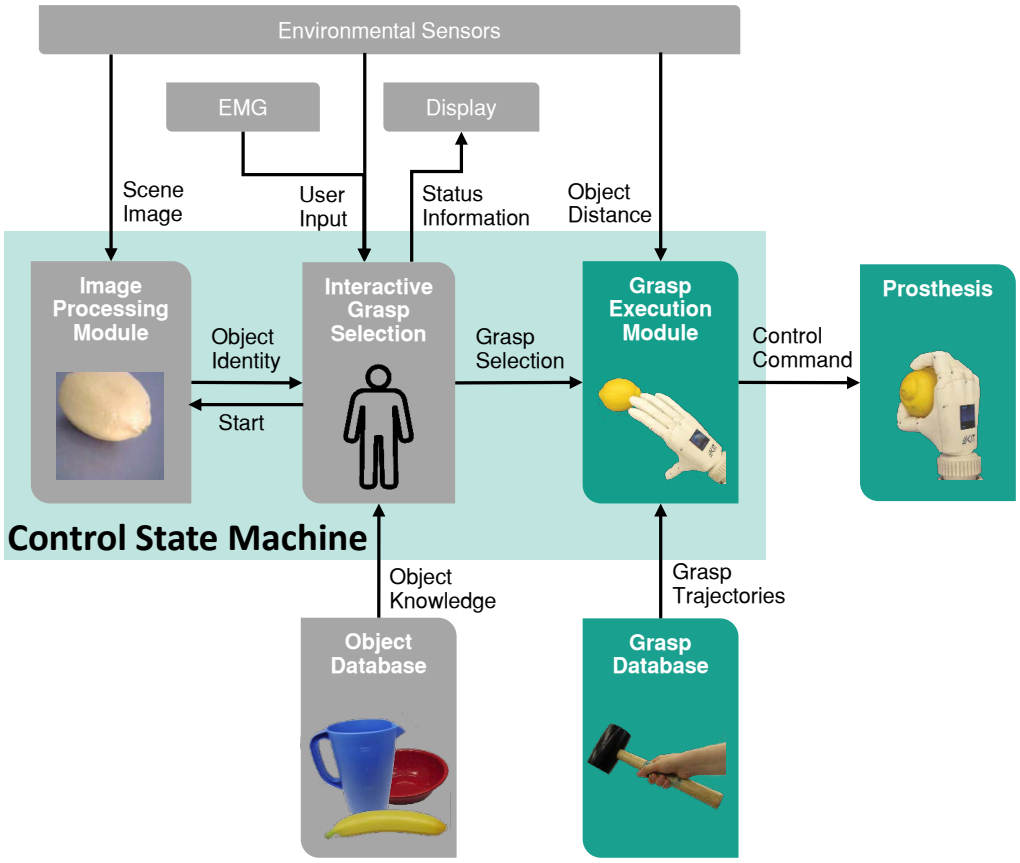

Figure 5.7: Architectural diagram of the semi-autonomous control with the control state machine including image processing, interactive grasp selection and grasp execution; the control uses information from sensors and databases to control the grasping motion of a prosthetic hand (adapted from (Starke, Weiner et al., 2022) © CC BY 4.0)

top grasp is chosen for a horizontal hand orientation while a rotation of $\geqslant \pm 15°$ commands a side grasp. This allows the intuitive differentiation of the grasp direction based on the inceptive approach performed by the user. Based on the intended grasp direction, a grasp control strategy can be chosen from the set of object-specific grasps from the human grasp database and the grasp can be suggested to the user on a display at the back of the prosthetic hand. The user is able to change the grasp direction by rotating the prosthesis or switch the suggested object by a quick shaking motion. The user can accept the suggested grasp with a single EMG signal.

During **grasp execution**, the corresponding motor trajectories for the preshape motion are performed on the prosthetic hand. The hand's state is continually monitored and the wrist orientation is adapted to compensate user-induced ro-

tations of the prosthetic hand. By these means, the correct orientation of the wrist is ensured irrespective of any rotations of the user's arm throughout the reaching motion. This prevents the need for uncomfortable compensatory shoulder motions for the user and allows them to approach the object with a comfortable arm motion.

Grasp closing is started once the hand reaches the object. This is detected using the distance sensor in the palm of the hand. As soon as the distance to the object falls below a predefined threshold, the final grasping motion is triggered without the need for any additional user commands. The grasping motion is then continued from the preshape pose and the fingers wrap around the object. Finally, a constant grasp force is applied on the object, which is defined based on the object's fragility known from the object database. By these means, a stable grasp is performed and the object can be securely lifted.

An **intervention by the user** is possible at any time throughout the entire grasp execution by quickly shaking the prosthetic hand. This aborts the grasping process and the hand returns to a relaxed open posture. The semi-autonomous control can then be started from the beginning by taking an image of the object to be grasped. Overall, the user only needs to provide two direct control inputs issued over the same EMG channel to use the semi-autonomous control. User intention is further indirectly assessed using the IMU measurements and a continuous, grasping motion learned from human demonstration is automatically executed supervised by the user.

5.4.2 Evaluation

The semi-autonomous control scheme is evaluated in a user study with 20 able-bodied participants. Half of the nine female and eleven male subjects had a background in robotics, five had no technical background at all. None of the subjects had experience with prosthetics or EMG control. To assess the merit of the semi-autonomous control scheme, it is compared to a conventional sequential control scheme used by commercial prosthetic hands as well as a hybrid approach.

- The *conventional sequential control* (CSC) is fully driven by EMG commands triggered by the user and is also applied in commercial hand prostheses as for example described by (Farina et al., 2014). It consists of two control modes driving the wrist rotation and hand closing respectively. In wrist rotation mode, the user can execute a clockwise rotation of the hand by

activating their extensor muscles and a counterclockwise rotation with the flexor muscle activation. For hand closing mode, the closing of the prosthesis is mapped to flexor muscle activation, while extensor muscle activation causes the fingers to open. Finger closing and opening or wrist rotation are performed at constant speed as long as the respective EMG electrode is activated. A muscle co-contraction triggers switching between the two control modes. This co-contraction is performed by simultaneously contracting flexor and extensor muscles. In order to execute a grasp, the user needs to activate the wrist rotation and the fingers sequentially. All motions are directly controlled by the user over two EMG electrodes at the forearm.

- The *semi-autonomous control* (SAC) autonomously executes a grasping motion learned from human demonstration under the supervision of the user, as explained in subsection 5.4.1. Triggered by an EMG signal, a grasp motion is suggested based on the information provided by an object and intention recognition system. The user can adapt or abort the suggested grasp by rotating or shaking the prosthetic hand without any targeted muscle contraction. Once the grasp is started by the user with a second EMG signal, a simultaneous grasping motion of wrist and fingers is executed autonomously, incorporating environmental sensor information. Therefore, there are only two active EMG control signals needed from the user to start the grasp, while the execution and coordination of the grasping motion is performed autonomously. The two EMG signals can be issued either by the flexor muscles, the extensor muscles or a cocontraction of both.
- The *hybrid semi-autonomous preshaping control* (SAP) provides an autonomous preshaping motion similar to the SAC. Again, the object detection is started by a first EMG signal and the grasp preshape is performed after the user accepts the grasp suggestion with a second EMG signal. Since the control of the temporal progress of the grasp execution is crucial, this hybrid approach leaves the timing of the grasping motion to the user. In contrast to the SAC, the final grasp motion is not automatically triggered and executed. Instead, the grasp motion starts when the user issues an EMG signal with a contraction of their flexor muscles. The motion continues as long as the flexor is contracted and the motion pauses whenever the user stops to provide an EMG flexor signal. By these means, the user is in full control of the start and continuation of the hand's closing motion. The closing trajectory of the prosthetic hand is still pro-

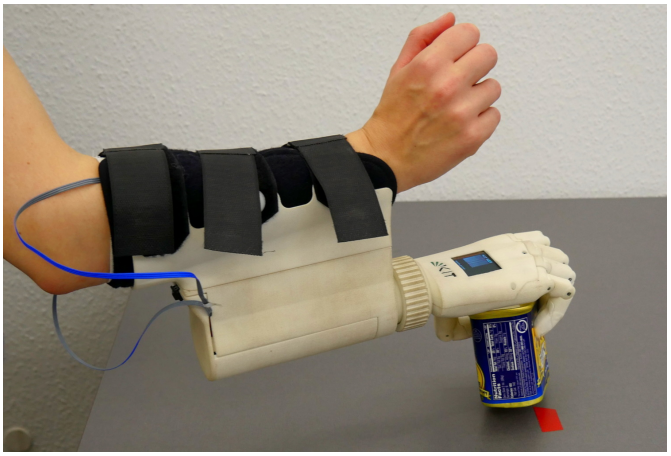

Figure 5.8: Study setup with an able-bodied subject wearing the prosthesis with a self-experience shaft while grasping a can of preserved meat (Starke, Weiner et al., 2022) © CC BY 4.0

vided by the human grasp database. Hence, the coordination of the finger and thumb motions as well as the wrist orientation is human-learned and autonomously controlled similar to the SAC.

In the **study procedure**, the subjects wear the prosthetic hand attached to the self-experience shaft below their own able hand, as shown in Fig. 5.8. Two EMG electrodes attached to the shaft were placed over the subjet's flexor and extensor muscles at the forearm and were calibrated regarding their sensitivity. Throughout all three control schemes, the same electrode calibration was kept. Subjects stood comfortably in front of a table with the object standing on top of the table before them. The prosthetic hand was placed on a mark on the table $13\,\mathrm{cm}$ to the right of the object.

For each control scheme, subjects got an explanation by the experimenter and were allowed to practice with an object not included in the study for $1\,\mathrm{min}$. Afterwards, twelve different objects were presented to the subjects in a randomized order. Subjects should perform both a top and a side grasp on the object, wherever the object allows for both approach directions. Otherwise, only a top grasp was performed. Subjects performed each grasp once, if the grasp failed, they were allowed a second trial. If the grasp failed a second time, it was marked as failed and excluded from the evaluation of grasp time. By these means, all three control schemes were evaluated in sequence. The order of the control schemes presented to each subject was varied in a counterbalanced crossover design. The order of objects was randomized between subjects but was kept constant for all three control schemes for the same subject.

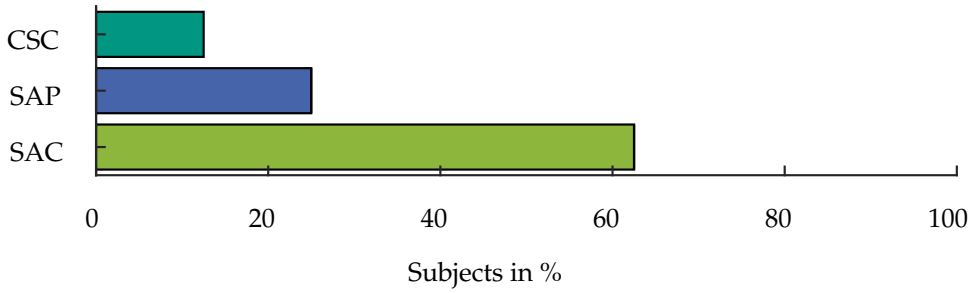

Figure 5.9: Preferred control scheme of the subjects in the user study (Starke, Weiner et al., 2022) © CC BY 4.0, most subjects prefer the presented semi-autonomous control scheme and the hybrid control with a semi-autonomous preshape and manual closing activation is ranked second

A number of **evaluation criteria** are gathered throughout and after the study. Throughout the user study, the grasping time and the EMG signals issued by the user were recorded. The grasping time was measured from a starting command given by the experimenter until the object was lifted from the table. A grasp was considered successful, if the object was held stably in the prosthesis for several seconds. For each control scheme, subjects completed a questionnaire directly after the experimental run. This questionnaire contained the NASA Task Load Index (NASA TLX) by (Hart and Staveland, 1988) to assess the user's workload, complemented with some additional questions on the intuitiveness, feeling of control and perception of feedback. After the entire study procedure including all three control schemes, subjects completed an additional questionnaire comparing the different control schemes.

Questionnaire results on **control scheme preference** show that $65.2\,\%$ of subjects prefer the SAC, as shown in Fig. 5.9. As depicted in Fig. 5.10 a), subjects further report an increase in intuitiveness of $30\,\%$ with the SAC compared to the CSC. This confirms the intuitiveness of the human-like grasping motions provided by the SAC.

The decrease in **workload** for both the SAC and the SAP compared to the CSC is statistically significant (Friedman's Anova[2] < 0.05) with a reduction of $45.1\,\%$ and $23.9\,\%$ respectively. This reduction of workload, shown in Fig. 5.10 b), is mainly caused by a reduced effort required to control the prosthesis and a reduced physical demand, as shown in Fig. 5.10 c) and d). The effort is significantly decreased from $75\,\%$ for the CSC to $40\,\%$ for the SAC. In the **physical demand**, an even larger decrease can be seen from $85\,\%$ to $25\,\%$ for the CSC

[2]The Friedman's Anova is a non-parametrical statistical test to measure the correlation between two variables.

and the SAC respectively. The objective **EMG measurements** support the subjective impression of the subjects. The integrated power of the generated EMG signal is presented in Fig. 5.10 e). Over the entire grasping process, the EMG power amounts to $203.7\,\mathrm{mV}$ in the CSC. Throughout the SAC, only $69.4\,\mathrm{mV}$ are measured. Therefore, the muscle power required to control the prosthetic grasp is reduced by $65.9\,\%$ by the SAC. By these means, grasp control becomes less exhausting for the user. Due to the need of only two explicit EMG control inputs, the SAC requires significantly less muscular power from the user than a conventional prosthesis control.

At the same time, no significant difference can be registered in the subjective **feeling of control**, as shown in Fig. 5.10 f). Despite the partial automation of the grasping process with only supervising control by the user, the SAC shows a perceived control of $62.5\,\%$, compared to $60\,\%$ with full control in the CSC. This indicates, that the human-like grasping motions provided by the SAC are intuitive for the user and thereby convey a direct feeling of control over the prosthetic device.

The **grasp execution time** is reduced from $9.8\,\mathrm{s}$ with the CSC to $8.4\,\mathrm{s}$ with the SAC in the median over all subjects and objects. One major factor for the grasping time in the SAC is the success of the visual object recognition. Since the object recognition is not part of this thesis, time needed for correcting a wrong object classification is excluded in the following, assuming ideal object information. Under this assumption, the median time for grasp execution with the SAC amounts to $7.9\,\mathrm{s}$. It is thereby $19.4\,\%$ faster than the CSC. The grasp execution time for the different grasps is shown in Fig. 5.11. The median grasp time is not significantly faster for the SAC compared to the CSC. However, it can be seen that the CSC has a significantly higher variance in grasp time than the SAC, especially including few very slow grasp demonstrations. This might be caused by the fact that some subjects had notable issues to perform the mode switching in the CSC. Similar to commercial sequential control, subjects did not get any feedback on the active prosthesis mode but had to rely on the accuracy of their own muscle signals. This leads to unintended movements of the wrist or fingers throughout or directly after mode switching, which prolonged the overall grasping process.

The **number of grasp attempts** needed for the different objects is shown in Fig. 5.12. Overall, there is no significant difference in the number of grasp attempts needed over the different control schemes. However, three object-specific differences can be seen. For the top grasp on the thin neck of a cola bottle, subjects had difficulties in aligning the fingers with the object while si-

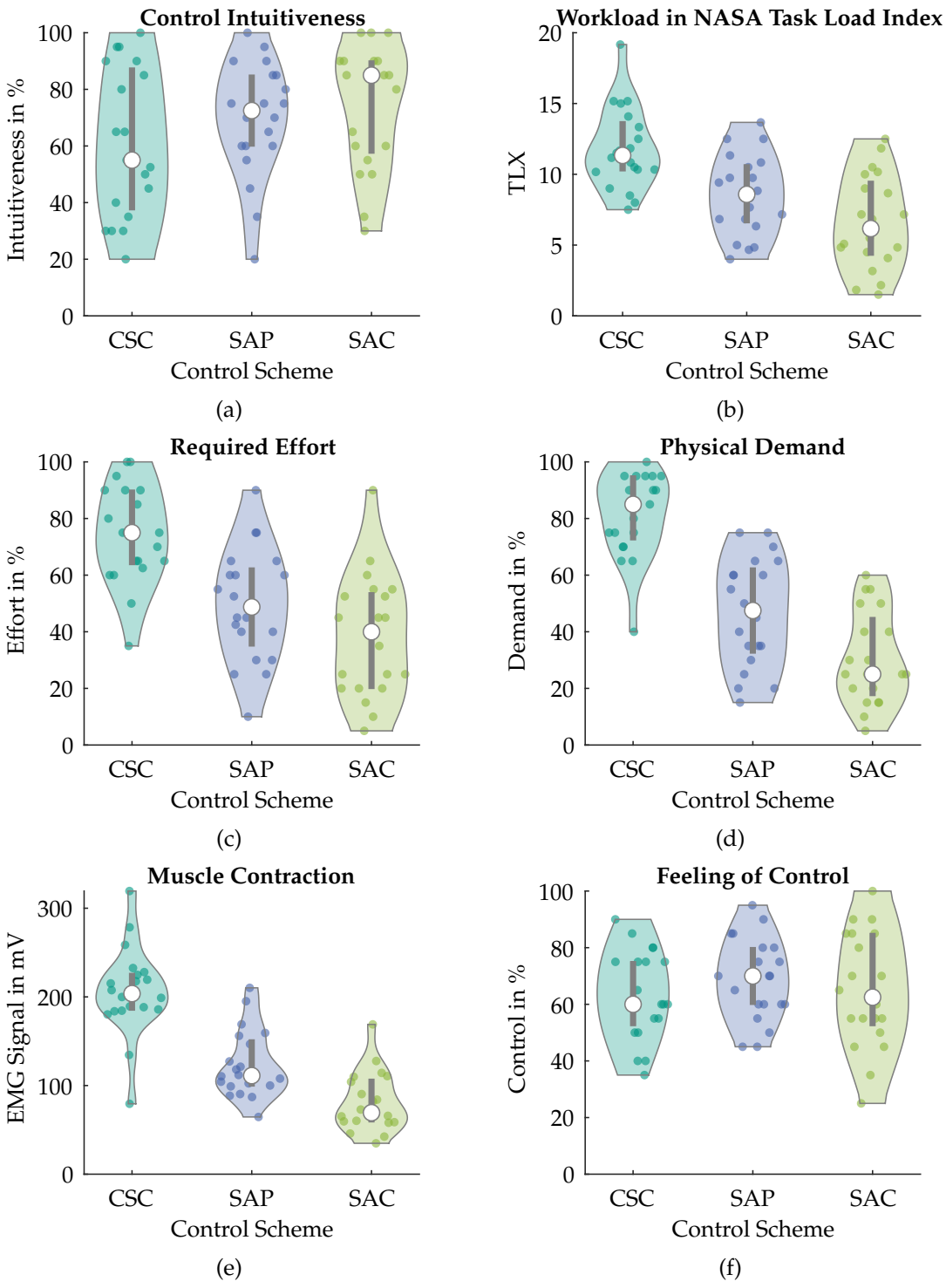

Figure 5.10: Results of the user study in terms of control intuitiveness (a), workload (b), required effort (c), physical demand (d), the integral of the EMG signals (e) and the feeling of control (f); all plots show the first to third quartile as a grey line with a white point marking the median, individual data points are shown as colored dots within the area of the vertically plotted kernel density function (Starke, Weiner et al., 2022) © CC BY 4.0

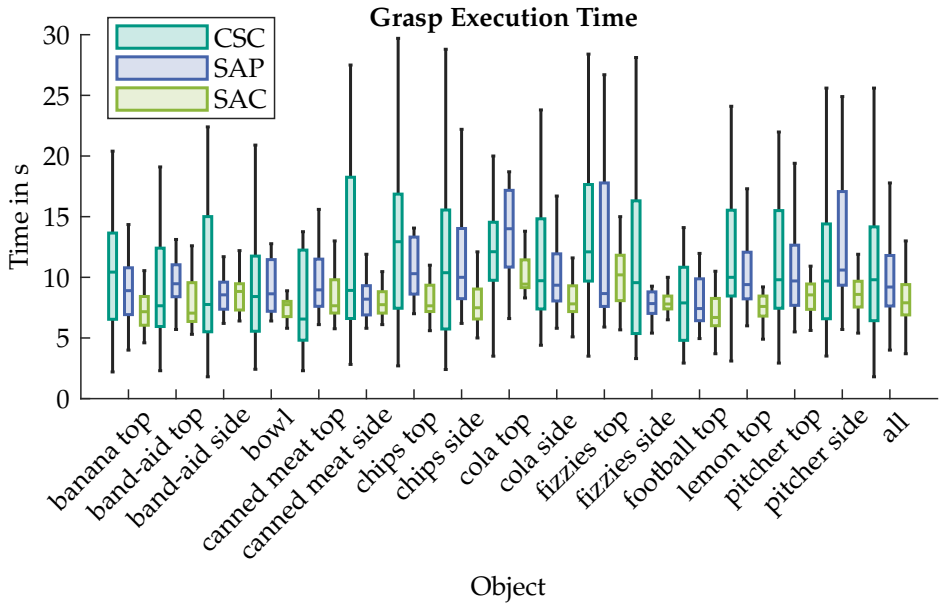

Figure 5.11: Grasp execution time over the three control schemes and all objects; the bars show the first to third quartile of measurements with the horizontal line marking the median time, the black line depict the data range excluding outliers (Starke, Weiner et al., 2022) © CC BY 4.0

multaneously tensing their muscles. Since the distance measurement replaces a muscle activation in triggering the grasp for the SAC, this grasp was easier to achieve with the semi-autonomous scheme. Similarly, the alignment of the fingers for the SAP was also difficult in a top grasp on a package of fizzy tablets. For the CSC, subjects were able to correct their grasp in the process to achieve an adequate grasp for the relatively light fizzy package at the expense of a prolonged grasp time. In contrast the lemon's shape complicates the alignment of the prosthesis with the object for a suitable grasp while simultaneously pointing the distance sensor in the palm towards the lemon surface. Thereby, several subjects had difficulties in triggering the final grasping motion with the SAC leading to a higher number of grasp attempts.

Overall, the semi-autonomous prosthesis control based on continuous grasp motions learned from human demonstration is more intuitive to the user than a sequential, EMG-based control. The partial automation of the grasping motion reduces the user's physical demand significantly, while they still feel in control of their prosthetic hand. Grasping is sped up compared to a sequential EMG-based control with a similar grasp success measured by the number of grasp attempts needed in the user study. The application of automated grasping motions learned from human demonstration thereby simplifies prosthetic

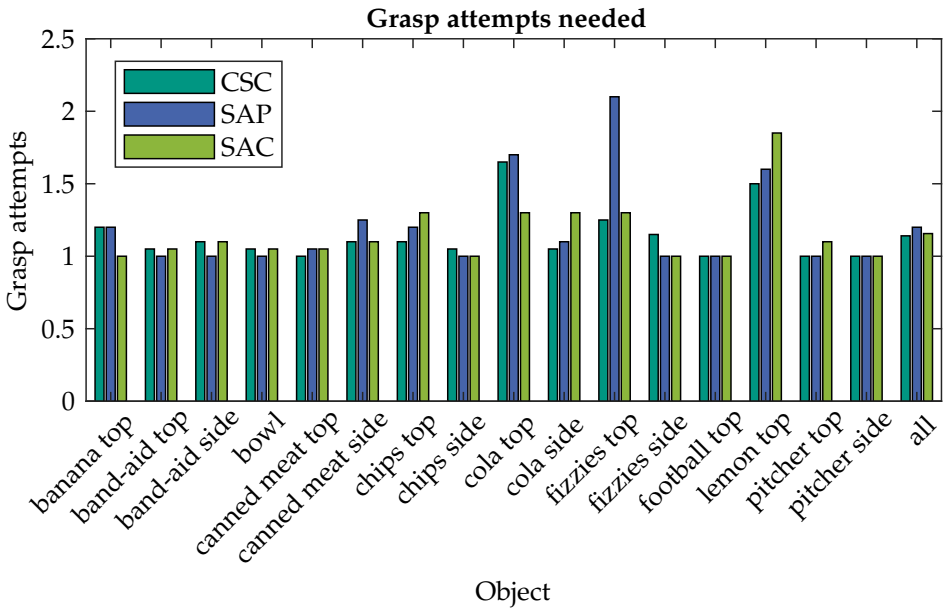

Figure 5.12: Number of attempts needed to grasp each object for all three control schemes; the ideal outcome of a grasp being successful in the first trial for all subjects is denoted as one (Starke, Weiner et al., 2022) © CC BY 4.0

grasping for the user while providing stable, coordinated grasping that feels natural to the user.

5.5 Summary and Conclusion

This chapter presents methods for human-inspired grasp control on prosthetic hands. The descriptive postural synergies are applied on a prosthetic hand. Further, a semi-autonomous control scheme is designed and evaluated, that simplifies grasp control for the user by automating parts of the grasping process. This control provides intuitive grasp motions that are learned from human demonstration and can be executed under the supervision of the user. This thesis expands the existing control of prosthetic hands in three main aspects:

- A descriptive postural synergy space is applied for prosthetic grasp control. It allows for a simple generation of specific grasp postures in hand control.
- A database of human grasp motions is built. It contains human demonstrations of power grasp motions for a wide variety of objects.
- A semi-autonomous grasp control is designed, that simplifies prosthesis control for the user. This control reduces the cognitive burden imposed

on the user when grasping with their prosthesis. It is the first prosthesis control that provides continuous, coordinated grasp motions of all DoF of the prosthetic hand and wrist.

The **descriptive postural synergy space** derived in this thesis is applied on a real robotic system. Synergy-generated grasp postures are mapped onto the prosthetic hand's kinematics and used as goal poses for a simple constant closing control. A range of different household and workshop objects is grasped with the prosthetic hand using this synergy-based control.

A **human grasp database** is learned from demonstrated human power grasps. It contains continuous, coordinated grasp trajectories for thumb and finger closing as well as wrist orientation. Trajectories in the database are generalized over several human subjects and mapped to the kinematics of the prosthetic hand. In addition, the grasp database provides a pregrasp segmentation, that is necessary to align the prosthetic grasping motion with the human arm approach motion in prosthesis control.

A **semi-autonomous grasp control** is designed based on the grasp trajectories from the human grasp database. It autonomously provides grasp suggestions based on the object and user intention. Once accepted by the user, an autonomous grasp motion is executed that compensates for hand rotations caused by the user's arm motion. The user can intervene at any time during the grasp process.

The **evaluation** shows that the descriptive postural synergies can be applied successfully in the control of prosthetic hands. The semi-autonomous control based on the human grasp database is preferred over a conventional prosthetic control by most subjects. Subjects can grasp objects faster with the semi-autonomous grasp control. It reduces the workload for the user while being very intuitive and evoking the same feeling of control over the prosthetic hand as a conventional, fully manual control.

CHAPTER 6

Conclusion

This thesis aims at understanding human grasping behavior to leverage the sophisticated human grasping knowledge for robotic hand control. To this end, grasp synergies representing both the posture and the forces of a grasp have been defined and analyzed. Structured grasp synergy spaces have been introduced to allow for an intuitive generation of new, human-like grasps for prosthetic hand control. In addition, a database of human grasps has been defined and used within a semi-autonomous control scheme for robotic prosthetic hands. In the following, the impact of the different contributions will be discussed and an outlook on possible directions for future extensions will be given.

6.1 Scientific Contributions

The posture and motion of the finger joint angles throughout the grasp is described by **postural and kinematic synergies**. An adaptable postural synergy space is learned in a latent space by an autoencoder network. In contrast to the state of the art, this synergy space has a non-linear structure and is thereby able to represent conceptual grasp characteristics. The postural synergy space is structured according to different grasp types and an additional parameter is encoding the diameter of the grasped object. By these means, new, human-like grasps, that were not directly demonstrated by humans can be generated

from the synergy space. The structure of the synergy space thereby allows to generate grasps of a specific type and size directly from the postural grasp synergies. The postural synergies have been evaluated in comparison to a state of the art representation of linear synergies derived by a PCA. The adaptable postural synergies have been published in Starke et al. (2018) and the generation of human-like grasps from these synergies has been presented in further detail in (Starke et al., 2020).

In addition, kinematic grasp synergy primitives are presented, that provide a generalized representation of kinematic synergy trajectories for a specific grasp type. From the demonstrated synergy trajectories, a via-point movement primitive is learned. This synergy primitive describes the general grasp motion for the particular grasp type in synergy space and also takes the variance of the synergy trajectories into account. A library of synergy primitives for different grasp types is built as a general representation of human grasp motions. Generalized kinematic synergy trajectories can be generated by executing the synergy primitives, which are adaptable in time, start and end position. In addition, the trajectory itself can be adapted within the learned human variance. Thereby the library of synergy primitives provides the first synergy representation of kinematic grasp motions, that allows the generation of human-like, adaptable grasp motions that have not been directly demonstrated by a human subject. The accuracy of demonstrated grasp motions regenerated from synergy primitives has been evaluated compared to state of the art kinematic synergies as well as the original human grasp trajectories.

Analyzing grasp contact forces between the hand and the object, **grasp force synergies** are comprehensively described for the first time. Compared to the state of the art, this work presents static force synergies, that encompass a wide range of different grasp types and are not limited to a specific grasp configuration. An analysis of grasp forces in unrestricted human grasping proves the existence of correlations between the forces at different contact locations especially for the fingers and the palm. Thereby, the presence of grasp force synergies in general human grasping is proven. Static grasp force synergies, that describe the grasp force configuration of the stable grasp are derived by a PCA. The static force synergies are evaluated regarding their ability to represent grasps demonstrated by humans. The grasp force analysis and comprehensive static force synergies have been published in (Starke et al., 2019).

Considering the entire force configuration process, two methods for the derivation of novel temporal force synergies are defined. These temporal synergies consider the contact force pattern over the entire grasping process from the

first contact of the hand and the object until the final stable grasp. Firstly, force synergy trajectories are defined in a static force synergy space learned from all contact force configurations irrespective of their timing. Secondly, a non-linear, temporal force synergy space is learned in the latent space of an LSTM-autoencoder trained with entire temporal grasp force patterns. This synergy space has an inherent notion of grasp progress and is structured according to the different grasp types. Both synergy spaces are evaluated regarding their reproduction quality for grasps demonstrated by humans. Human-like grasp force patterns generated from the temporal synergy space are further evaluated regarding their grasp success in comparison to human-demonstrated grasps. The temporal force synergies have been published in (Starke et al., 2021).

Finally, a **semi-autonomous grasping** procedure is presented to simplify grasp control for prosthetic hands. The control is based on a human grasp database providing continuous coordinated grasp motions learned from human demonstration. The grasp motions include both finger and thumb closure as well as the wrist rotation, all controlled together in a coordinated manner. Using environmental information gained from sensors within the prosthetic hand, the user is able to control a human-like grasping motion including motion in all degrees of freedom of the prosthetic hand simultaneously. Simultaneously, the semi-autonomous grasp control requires only two EMG commands directly issued by the user. Thereby, it reduces the workload of the user significantly. The semi-autonomous control scheme is evaluated regarding grasp time, grasp success and user workload in comparison to a manual sequential control and a hybrid control with semi-autonomous grasp selection and manual finger closing. The semi-autonomous prosthesis control has been published in (Starke, Weiner et al., 2022).

6.2 Discussion and Outlook

This thesis introduces a novel adaptable representation for postural synergies and kinematic synergy primitives to generate new, human-like grasp postures and motions with defined grasp characteristics for humanoid robotic hands. Further, it presents the first force synergy representation that covers a wide range of different objects and grasp types as well as novel temporal force synergies to describe the temporal grasp force patterns over the entire grasping process. Finally, a semi-autonomous prosthesis control based on human grasping motions is developed, that simplifies the control of coordinated, continuous

grasping motions for the user. In summary, this work contributes to the development of simple, intuitive grasp control learned from human demonstration by providing synergy representations to model human grasp strategies and a control scheme to apply these human strategies onto robotic prosthetic hands. In continuation, this thesis can be extended in several directions pushing further towards the goal of a versatile, human-inspired robotic hand with human-like grasping abilities.

Based on the kinematic synergy primitives, **generalized primitives for manipulation actions** can be learned. The grasp synergy primitives presented in this work cover grasping motions of the fingers for a set of different grasp types. By considering human demonstrations of more complex manipulation actions, this method could be extended to a more general representation of goal-oriented finger motions. The most paramount research question in this context is whether the concept of grasp synergies can generally be transferred to in-hand manipulation. In addition, the classification of manipulation motions and the definition of appropriate motion primitives taking into account variability in demonstrations as well as possible variations of the manipulation strategy itself introduce questions for further research.

Similar to the application of the postural synergies on a prosthetic robotic hand presented in this thesis, a **synergy-based force control for robotic hands** can be defined. The adaptable postural synergies have been evaluated on the KIT Prosthetic Hand within this work. Recent developments in humanoid hand design have generated hands equipped with tactile sensing abilities trying to mimic the human sense of touch, e. g. the KIT Sensorized Soft Hand by Weiner et al. (2021). Such hands allow for direct grasp force control based on the tactile sensor information. To this end, the temporal force synergies presented in this work could set the foundation for an intelligent, human-like grasp force control for robotic hands. Open research questions in this area include the consolidation of hand motion trajectories and temporal force patterns in hand control. Further, the mapping of human force patterns to the kinematic and sensor structure of robotic hands remains to be determined.

Finally, an **extension of the semi-autonomous grasp control** can be designed to suit prosthetic hands with different functionalities. The presented semi-autonomous control scheme is tailored to the three degrees of actuation of the female KIT Prosthetic Hand, being thumb and finger flexion as well as wrist rotation. Applying the methodical approach of the kinematic synergy primitives, the database can be extended to provide human-learned grasp strategies for varying hand kinematics. This could include individual finger motions, en-

abling precision grasps or an active thumb abduction, which is required for platform grasps. In addition, unknown objects can be included based on visual object segmentation algorithms (e. g. by Hundhausen et al. (2019)), which obviously cannot rely on an object database providing very detailed object information. While the extension of the grasp database itself is a straightforward task, open research questions remain in the generalization of the semi-autonomous control scheme. This includes choosing a grasp strategy based on less specific object information to handle unknown objects as well as the adequate participation of the user in these increasingly complex grasp choices. Further, explicit grasp force control based on the human control strategies described by the temporal force synergies can be included in the semi-autonomous prosthetic control.

Overall, this thesis presents a representation of human grasp strategies including finger and hand motion as well as grasp force progression by lower-dimensional synergies. Both kinematic synergy primitives and temporal force synergies are generalizable and can be used for the generation of new, human-like grasps for robotic hands. In addition, a semi-autonomous grasp control is presented for prosthetic hands based on coordinated, human-like grasp motions. Based on a human grasp database this control achieves intuitive grasping behavior while reducing the cognitive burden of the user.

List of Figures

List of Tables

List of Algorithms

Bibliography

Belter, J. T., Segil, J. L., Dollar, A. M., and Weir, R. F. (2013). Mechanical design and performance specifications of anthropomorphic prosthetic hands: A review. *The Journal of Rehabilitation Research and Development*, 50(5):599–617. *Cited on page 79.*

Bennett, D. A., Member, S., and Goldfarb, M. (2018). IMU-Based Wrist Rotation Control of a Transradial Myoelectric Prosthesis. *IEEE Transactions on Neural Systems and Rehabilitation Engineering*, 26(2):419–427. *Cited on page 18.*

Bicchi, A., Gabiccini, M., and Santello, M. (2011). Modelling natural and artificial hands with synergies. *Philosophical Transactions of the Royal Society B: Biological Sciences*, 366(1581):3153–3161. *Cited on pages 12, 15, 29, and 31.*

Biddiss, E. A. and Chau, T. T. (2007). Upper limb prosthesis use and abandonment : A survey of the last 25 years. *Prosthetics and Orthorics International*, 31(3):236–257. *Cited on page 17.*

Brown, C. and Asada, H. (2007). Inter-Finger Coordination and Postural Synergies in Robot Hands Via Mechanical Implementation of Principal Components Analysis. In *IEEE/RSJ Int. Conf. on Intelligent Robots and Systems*, pages 2877–2882. *Cited on page 12.*

Buckley, M., Vaidyanathan, R., and Mayol-Cuevas, W. (2011). Sensor suites for assistive arm prosthetics. In *IEEE Symposium on Computer-Based Medical Systems*, pages 1–6. *Cited on page 20.*

Bullock, I., Zheng, J. Z., De La Rosa, S., Guertler, C., and Dollar, A. M. (2013a). Grasp Frequency and Usage in Daily Household and Machine Shop Tasks. *IEEE Transactions on Haptics*, 6(3):296–308. *Cited on pages 9 and 25.*

Bullock, I. M., Ma, R. R., and Dollar, A. M. (2013b). A Hand-Centric Classification of Human and Robot Dexterous Manipulation. *IEEE Transactions on Haptics*, 6(2):129–144. *Cited on page 9.*

Calli, B., Walsman, A., Singh, A., Srinivasa, S., Abbeel, P., and Dollar, A. (2015). Benchmarking in Manipulation Research : The YCB Object and Model Set and Benchmarking Protocols. *IEEE Robotics & Automation Magazine*, 22(3):184–185. *Cited on pages 26, 52, 80, and 81.*

Casini, S., Tincani, V., Averta, G., Poggiani, M., Santina, C. D., Battaglia, E., Catalano, M. G., Bianchi, M., Grioli, G., and Bicchi, A. (2017). Design of an underactuated wrist based on adaptive synergies. In *IEEE International Conference on Robotics and Automation (ICRA)*, pages 6679–6686. IEEE. *Cited on page 14.*

Castellini, C. and Van Der Smagt, P. (2013). Evidence of muscle synergies during human grasping. *Biological Cybernetics*, 107(2):233–245. *Cited on page 10.*

Catalano, M., Grioli, G., Farnioli, E., Serio, A., Piazza, C., and Bicchi, A. (2014). Adaptive Synergies for the Design and Control of the Pisa/IIT SoftHand. *Int. Journal of Robotics Research*, 33(5):768–782. *Cited on page 12.*

Catalano, M. G., Grioli, G., Serio, A., Farnioli, E., Piazza, C., and Bicchi, A. (2012). Adaptive Synergies for a Humanoid Robot Hand. In *IEEE-RAS Int. Conf. on Humanoid Robots*, pages 7–14. *Cited on page 12.*

Chadwell, A., Kenney, L., Thies, S., Galpin, A., and Head, J. (2016). The reality of myoelectric prostheses: Understanding what makes these devices difficult for some users to control. *Frontiers in Neurorobotics*, 10:1–21. *Cited on page 17.*

Chen, T., Haas-Heger, M., and Ciocarlie, M. (2018). Underactuated Hand Design Using Mechanically Realizable Manifolds. In *IEEE Int. Conf. on Robotics and Automation*, pages 7392–7398. *Cited on page 12.*

Chen, W., Xiong, C., and Yue, S. (2015). Mechanical Implementation of Kinematic Synergy for Continual Grasping Generation of Anthropomorphic Hand. *IEEE/ASME Transactions on Mechatronics*, 20(3):1249–1263. *Cited on page 12.*

Ciancio, A. L., Cordella, F., Barone, R., Romeo, R. A., Bellingegni, A. D., Sacchetti, R., Davalli, A., Pino, G. D., Ranieri, F., Lazzaro, V. D., Guglielmelli, E., and Zollo, L. (2016). Control of prosthetic hands via the peripheral nervous system. *Frontiers in Neuroscience*, 10:1–17. *Cited on page 18.*

Ciocarlie, M., Goldfeder, C., and Allen, P. (2007a). Dexterous Grasping via Eigengrasps: A Low-dimensional Approach to a High-complexity Problem. *Proceedings of the Robotics: Science & Systems 2007 Workshop-Sensing and Adapting to the Real World, Electronically published*. *Cited on page 15.*

Ciocarlie, M., Goldfeder, C., and Allen, P. (2007b). Dimensionality reduction for hand-independent dexterous robotic grasping. In *IEEE Int. Conf. on Intelligent Robots and Systems*, pages 3270–3275. *Cited on pages 15 and 21.*

Ciocarlie, M. T. and Allen, P. K. (2009). Hand Posture Subspaces for Dexterous Robotic Grasping. *Int. Journal of Robotics Research*, 28(7):851–867. *Cited on page 15.*

Cipriani, C., Zaccone, F., Micera, S., and Carrozza, M. (2008). On the Shared Control of an EMG-Controlled Prosthetic Hand: Analysis of User-Prosthesis Interaction. *IEEE Transactions on Robotics*, 24(1):170–184. *Cited on page 19.*

Cordella, F., Ciancio, A. L., Sacchetti, R., Davalli, A., Cutti, A. G., Guglielmelli, E., and Zollo, L. (2016). Literature review on needs of upper limb prosthesis users. *Frontiers in Neuroscience*, 10:1–14. *Cited on page 17.*

Cutkosky, M. R. (1989). On Grasp Choice, Grasp Models, and the Design of Hands for Manufacturing Tasks. *IEEE Transactions on Robotics and Automation*, 5(3):269–279. *Cited on pages 8, 25, 26, and 35.*

Dalley, S. A., Varol, H. A., and Goldfarb, M. (2011). A Method for the Control of Multigrasp MyoelectricProsthetic Hands. *Neural Systems and Rehabilitation Engineering, IEEE Transactions on*, 20(1):58–67. *Cited on page 18.*

d'Avella, A., Saltiel, P., and Bizzi, E. (2003). Combinations of muscle synergies in the construction of a natural motor behavior. *nature neuroscience*, 6(3). *Cited on page 10.*

De Souza, R., El Khoury, S., Santos-Victor, J., and Billard, A. (2014). Towards comprehensive capture of human grasping and manipulation skills. In *Proceedings of the 13th International Symposium on 3D Analysis of Human Movement*, pages 84–87. *Cited on page 16.*

De Souza, R., El-Khoury, S., Santos-Victor, J., and Billard, A. (2015). Recognizing the Grasp Intention from Human Demonstration. *Robotics and Autonomous Systems*, 74:108–121. *Cited on pages 16 and 49.*

Degol, J., Akhtar, A., Manja, B., and Bretl, T. (2016). Automatic grasp selection using a camera in a hand prosthesis. In *International Conference of the IEEE Engineering in Medicine and Biology Society (EMBC)*, pages 431–434. *Cited on page 18.*

Della Santina, C., Arapi, V., Averta, G., Damiani, F., Fiore, G., Settimi, A., Catalano, M. G., Bacciu, D., Bicchi, A., and Bianchi, M. (2019). Learning From Humans How to Grasp : A Data-Driven Architecture for Autonomous Grasping With Anthropomorphic Soft Hands. *IEEE Robotics and Automation Letters*, 4(2):1533–1540. *Cited on pages 15 and 83.*

Della Santina, C., Bianchi, M., Averta, G., Ciotti, S., Arapi, V., Fani, S., Battaglia, E., Catalano, M. G., Santello, M., and Bicchi, A. (2017). Postural Hand Synergies during Environmental Constraint Exploitation. *Frontiers in Neurorobotics*, 11:41. *Cited on page 11.*

Dimou, D., Santos-Victor, J., and Moreno, P. (2021). Learning Conditional Postural Synergies for Dexterous Hands: A Generative Approach Based on Variational Auto-Encoders and Conditioned on Object Size and Category. In *IEEE International Conference on Robotics and Automation*, pages 4710–4716. *Cited on page 12.*

Došen, S., Cipriani, C., Kostić, M., Controzzi, M., Carrozza, M., and Popović, D. (2010). Cognitive vision system for control of dexterous prosthetic hands: Experimental evaluation. *Journal of NeuroEngineering and Rehabilitation*, 7(1):42. *Cited on page 19.*

Došen, S. and Popović, D. B. (2011). Transradial Prosthesis: Artificial Vision for Control of Prehension. *Artificial Organs*, 35(1):37–48. *Cited on page 19.*

Ekvall, S. and Kragic, D. (2004). Interactive grasp learning based on human demonstration. In *IEEE International Conference on Robotics and Automation*, pages 3519–3524, New Orleans. *Cited on page 83.*

Farina, D., Jiang, N., Rehbaum, H., Holobar, A., Graimann, B., Dietl, H., and Aszmann, O. C. (2014). The extraction of neural information from the surface emg for the control of upper-limb prostheses: emerging avenues and

challenges. *IEEE Transactions on Neural Systems and Rehabilitation Engineering*, 22(4):797–809. *Cited on pages 82, 87, and 91.*

Feix, T., Romero, J., Schmiedmayer, H.-B., Dollar, A. M., and Kragic, D. (2016). The GRASP Taxonomy of Human Grasp Types. *IEEE Transactions on Human-Machine Systems*, 46(1):66–77. *Cited on pages 8, 35, 36, 37, 38, and 54.*

Ferrari, C. and Canny, J. (1992). Planning Optimal Grasps. *1992 IEEE International Conference on Robotics and Automation*, pages 2290–2295. *Cited on pages 31 and 72.*

Fougner, A., Stavdahl, Ø., Kyberd, P. J., Losier, Y. G., and Parker, P. A. (2012). Control of Upper Limb Prostheses : Terminology and Proportional Myoelectric Control — A Review. *IEEE Transactions on Neural Systems and Rehabilitation Engineering*, 20(5):663–677. *Cited on page 18.*

Gabiccini, M., Bicchi, A., Prattichizzo, D., and Malvezzi, M. (2011). On the Role of Hand Synergies in the Optimal Choice of Grasping Forces. *Autonomous Robots*, 31(2-3):235–252. *Cited on pages 12 and 15.*

Gardner, M., Vaidyanathan, R., Burdet, E., and Khoo, B. C. (2015). Motion-based grasp selection: Improving traditional control strategies of myoelectric hand prosthesis. In *IEEE International Conference on Rehabilitation Robotics*, pages 307–312. *Cited on page 18.*

George, J. A., Davis, T. S., Brinton, M. R., and Clark, G. A. (2020). Intuitive neuromyoelectric control of a dexterous bionic arm using a modified Kalman filter. *Journal of Neuroscience Methods*, 330:108462. *Cited on page 18.*

Ghazaei, G., Alameer, A., Degenaar, P., Morgan, G., and Nazarpour, K. (2015). An exploratory study on the use of convolutional neural networks for object grasp classification. In *IET International Conference on Intelligent Signal Processing*, pages 5 .–5 .(1). *Cited on page 18.*

Ghazaei, G., Alameer, A., Degenaar, P., Morgan, G., and Nazarpour, K. (2017). Deep learning-based artificial vision for grasp classification in myoelectric hands. *Journal of Neural Engineering*, 14(3):aa6802. *Cited on page 18.*

Godfrey, S. B., Ajoudani, A., Catalano, M., Grioli, G., and Bicchi, A. (2013). A synergy-driven approach to a myoelectric hand. In *IEEE Int. Conf. on Rehabilitation Robotics*. *Cited on page 12.*

Gonzalez, V., Rowson, J., and Yoxall, A. (2017). Analyzing finger interdependencies during the Purdue Pegboard Test and comparative activities of daily living. *Journal of Hand Therapy*, 30(1):80–88. *Cited on page 14.*

Gonzalez-Vargas, J., Dosen, S., Amsuess, S., Yu, W., and Farina, D. (2015). Human-machine interface for the control of multi-function systems based on electrocutaneous menu: Application to multi-grasp prosthetic hands. *PLOS ONE*, 10(6):1–26. *Cited on page 19.*

Gracia-Ibáñez, V., Vergara, M., Buffi, J. H., Murray, W. M., and Sancho-Bru, J. L. (2017). Across-subject calibration of an instrumented glove to measure hand movement for clinical purposes. *Computer Methods in Biomechanics and Biomedical Engineering*, 19(16):1–11. *Cited on page 26.*

Grodd, W., Hülsmann, E., Lotze, M., Wildgruber, D., and Erb, M. (2001). Sensorimotor mapping of the human cerebellum: fMRI evidence of somatotopic organization. *Human Brain Mapping*, 13(2):55–73. *Cited on page 1.*

Hahne, J. M., Bießmann, F., Jiang, N., Rehbaum, H., Farina, D., Meinecke, F. C., Müller, K. ., and Parra, L. C. (2014). Linear and nonlinear regression techniques for simultaneous and proportional myoelectric control. *IEEE Transactions on Neural Systems and Rehabilitation Engineering*, 22(2):269–279. *Cited on page 18.*

Hansen, T. C., Trout, M. A., Segil, J. L., Warren, D. J., and George, J. A. (2021). A Bionic Hand for Semi-Autonomous Fragile Object Manipulation via Proximity and Pressure Sensors. In *International Conference of the IEEE Engineering in Medicine and Biology Society*, pages 6465–6469. *Cited on page 19.*

Hao, Y., Controzzi, M., Cipriani, C., Popović, D. B., Yang, X., Chen, W., Zheng, X., and Carrozza, M. C. (2013). Controlling Hand-Assistive Devices. *IEEE Robotics and Automation Magazine*, 20(1):40–52. *Cited on page 19.*

Hart, S. G. and Staveland, L. E. (1988). Development of NASA-TLX (Task Load Index): Results of Empirical and Theoretical Research. *Advances in Psychology*, 52:139–183. *Cited on page 94.*

Hundhausen, F., Megerle, D., and Asfour, T. (2019). Resource-aware object classification and segmentation for semi-autonomous grasping with prosthetic hands. In *IEEE/RAS International Conference on Humanoid Robots (Humanoids)*, Toronto, Canada. *Cited on pages 89 and 105.*

Iberall, T. (1997). Human Prehension and Dexterous Robot Hands. *The International Journal of Robotics Research*, 16(3):285–299. *Cited on pages 8, 37, and 84.*

Ijspeert, A., Nakanishi, J., and Schaal, S. (2002). Learning Attractor Landscapes for Learning Motor Primitives. In *Conference on Neural Information Processing Systems*, pages 1–8. *Cited on page 42.*

Ingram, J. N., Körding, K. P., Howard, I. S., and Wolpert, D. M. (2008). The statistics of natural hand movements. *Experimental Brain Research*, 188(2):223–236. *Cited on page 13.*

Jafarzadeh, M. and Tadesse, Y. (2019). Convolutional Neural Networks for Speech Controlled Prosthetic Hands. In *International Conference on Transdisciplinary AI (TransAI)*, pages 35–42. *Cited on page 20.*

Jarque-Bou, N. J., Scano, A., Atzori, M., and Müller, H. (2020). Kinematic synergies of hand grasps: a comprehensive study on a large publicly available dataset. *Journal of NeuroEngineering and Rehabilitation*, 16(63):1–14. *Cited on pages 2, 11, and 21.*

Jones, L. A. and Lederman, S. J. (2006). *Human hand function*. Oxford University Press. *Cited on page 1.*

Kamakura, N., Matsuo, M., Ishii, H., Mitsuboshi, F., and Miura, Y. (1980). Patterns of Static Prehension in Normal Hands. *The American Journal of Occupational Therapy*, 34(7):437–445. *Cited on pages 8 and 35.*

Karnati, N., Kent, B. A., and Engeberg, E. D. (2013). Bioinspired sinusoidal finger joint synergies for a dexterous robotic hand to screw and unscrew objects with different diameters. *IEEE/ASME Transactions on Mechatronics*, 18(2):612–623. *Cited on page 14.*

Kasper, A., Xue, Z., and Dillmann, R. (2012). The KIT object models database: An object model database for object recognition, localization and manipulation in service robotics. *Int. Journal of Robotics Research*, 31(8):927–934. *Cited on pages 26, 52, and 80.*

Kent, B. A., Lavery, J., and Engeberg, E. D. (2014). Anthropomorphic Control of a Dexterous Artificial Hand via Task Dependent Temporally Synchronized Synergies. *Journal of Bionic Engineering*, 11(2):236–248. *Cited on page 13.*

Konnaris, C., Thomik, A. A. C., and Faisal, A. A. (2016). Sparse eigenmotions derived from daily life kinematics implemented on a dextrous robotic hand.

2016 6th IEEE International Conference on Biomedical Robotics and Biomechatronics (BioRob), pages 1358–1363. *Cited on page 14.*

Kyranou, I., Krasoulis, A., Erden, M. S., Nazarpour, K., and Vijayakumar, S. (2016). Real-Time Classification of Multi-Modal Sensory Data for Prosthetic Hand Control. In *IEEE RAS/EMBS International Conference on Biomedical Robotics and Biomechatronics*, pages 536–541, Singapore. *Cited on page 18.*

León, B., Morales, A., and Sancho-Bru, J. (2014). The Model of the Human Hand. In *From Robot to Human Grasping Simulation*, volume 19, chapter 5, pages 123–173. Springer International Publishing. *Cited on page 1.*

Light, C. M., Chappell, P. H., Hudgins, B., and Engelhart, K. (2002). Intelligent multifunction myoelectric control of hand prosthesis. *Journal of Medical Engineering & Technology*, 26(4):139–146. *Cited on page 18.*

Liu, J., Feng, F. X., Nakamura, Y. C., and Pollard, N. S. (2014). A taxonomy of everyday grasps in action. In *IEEE-RAS International Conference on Humanoid Robots*, pages 573–580. *Cited on page 9.*

Mandery, C., Terlemez, O., Do, M., Vahrenkamp, N., and Asfour, T. (2016). Unifying representations and large-scale whole-body motion databases for studying human motion. *IEEE Transactions on Robotics*, 32(4):796–809. *Cited on pages 28, 31, 35, 70, 72, and 83.*

Markovic, M., Došen, S., Cipriani, C., Popovic, D., and Farina, D. (2014). Stereovision and augmented reality for closed-loop control of grasping in hand prostheses. *Journal of Neural Engineering*, 11(4):046001. *Cited on page 19.*

Markovic, M., Došen, S., Popovic, D., Graimann, B., and Farina, D. (2015). Sensor fusion and computer vision for context-aware control of a multi degree-of-freedom prosthesis. *Journal of Neural Engineering*, 12(6):066022. *Cited on page 19.*

Marneweck, M., Lee-Miller, T., Santello, M., and Gordon, A. M. (2016). Digit Position and Forces Covary during Anticipatory Control of Whole-Hand Manipulation. *frontiers in Human Neuroscience*, 10:1–10. *Cited on pages 16 and 56.*

McMullen, D. P., Hotson, G., Katyal, K. D., Wester, B. A., Fifer, M. S., McGee, T. G., Harris, A., Johannes, M. S., Vogelstein, R. J., Ravitz, A. D., Anderson, W. S., Thakor, N. V., and Crone, N. E. (2014). Demonstration of a semi-autonomous hybrid brain-machine interface using human intracranial EEG,

eye tracking, and computer vision to control a robotic upper limb prosthetic. *IEEE Transactions on Neural Systems and Rehabilitation Engineering*, 22(4):784–796. *Cited on page 20.*

Monforte, M. and Ficuciello, F. (2020). A Reinforcement Learning Method Using Multifunctional Principal Component Analysis for Human-like Grasping. *IEEE Transactions on Cognitive and Developmental Systems*. *Cited on page 15.*

Mouchoux, J., Carisi, S., Došen, S., Farina, D., Schilling, A. F., and Markovic, M. (2021). Artificial Perception and Semiautonomous Control in Myoelectric Hand Prostheses Increases Performance and Decreases Effort. *Transactions on Robotics*, 37(4):1298–1312. *Cited on page 19.*

Naceri, A., Moscatelli, A., Santello, M., and Ernst, M. O. (2014). Multi-digit Position and Force Coordination in Three- and Four-digit Grasping. In Auvray, M. and Duriez, C., editors, *Haptics: Neuroscience, Devices, Modeling, and Applications*, pages 101–108, Berlin, Heidelberg. Springer Berlin Heidelberg. *Cited on pages 16 and 56.*

Nobre Castro, M. and Došen, S. (2022). Continuous Semi-autonomous Prosthesis Control Using a Depth Sensor on the Hand. *Frontiers in Neurorobotics*, 16:814973. *Cited on page 19.*

Ortiz-Catalan, M., Håkansson, B., and Brånemark, R. (2014). Real-time and simultaneous control of artificial limbs based on pattern recognition algorithms. *IEEE Transactions on Neural Systems and Rehabilitation Engineering*, 22(4):756–764. *Cited on page 18.*

Palermo, F., Cognolato, M., Gijsberts, A., Müller, H., Caputo, B., and Atzori, M. (2017). Repeatability of grasp recognition for robotic hand prosthesis control based on sEMG data. In *IEEE International Conference on Rehabilitation Robotics*, pages 1154–1159. *Cited on page 18.*

Paraschos, A., Daniel, C., Peters, J. R., and Neumann, G. (2013). Probabilistic Movement Primitives. In Burges, C. J. C., Bottou, L., Welling, M., Ghahramani, Z., and Weinberger, K. Q., editors, *Advances in Neural Information Processing Systems*, pages 1–9. *Cited on page 42.*

Parikh, P. J., Fine, J. M., and Santello, M. (2019). Dexterous Object Manipulation Requires Context-Dependent Sensorimotor Cortical Interactions in Humans. *Cerebral Cortex*, 30(5):3087–3101. *Cited on page 16.*

Paskett, M. D., Brinton, M. R., Hansen, T. C., George, J. A., Davis, T. S., Duncan, C. C., and Clark, G. A. (2021). Activities of daily living with bionic arm improved by combination training and latching filter in prosthesis control comparison. *Journal of NeuroEngineering and Rehabilitation*, 18(45):1743–0003. *Cited on page 18.*

Peer, A., Einenkel, S., and Buss, M. (2008). Multi-fingered Telemanipulation - Mapping of a Human Hand to a Three Finger Gripper. In *IEEE International Symposium on Robot and Human Interactive Communication*, pages 465–470, Munich. *Cited on page 84.*

Pei, D., Patel, V., Burns, M., Chandramouli, R., and Vinjamuri, R. (2019). Neural Decoding of Synergy-Based Hand Movements Using Electroencephalography. *IEEE Access*, 7(1):18155–18163. *Cited on page 11.*

Piazza, C., Grioli, G., Catalano, M. G., and Bicchi, A. (2019). A Century of Robotic Hands. *Annual Review of Control, Robotics, and Autonomous Systems*, 2(1):1–32. *Cited on page 13.*

Piazza, C., Santina, C. D., Catalano, M., Grioli, G., Garabini, M., and Bicchi, A. (2016). SoftHand Pro-D: Matching dynamic content of natural user commands with hand embodiment for enhanced prosthesis control. In *IEEE International Conference on Robotics and Automation*, pages 3516–3523. *Cited on page 18.*

Piazza, C., Simon, A. M., Turner, K. L., Miller, L. A., Catalano, M. G., Bicchi, A., and Hargrove, L. J. (2020). Exploring augmented grasping capabilities in a multi-synergistic soft bionic hand. *Journal of NeuroEngineering and Rehabilitation*, 17(116):1–16. *Cited on pages 18 and 79.*

Prattichizzo, D., Malvezzi, M., and Bicchi, A. (2010). On Motion and Force Control of Grasping Hands with Postural Synergies. *Robotics: Science and Systems*. *Cited on pages 12 and 15.*

Prattichizzo, D., Malvezzi, M., Gabiccini, M., and Bicchi, A. (2013). On Motion and Force Controllability of Precision Grasps with Hands Actuated by Soft Synergies. *IEEE Transactions on Robotics*. *Cited on pages 12 and 15.*

Rearick, M. P. and Santello, M. (2002). Force synergies for multifingered grasping : effect of predictability in object center of mass and handedness. *Experimental Brain Research*, 144(1):38–49. *Cited on pages 16, 52, and 56.*

Romero, J., Feix, T., Ek, C. H., Kjellström, H., and Kragic, D. (2013). Extracting Postural Synergies for Robotic Grasping. *IEEE Transactions on Robotics*, 29(6):1342–1352. *Cited on pages 13, 14, 17, 34, 35, 61, and 75.*

Rosmarin, J. B. and Asada, H. H. (2008). Synergistic Design of a Humanoid Hand with Hybrid DC motor-SMA Array Actuators Embedded in the Palm. In *IEEE Int. Conf. on Robotics and Automation*, pages 773–778. *Cited on page 12.*

Sancho-Bru, J. L., Péréz-González, A., Vergara, M., and Guirintano, D. J. (2003). A 3D Biomechanical Model of the Hand for Power Grip. *Journal of Biomechanical Engineering*, 125(1):78–83. *Cited on page 21.*

Santello, M., Bianchi, M., Gabiccini, M., Ricciardi, E., Salvietti, G., Prattichizzo, D., Ernst, M., Moscatelli, A., Jörntell, H., Kappers, A. M., Kyriakopoulos, K., Albu-Schäffer, A., Castellini, C., and Bicchi, A. (2016). Hand synergies: Integration of robotics and neuroscience for understanding the control of biological and artificial hands. *Physics of Life Reviews*, 17:1–23. *Cited on page 12.*

Santello, M., Flanders, M., and Soechting, J. F. (1998). Postural Hand Synergies for Tool Use. *The Journal of Neuroscience*, 18(23):10105–10115. *Cited on pages 2, 11, 21, 23, 29, 57, 58, 59, and 75.*

Santello, M. and Soechting, J. F. (2000). Force synergies for multifingered grasping. *Experimental Brain Research*, 133(4):457–467. *Cited on page 16.*

Schweitzer, W., Thali, M. J., and Egger, D. (2018). Case-study of a user-driven prosthetic arm design: Bionic hand versus customized body-powered technology in a highly demanding work environment. *Journal of NeuroEngineering and Rehabilitation*, 15(1):1–27. *Cited on page 17.*

Segil, J. L., Controzzi, M., ff. Weir, R. F., and Cipriani, C. (2014). Comparative study of state-of-the-art myoelectric controllers for multigrasp prosthetic hands. *Journal of Rehabilitation Research and Development*, 51(9):1439–1454. *Cited on page 18.*

Shafti, A., Orlov, P., and Faisal, A. A. (2019). Gaze-based, Context-aware Robotic System for Assisted Reaching and Grasping. In *International Conference on Robotics and Automation (ICRA)*, pages 863–869. *Cited on page 20.*

Smit, G., Plettenburg, D. H., and van der Helm, F. C. T. (2015). The Lightweight Delft Cylinder Hand: First Multi-Articulating Hand That Meets the Basic User Requirements. *Transactions on Neural Systems and Rehabilitation Engineering*, 23(3):431–440. *Cited on page 78.*

Starke, J., Chatzilygeroudis, K., Billard, A., and Asfour, T. (2019). On force synergies in human grasping behavior. In *IEEE/RAS International Conference on Humanoid Robots (Humanoids)*, pages 72–78, Toronto, Canada. *Cited on pages 50, 52, 53, 54, 56, 58, 59, 60, and 102.*

Starke, J., Eichmann, C., Ottenhaus, S., and Asfour, T. (2018). Synergy-based, data-driven generation of object-specific grasps for anthropomorphic hands. In *IEEE/RAS International Conference on Humanoid Robots (Humanoids)*, pages 327–333, Beijing, China. *Cited on pages 23, 29, 32, and 102.*

Starke, J., Eichmann, C., Ottenhaus, S., and Asfour, T. (2020). Human-inspired representation of object-specific grasps for anthropomorphic hands. *International Journal of Humanoid Robotics (IJHR)*, 17(2):2050008. *Cited on pages 12, 23, 24, 26, 27, 28, 30, 31, 32, 33, and 102.*

Starke, J., Keller, M., and Asfour, T. (2021). Temporal force synergies in human grasping. In *IEEE/RSJ International Conference on Intelligent Robots and Systems (IROS)*, pages 3940–3947, Prague, Czech Republic. *Cited on pages 50, 62, 63, 64, 65, 67, 68, 69, 70, 71, 72, 73, and 103.*

Starke, J., Weiner, P., Crell, M., and Asfour, T. (2022). Semi-autonomous control of prosthetic hands based on multimodal sensing, human grasp demonstration and user intention. *Robotics and Autonomous Systems*. *Cited on pages 78, 80, 85, 86, 89, 90, 93, 94, 96, 97, 98, and 103.*

Sundaram, S., Kellnhofer, P., Li, Y., Zhu, J.-Y., Torralba, A., and Matusik, W. (2019). Learning the signatures of the human grasp using a scalable tactile glove. *Nature*, 569:698–702. *Cited on pages 16 and 49.*

Swain, I. D. and Nightingale, J. M. (1980). An adaptive control system for a complete hand/arm prosthesis. *Journal of Biomedical Engineering*, 2(3):163–166. *Cited on page 18.*

Thomik, A. A. C., Fenske, S., and Faisal, A. A. (2015). Towards Sparse Coding of Natural Movements for Neuroprosthetics and Brain – Machine Interfaces. In *International IEEE EMBS Conference on Neural Engineering*, pages 938–941, Montpellier, France. *Cited on page 13.*

Vahrenkamp, N., Asfour, T., and Dillmann, R. (2010). Simox: A Simulation and Motion Planning Toolbox for C++. Technical report, Karlsruhe Institute of Technology (KIT). *Cited on pages 31 and 72.*

Vergara, M., Sancho-Bru, J. L., Gracia-Ibáñez, V., and Pérez-González, A. (2014). An introductory study of common grasps used by adults during performance of activities of daily living. *Journal of Hand Therapy*, 27(3):225–234. *Cited on pages 10 and 26.*

Volkmar, R., Došen, S., Gonzalez-Vargas, J., Baum, M., and Markovic, M. (2019). Improving bimanual interaction with a prosthesis using semi-autonomous control. *Journal of NeuroEngineering and Rehabilitation*, 16(140):1–13. *Cited on page 18.*

Weiner, P., Hundhausen, F., Grimm, R., and Asfour, T. (2021). Detecting grasp phases and adaption of object-hand interaction forces of a soft humanoid hand based on tactile feedback. In *IEEE/RSJ International Conference on Intelligent Robots and Systems (IROS)*, pages 3956–3963, Prague, Czech Republic. *Cited on page 104.*

Weiner, P., Starke, J., Hundhausen, F., Beil, J., and Asfour, T. (2018). The kit prosthetic hand: Design and control. In *IEEE/RSJ International Conference on Intelligent Robots and Systems (IROS)*, pages 3328–3334, Madrid, Spain. *Cited on pages 77 and 79.*

Weiner, P., Starke, J., Rader, S., Hundhausen, F., and Asfour, T. (2022). Designing prosthetic hands with embodied intelligence: The kit prosthetic hands. *Frontiers in Neurorobotics*, tbd:1–21. *Cited on pages 20, 77, and 79.*

Weiss, E. J. and Flanders, M. (2004). Muscular and Postural Synergies of the Human Hand. *Journal of Neurophysiology*, 92(1):523–535. *Cited on page 11.*

Weisz, J. and Allen, P. K. (2012). Pose Error Robust Grasping from Contact Wrench Space Metrics. *2012 IEEE International Conference on Robotics and Automation*, pages 557–562. *Cited on page 32.*

Wijk, U. and Carlsson, I. (2015). Forearm amputees' views of prosthesis use and sensory feedback. *Journal of Hand Therapy*, 28:269–278. *Cited on page 17.*

Wilson, S. and Vaidyanathan, R. (2017). Upper-limb prosthetic control using wearable multichannel mechanomyography. In *International Conference on Rehabilitation Robotics*, pages 1293–1298. *Cited on page 18.*

Wimböck, T., Reinecke, J., and Chalon, M. (2012). Derivation and Verification of Synergy Coordinates for the DLR Hand Arm System. In *IEEE Int. Conf. on Automation Science and Engineering*, pages 454–460. *Cited on pages 15 and 21.*

Xu, K., Liu, Z., Zhao, B., Liu, H., and Zhu, X. (2019). Composed continuum mechanism for compliant mechanical postural synergy : An anthropomorphic hand design example. *Mechanism and Machine Theory*, 132:108–122. *Cited on page 13.*

Zhou, Y., Gao, J., and Asfour, T. (2019). Learning via-point movement primitives with inter- and extrapolation capabilities. In *IEEE/RSJ International Conference on Intelligent Robots and Systems (IROS)*, pages 4301–4308, Macau, China. *Cited on page 43.*

Zhuang, K. Z., Sommer, N., Mendez, V., Aryan, S., Formento, E., D'Anna, E., Artoni, F., Petrini, F., Granata, G., Cannaviello, G., et al. (2019). Shared human–robot proportional control of a dexterous myoelectric prosthesis. *Nature Machine Intelligence*, 1(9):400–411. *Cited on pages 18 and 20.*

List of Publications

N. Jaquier, Y. Zhou, **J. Starke**, and T. Asfour, "Learning to Sequence and Blend Robot Skills via Differentiable Optimization," *IEEE Robotics and Automation Letters*, 2022.

J. Starke, P. Weiner, M. Crell, and T. Asfour, "Semi-autonomous control of prosthetic hands based on multimodal sensing, human grasp demonstration and user intention," *Robotics and Autonomous Systems*, vol. 154, p. 104123, 2022.

P. Weiner, **J. Starke**, S. Rader, F. Hundhausen, and T. Asfour, "Designing Prosthetic Hands with Embodied Intelligence: The KIT Prosthetic Hands," *Frontiers in Neurorobotics*, vol. 16, pp. 1–14, 2022.

J. Starke, M. Keller, and T. Asfour, "Temporal Force Synergies in Human Grasping," in *IEEE/RSJ International Conference on Intelligent Robots and Systems (IROS)*, 2021, pp. 3940–3947.

F. Hundhausen, **J. Starke**, and T. Asfour, "A Soft Humanoid Hand with In-Finger Visual Perception," in *IEEE/RSJ International Conference on Intelligent Robots and Systems (IROS)*, 2020, pp. 8722–8728.

J. Starke, C. Eichmann, S. Ottenhaus, and T. Asfour, "Human-Inspired Representation of Object-Specific Grasps for Anthropomorphic Hands," *International Journal of Humanoid Robotics (IJHR)*, vol. 17, no. 2, p. 2050008, 2020.

I. Llop-Harillo, A. Pérez-González, **J. Starke**, and T. Asfour, "The Anthropomorphic Hand Assessment Protocol (AHAP)," *Robotics and Autonomous Systems*, vol. 121, p. 103259, 2019.

J. Starke, K. Chatzilygeroudis, A. Billard, and T. Asfour, "On Force Synergies in Human Grasping Behavior," in *IEEE/RAS International Conference on Humanoid Robots (Humanoids)*, 2019, pp. 72–78.

J. Starke, C. Eichmann, S. Ottenhaus, and T. Asfour, "Synergy-Based, Data-Driven Generation of Object-Specific Grasps for Anthropomorphic Hands," in *IEEE/RAS International Conference on Humanoid Robots (Humanoids)*, 2018, pp. 327–333.

P. Weiner, **J. Starke**, F. Hundhausen, J. Beil, and T. Asfour, "The KIT Prosthetic Hand: Design and Control," in *IEEE/RSJ International Conference on Intelligent Robots and Systems (IROS)*, 2018, pp. 3328–3334.

M. T. Chikhaoui, J. Granna, **J. Starke**, and J. Burgner-Kahrs, "Toward Motion Coordination Control and Design Optimization for Dual-Arm Concentric Tube Continuum Robots," *IEEE Robotics and Automation Letters (RAL)*, vol. 3, no. 3, pp. 1793–1800, 2018.

J. Starke, E. Amanov, M. T. Chikhaoui, and J. Burgner-Kahrs, "On the Merits of Helical Tendon Routing in Continuum Robots," in *IEEE/RSJ International Conference on Intelligent Robots and Systems (IROS)*, 2017, pp. 6470–6476.

Underlined authors share first authorship